

**UNCLASSIFIED**

---

---

**AD 274 340**

*Reproduced  
by the*

ARMED SERVICES TECHNICAL INFORMATION AGENCY  
ARLINGTON HALL STATION  
ARLINGTON 12, VIRGINIA



---

---

**UNCLASSIFIED**

NOTICE: When government or other drawings, specifications or other data are used for any purpose other than in connection with a definitely related government procurement operation, the U. S. Government thereby incurs no responsibility, nor any obligation whatsoever; and the fact that the Government may have formulated, furnished, or in any way supplied the said drawings, specifications, or other data is not to be regarded by implication or otherwise as in any manner licensing the holder or any other person or corporation, or conveying any rights or permission to manufacture, use or sell any patented invention that may in any way be related thereto.

274340



RADIO CORPORATION OF AMERICA  
RCA LABORATORIES

FINAL REPORT

RESEARCH AND DEVELOPMENT ON  
SEMICONDUCTOR PARAMETRIC AND TUNNEL DIODE  
MICROWAVE DEVICES

CONTRACT NO. AF19(604)-4980  
AIR FORCE CAMBRIDGE RESEARCH CENTER  
AIR RESEARCH AND DEVELOPMENT COMMAND

REPORT DATE: OCTOBER 31, 1961



DAVID SARNOFF RESEARCH CENTER  
PRINCETON, NEW JERSEY

AFCRL-62-46

FINAL REPORT

*For the Period*

January 1, 1959 to October 31, 1961

*Report Date:* October 31, 1961

**RESEARCH AND DEVELOPMENT ON SEMICONDUCTOR  
PARAMETRIC AND TUNNEL DIODE MICROWAVE DEVICES**

**Contract No. AF19(604)-4980**

**Project - 4645**

**Task - 4645-01**

*Prepared for*

ELECTRONICS RESEARCH DIRECTORATE  
AIR FORCE CAMBRIDGE RESEARCH LABORATORIES  
OFFICE OF AEROSPACE RESEARCH  
UNITED STATES AIR FORCE  
BEDFORD, MASSACHUSETTS

*Report Prepared by:* K.K.N. Chang  
G. Conrad  
G.H. Heilmeier  
N.J. Kolettis  
H.J. Prager  
C.F. Stocker

RADIO CORPORATION OF AMERICA  
RCA LABORATORIES  
PRINCETON, NEW JERSEY

Requests for additional copies by Agencies of the  
Department of Defense, their contractors, and other  
Government agencies should be directed to the:

**ARMED SERVICES TECHNICAL INFORMATION AGENCY**  
**ARLINGTON HALL STATION**  
**ARLINGTON 12, VIRGINIA**

Department of Defense contractors must be established for ASTIA services or have their  
"need-to-know" certified by the cognizant military agency of their project or contract.

## TABLE OF CONTENTS

	PAGE
I. SUMMARY .....	1
II. PARAMETRIC AMPLIFIERS .....	5
A. Single Diode Parametric Amplifier Using Lower Frequency Pumping .....	5
B. Cavity-Type Amplifier (Coaxial-Line Distributed Amplifier) .....	7
C. Helix-Type Parametric Amplifier.....	10
D. Millimeter Wave Generation by Parametric Methods .....	17
III. TUNNEL DIODE AMPLIFIERS .....	21
A. Tunnel Diode Characteristic .....	21
B. Tunnel Diode Amplifier .....	22
C. Noise Theory .....	26
D. Semiconductor Oscillators .....	29
IV. TUNNEL DIODE CONVERTERS .....	34
A. Small Pump Theory .....	34
B. Coaxial Line Circuit for UHF Down Converter .....	39
C. S-Band Down Converter.....	41
D. Lumped Parameter Circuit for UHF Down Converter .....	42
E. Method of Optimization of Noise Factor .....	48
F. Large Pump Theory .....	49
G. Millimeter Wave Tunnel Diode Down Converter .....	59
V. SOLID-STATE MICROWAVE DEVICES .....	60
A. Negative-Resistance Transmission Line Amplifier .....	60
B. Two-Port Microwave Devices .....	68
VI. GERMANIUM AND GALLIUM ANTIMONIDE TUNNEL DIODES .....	79
A. Germanium Tunnel Diodes .....	79
B. Gallium Antimonide Tunnel Diodes .....	84
C. Appendix - A General Model for the Source of Tunnel Diode Valley Current .....	86
REFERENCES .....	89

## I. SUMMARY

This technical report covers work done under Contract No. AF19(604)-4980 entitled "Research and Development on Semiconductor Parametric and Tunnel Diode Microwave Devices.

The object of the work is briefly as follows.

(a) Undertake a theoretical investigation of the behavior of parametric amplifiers including:

- (1) Low-frequency pumping
- (2) Noise properties
- (3) Gain, bandwidth, linearity
- (4) Intermodulation effects
- (5) Signal modulation
- (6) New concepts employing varying degrees of non-linearity.

(b) Carry on an experimental program with special attention to:

- (1) Broad banding
- (2) Lower pumping power
- (3) Optimum noise factor

(c) Search for novel active semiconductor microwave devices

- (1) Two-terminal type
- (2) Four-terminal nonreciprocal type

(d) Develop improved varactors and tunnel diodes with:

- (1) Lower losses
- (2) Greater non-linearities
- (3) Higher cut-off frequencies

Prior to the starting date for the contract RCA Laboratories had made important contributions to the general advance of parametric amplifiers. In particular, it had been shown that they can be pumped at frequencies lower than the signal frequency, permitting them to be used at frequencies where higher-frequency pumps are not available. Furthermore, two-

port devices have been demonstrated which do not require isolators. This had been achieved by using a composite amplifier comprising two converters and one amplifier.<sup>2</sup>

In a first attempt to obtain broad-band parametric amplification, work was begun on an S-band distributed amplifier made of a length of coaxial line. Because the line was heavily loaded with parametric diodes, the amplifier produced power gains of 15 db with bandwidths only of 30-40 mc. To obtain higher gains with broader bandwidths a second approach was undertaken. This new approach called for the design of p-n junction diodes which are not conventionally mounted or wired. Instead, individual units of p-n junctions are attached directly to a non-dispersive slow-wave structure such as a helix. By carefully mounting three individual parametric diodes on the helix turns, net power gains of 26 db have been obtained. Noise factors of 5 to 7 db were measured. An improved version of an helix type amplifier using 18 distributed parametric diodes has achieved bandwidths of the order of 200 mc.

Work on low-frequency pumping was also extended to an investigation of the possibility of harmonic generation of millimeter waves using nonlinear reactances. A parametric frequency doubler has been studied. Measurements on a gallium arsenide point-contact diode have given a conversion efficiency of -9 db for the second harmonic of a 24 kMc input. The new results represent a 6 to 7 db improvement over conventional nonlinear resistance conversion.

The lowest possible pump frequency for parametric devices is, of course, zero frequency, i.e., D.C. battery. The introduction of tunnel diodes prompted us to investigate a new set of semiconductor microwave amplifiers and frequency converters with a D.C. pump. A tunnel diode amplifier was first investigated. The expressions for gain, bandwidth and noise factor of this amplifier are shown to be analogous to those found for a cavity-type parametric amplifier with one striking difference, the bandwidth of the tunnel diode amplifier is comparatively broad.

An experimental lumped-circuit amplifier has been built for demonstration purposes. The operating frequencies were 80 mc, 66 mc, and 30 mc. These all gave stable power gains of about 15 db with bandwidths of the order of a few megacycles. The noise factors were measured to be of the order of 4 db. The tunnel diodes which were used in the experimental amplifier had only a small amount of negative conductance. It is pointed out that a diode with a higher negative conductance at the same DC current would have a much lower noise factor.

The noise in the tunnel diode was found to be essentially of the shot-effect type. It is generally believed that low-noise operation is possible by choosing low biasing currents,

but no quantitative analysis had been done. An analysis was made which indicates that with a given I-V characteristic of a tunnel diode a minimum noise factor exists at a unique point on the characteristic. Furthermore, an ideal I-V characteristic which can be a guide for the design of tunnel diode devices with low noise factors is suggested.

When the tunnel diode amplifier operates at infinite gain, oscillation takes place. A simple theory for a tunnel diode oscillator was derived.

In addition to amplifiers and oscillators, tunnel diodes can be used as frequency converters. In practice, the low-noise, high-gain, conversion of a high-frequency signal to a lower frequency signal has not been possible with previous mixer devices. Ordinary crystal detectors, which make use of the nonlinear behavior of their positive resistance, exhibit a conversion loss and a poor noise factor. On the other hand, parametric converters, which operate on a nonlinear capacitance or inductance basis, have achieved good noise factors with up-conversion gain. Parametric down converters, however, have poor noise factors. For such down converters it is found that the excess noise factor (i.e. the noise factor minus unity) goes roughly as the ratio of the input frequency to the output frequency. Thus for a ten-to-one frequency down-conversion, the noise factor is about 10 db. Because of this frequency dependence, it is difficult to convert a microwave frequency into a low intermediate frequency with a reasonable noise factor by parametric converters.

The unusual I-V characteristic of tunnel diodes suggested a down converter which can exhibit both conversion gain and low noise factor. To demonstrate this low noise, high-gain down conversion, an experimental UHF tunnel-diode converter, which converts a UHF signal to a 30 mc intermediate frequency, was built. This converter yields conversion gains of 10 to 20 db and noise factors of 2 to 5 db. In particular, the effect of large pump voltage on the overall tunnel-diode converter performance was thoroughly investigated. It was found that a further reduction in noise factor and an improvement in circuit stability were obtained through the application of the large pump<sup>3</sup> voltage.

Parametric and tunnel diodes are both two-terminal devices. To achieve four-terminal amplifiers with these devices, a traveling-wave scheme using a series of distributed diodes has been suggested. A transmission line with distributed positive and negative resistance as well as with distributed diode noise generators was analyzed. Gain and noise factors were derived as a function of boundary conditions, matching conditions and distributed noise. It was found that low-noise amplification can be achieved on such a line provided the line is characterized by high gain per unit length, high total gain, good matching and low distributed noise. A distortionless active line for such low-noise amplifiers appears attractive.

Ever since the parametric and tunnel diodes were introduced, it has been generally felt that these devices would be more useful if somehow they could be modified to four terminal devices. A general study is underway toward realization of a four terminal active semiconductor device. A new scheme which utilizes a unique interaction between Hall-effect and magneto resistance was proposed. Early experimental results indicate that a novel nonreciprocal active semiconductor device is possible and it is hoped that the new scheme would lead to many important high-frequency applications.

In the field of device study, the degradation of tunnel-diode valley current with overcooking at alloying temperatures has recently been observed. An impurity diffusion mechanism has been postulated and vindicated in a test experiment. Alloy dots of known high dopant densities (e.g. eutectics) have been used as the diffusion source. While quantitative agreement is more easily approached in germanium since its relevant parameters are more accurately known, eutectic alloys have proved especially fruitful for the fabrication of gallium antimonide tunnel diodes.

## II. PARAMETRIC AMPLIFIERS

### A. SINGLE DIODE PARAMETRIC AMPLIFIER USING LOWER FREQUENCY PUMPING

#### Introduction

Parametric amplifiers of the nonlinear-reactance type have received periodic attention in the past. More recently, parametric amplification in the microwave region using the nonlinear inductance property of ferromagnetic resonance has been described. These amplifiers have, however, conventionally drawn their energy from an RF pump-power supply having a frequency higher than that of the signal to be amplified. A higher frequency source is usually not practical, particularly when the signal is at a microwave frequency.

To remedy this fundamental drawback, a parametric amplifier using lower-frequency pumping has been suggested<sup>1</sup> in which two or more pump sources at frequencies lower than the signal frequency are employed. In addition, to be compatible with the multiple lump system, a reactance sample of a higher than quadratic order of nonlinearity is necessary for amplification.

In the following a series of experiments which verify the principle of lower-frequency pumping is discussed. The experiments contain a first realization which made use of a nickel-manganese ferrite as the nonlinear reactance. Later experiments were performed with a germanium junction diode having a large degree of nonlinearity between the capacitance and the biasing voltage. Measurements of gain, bandwidth, and noise figure were made and found to be in substantial agreement with theory. Because of the large amount of nonlinearity existing in these junction diodes, the necessary pumping power was found to be exceedingly small.

#### Theoretical Background

Although a general theory on parametric amplifiers has been given in two previous articles,<sup>1,2</sup> it is still worthwhile to review in brief some of the basic equations, particularly because the case discussed here involves the use of a nonlinear capacitance instead of the nonlinear inductance treated before.

Consider the four resonant circuits of Fig. 1, coupled through a nonlinear capacitance whose charge,  $q$ , is a cubic function of the voltage,  $v$ .

$$q = C_0 v + Cv^3 \quad (\text{II-1})$$

Here  $C_0$  is the linear capacitance, and  $C$  is the coefficient of nonlinearity. The two pump circuits are resonant at frequencies  $\omega_3$ ,  $\omega_4$ , the signal circuit is at  $\omega_1$ , and the idler is at  $\omega_2 = \omega_3 + \omega_4 - \omega_1$ .

It can then be shown<sup>2</sup> that a negative conductance  $G$  is formed in the signal circuit:

$$G = a G_T \frac{\omega(\omega_3 + \omega_4 - \omega)/\omega_1 \omega_2}{1 + \left(\frac{B_2}{G_2}\right)^2}, \quad (\text{II-2})$$

where

$$a = \frac{9}{4} C^2 \left| \frac{I_3}{Y_3} \right|^2 \left| \frac{I_4}{Y_4} \right|^2 \frac{\omega_1(\omega_3 + \omega_4 - \omega_1)}{G_T G_2} \quad (\text{II-3})$$

The  $I$ 's are the pumping currents,  $Y$ 's are the admittances, and the  $G$ 's are conductances. The total conductance,  $G_T$ , of the signal circuit includes the signal generator conductance,  $G_g$ , the signal tank conductance  $G_T$ , and the load conductance  $G_L$ .

If the maximum available power output from the signal generator is  $I_1^2/4G_g$ , then the power gain  $G_p$  is

$$G_p = \frac{4G_g G_L}{(G_T + G)^2 + \left(B_1 - G \frac{B_2}{G_2}\right)^2} \quad (\text{II-4})$$

The expressions for the product of voltage gain ( $G_v$ ) and bandwidth ( $B$ ) and for the ultimate noise factor ( $F$ ) are the same as those found<sup>2</sup> for the case of higher-frequency pumping:

$$G_v B = \frac{G_L \omega_2}{G_T \omega_1 Q_2}, \quad (\text{II-5})$$

$$F = 1 + \frac{T}{T_o} \left( \frac{G_L}{G_g} + \frac{\omega_1}{\omega_2} - \frac{a G_T}{G_g} \right) \quad (\text{II-6})$$

The experiments described in this paper were greatly simplified through the choice of equal pump frequencies,  $\omega_3 = \omega_4$ . In this case only one pump source and one pump circuit were necessary. The gain and noise factor equations for this single pump case remain the same as above, provided  $a$  is placed by

$$\alpha' = \frac{9}{16} C^2 \left| \frac{I_3}{Y_3} \right|^4 \frac{\omega_1(2\omega_3 - \omega_1)}{G_T G_2} \quad (II-7)$$

### Experimental Results

The experimental setup for the noise factor measurement of an S-band parametric amplifier is shown in Fig. II-2. A coaxial T-section, which has three branches resonating respectively at signal frequency ( $\omega_1$ ), the pump frequency ( $\omega_3$ ) and the idling frequency ( $\omega_2$ ), is employed as the amplifier circuit. A germanium junction diode is mounted at the junction of the T-section. The diode is self-biased through a resistance of 1000 ohms.

The following results have been measured.

TABLE II-1

$f_1$ (signal frequency)	2300 mc
$f_3$ (pump frequency)	1800 mc
$f_2$ (idling frequency)	1300 mc
$F_1$ (N.F. of receiver alone)	16 db
$F_{12}$ (N.F. of amplifier plus 10 db attenuator plus receiver)	8 db
$F_2$ (N.F. of 10 db attenuator plus receiver)	17 db
$G_p$ (net power gain of amplifier)	15 db
$P_p$ (pumping power)	20 mw

The above measurements thus gave a noise factor for the amplifier of 6.8 db. The noise factor computed from Eq. (II-6) is 6.6 db which agrees very well with the experimental value. It is understood that these noise factors are deduced for a two-terminal, non-isolated system. The noise factor would be lower if a circulator had been used. Furthermore, by using higher orders of nonlinearity the noise factor would also be improved.

### B. CAVITY-TYPE AMPLIFIER (COAXIAL-LINE DISTRIBUTED AMPLIFIER)

The traveling-wave parametric amplifier offers an attractive means of obtaining broadband microwave amplification. It employs the nonlinear reactance necessary for parametric amplification as part of a transmission line. If the line is terminated in its characteristic impedance, there is no reflection of the signal, idle, or pump frequencies, and hence isolation between input and output is obtained. The narrow-bandwidth restriction of conventional parametric amplifiers is not a limitation of the traveling-wave scheme because resonant circuits are not employed.

Since the semiconductor diode is essentially a two-terminal device, one of the convenient ways to make a four-terminal device with such active diodes is to load a smooth transmission line with diodes in a distributed way. In order that lumped loading capacitances of the diodes may have the same effect as though their impedances were uniformly distributed, it is necessary that the loading diodes be spaced at distances that do not exceed a quarter wave length.<sup>4</sup> If the spacing is greater, the loading impedances tend to act as irregularities or chokes and interfere with transmission.

The effect of loading the diodes on a line can be analyzed as follows. The section of line between a pair of diodes and the effect of the diodes may be represented by a  $\pi$ -section as in Fig. II-3. Here  $Z$  and  $Y$  are respectively the series impedance and the shunt admittance per unit length of line.

If the line is lossless, the cosine of the propagation constant ( $\beta_o$ ) of the unloaded line is

$$\cos \beta_o \ell = 1 + \frac{1}{2} Z Y, \quad (\text{II-9})$$

where

$$Z = z\ell \frac{\sin \beta_o \ell}{\beta_o \ell} \quad (\text{II-10})$$

and

$$\frac{1}{2} Y = y\ell \frac{\tan \frac{1}{2} \beta_o \ell}{\frac{1}{2} \beta_o \ell} \quad (\text{II-11})$$

The loading of the diode will change the propagation constant from  $\beta_o$  to  $\beta_d$ , which satisfies

$$\cos \beta_d \ell = 1 + \frac{1}{2} Z [Y + Y_d] = \cos \beta_o \ell + i \frac{Z_o}{2} Y_d \sin \beta_o \ell \quad (\text{II-12})$$

where  $Z_o$  is the characteristic impedance of the line and

$$Y_d = \frac{j\omega C_o}{1 + j\omega C_o R} \quad (\text{II-13})$$

$C_o$  and  $R$  are the diode capacitance and series resistance respectively.

In the presence of the signal frequency ( $\omega_1$ ) the pump frequency ( $\omega_3$ ), and the idling frequency ( $\omega_2 = \omega_3 - \omega_1$ ), nonlinear interaction takes place in the diode, and  $Y_d$  in

Eq. (II-12) becomes current-and voltage-dependent. The cosine of the new propagation constant ( $\beta_d$ ) under the amplifying condition is then

$$\cos \beta_d \ell = \cos \beta_o \ell + j \frac{Z_o}{2} \frac{i}{V} \sin \beta_o \ell , \quad (\text{II-14})$$

where  $i$  and  $V$  are respectively the diode current and voltage.

By assuming a quadratic nonlinearity between charge and voltage<sup>1</sup> (i.e.  $q = C_o V - CV^2$ ), the change of the propagation constant under small-signal amplifying conditions is found to be

$$\beta_{d1} = \beta_{d2} + j\alpha \quad (\text{II-15})$$

where

$$\alpha = \sqrt{\frac{\omega_1 \omega_2}{\omega_3^2} \left| \frac{V_3 C}{C_o} \right| \left( \frac{\omega_3 C_o Z_o}{2} \right)^2 \frac{\sin \beta_{o1} \ell \sin \beta_{o2} \ell}{\ell^2 \sin \beta_{d1} \ell \sin \beta_{d2}} - \left( \frac{\delta \beta}{2} \right)^2} \quad (\text{II-16})$$

and

$$\delta \beta = \beta_{d1} + \beta_{d2} - \beta_{d3} \quad (\text{II-17})$$

Here  $\alpha \ell$  is the gain parameter per diode. The voltage gain ( $G_V$ ) per diode is

$$G_V = e^{\alpha \ell} \quad (\text{II-18})$$

In the case where  $\ell \rightarrow 0$ , Eq. (II-16) degenerates into an expression which has the same form as that for a smooth transmission line.<sup>5</sup>

An active coaxial-line, has been built with germanium diodes in place of the usual shunt capacitors. Using six diodes, gains as high as 15 db were observed with a signal frequency of 3440 mc, a pumping frequency of 4250 mc and idle frequency of 810 mc. The pumping power was in the order of 400 milliwatts. Each of the three frequencies of concern were placed in a different pass band of the line.

The structure did not possess the wide-band properties predicted for it. The bandwidth was found to be 30-40 megacycles. This can be explained by the fact that in order to obtain high gain from such a small number of diodes, the loading of the line must be considerable. The distortion of the line parameters in this manner leads to amplification over a relatively narrow band. If the loading of the line were lighter, the broadband capabilities would necessitate high Q diodes, and much smaller gains per stage. Hence many diodes would be required for the gain observed if the bandwidth were to be of the order of 20%.

Parametric amplification in periodically loaded transmission lines was also observed with a pump frequency lower than that of the signal frequency. In particular, the 6-diode line yielded net gains of from 6 to 10 db with proper bias adjustment at a pump frequency of 2130 mc and a signal frequency of 3500 mc. Pumping power was of the order of 500 milliwatts. This device suffered also from the narrow-band limitations of the conventional higher-frequency pumping scheme for much the same reasons. A bandwidth of 30 mc was obtained experimentally. It is felt that the ability to pump at a frequency lower than the signal in this case was due to a doubling process in the diodes. This is substantiated by the fact that the line possessed a pass band at the 2nd harmonic of the pump (4260 ac) and required slightly greater pumping power for gains which were lower than those observed in the conventional case.

### C. HELIX-TYPE PARAMETRIC AMPLIFIER

It has been pointed out that to obtain high gains with broader bandwidths, many diodes must be employed. Since the physical size of conventional commercial diodes makes it virtually impossible to construct a structure with sufficient diodes per wavelength at microwave frequencies to yield appreciable gains, a new approach was tried.

Diodes were fabricated using strips of n-type germanium with alloy dots spaced periodically at a convenient small distance. The strips were mounted on quartz rods for mechanical support. Three such diode structures were mounted symmetrically about an S-band helix. The pitch of the helix was made equal to the spacing between adjacent dots so that the dots made contact with each turn of the helix. (Fig. II-4a).

Diodes shown in Fig. II-4a are activated by the radial rf field. Alternatively, they can be arranged so that they can be activated by the axial field (Fig. II-4b). In Fig. II-4c, coaxial-line feed is shown for the signal, and coupled helix feed is shown for the pump. The helix is an excellent circuit for this purpose since it is nondispersive. It can be designed to transmit simultaneously the pump frequency, the signal frequency and the idling frequency. In addition, the fabrication of the helix structure is simple in that the diodes require no external wiring since they are activated by the rf electric field between adjacent turns of the helix. In addition, by introducing the pump signal through a coupled helix, some isolation between the signal and pump sources can be achieved.

The first helix-type amplifier is shown in Fig. II-5. The diodes, mounted between turns of the coil, are of germanium, alloyed-diffused and have the following characteristics:

Capacitance (-1 volt)	0.2 - 1 $\mu\text{f}$
Series resistance	2 - 15 ohms
Cutoff frequency (nominal)	20 - 100 kMc

The test apparatus is shown schematically in Fig. II-6. Typical operating data are as follows:

TABLE II-2

Signal Frequency	2800 mc
Pump Frequency	3800 mc
Number of Diodes	2
Pump Power	60 mw
Unloaded helix insertion loss	- 6 db
New Power Gain	26 db
Voltage Gain Bandwidth	30 mc
Noise Figure	5 - 7 db

It can be seen that the bandwidth is quite low, presumably due to the loading introduced by the diodes. To preserve the necessary dispersionless characteristics of a propagating structure, the diode loading must be light. This necessitates many diodes for significant gain, because the gain per diode is small. A second helix was designed so that more diodes per wavelength could be incorporated in the amplifier. In the new structure, the diodes were mounted symmetrically in three stacks on a polystyrene rod. The rod with diodes was then mounted coaxially in the helix structure as shown in Fig. II-7. The new design permitted tighter coupling to the diodes at the pump frequency, resulting in lower pumping powers. Coupled helices were again used to couple power to the helix structure. Experimental results are as follows:

TABLE II-3

Number of diodes	18
Pump frequency	2020 mc
Pumping power	250 mw
Signal frequency	1300 mc to 1525 mc
Net gain	8 db
Diode characteristics	
$C = .8 - 1.2 \mu\text{uf}$	
$f_c$ (cutoff freq.)	20 - 90 kMc

The plot of gain vs. frequency is shown in Fig. II-8. The term electronic gain refers to the gain at the signal frequency when the pump power is applied. It does not include the cold insertion loss of the amplifier. The net gain of the structure is shown by the solid curve in Fig. II-8. The actual amount of pumping power supplied to the diodes was 150 mw. The remaining 100 mw was reflected at the input coupler, and could be reduced by improving the input match. A saturation effect in the gain of the structure was noted. It was found that the gain increased with increased pumping power up to a level of 250 mw (total

pumping power supplied from pump source). Further increases in pumping power did not result in increased gain, and at approximately the 800 mw level, a decrease in gain with increased pumping power was noted. This effect is attributed to increased diode losses due to reverse breakdown over part of the cycle.

### Extension of Experiments

Another and more recent experimental study of the transmission and coupling characteristics of a helix periodically loaded by variable-capacitance diodes along a portion of its length was undertaken by the RCA Electron Tube Division in conjunction with the RCA Laboratories<sup>6</sup>. In this structure, the helix is supported by ceramic rods, and a direct connection is made to each end of the helix.

Semiconductor variable-capacitance diodes were used as helix-turn loading elements. These germanium-type diodes have capacitances of the order of one picofarad. They are encapsulated in small cylindrical packages approximately one-tenth of an inch in diameter. The helix was similar to those used in RCA medium-power S-band traveling-wave tubes.

One end of the helix was terminated in a matched load and the input VSWR was measured on a reflectometer over the 2000- to 4000-megacycle frequency range. The diodes were spaced at intervals of two, three, and four turns. The periodicity of the low-VSWR regions decreased with decreasing diode spacing from an average of approximately 1000 megacycles for a diode in every fourth turn to about 300 megacycles for a diode in every second turn. Figure II-9 shows the VSWR with diodes positioned in every second turn. The several match ranges in the 2000- to 4000-megacycle frequency range include a relatively broadband of very low VSWR in the 2000- to 2300-megacycle range, and a narrower band of very low VSWR near 3000 megacycles. Small shifts in diode position and spacing produced substantial shifts in the frequency locations of these ranges of low VSWR.

The curves of Fig. II-10 show insertion-loss measurements on the diode-loaded helix structure under conditions of no diode loading, a single diode loading per one helix turn, and diodes loading alternate turns. The unloaded helix has an insertion loss of from one to six decibels over the entire frequency octave from 2000 to 4000 megacycles.

The loading of the helix with a single diode provided only a point of impedance discontinuity and did not constitute periodic loading. For this case, the measured insertion loss generally occurred in the neighborhood of 12 to 15 decibels over the 2000- to 4000-megacycle frequency range. The insertion loss resulting from the insertion of three diodes into the helix (a diode loading alternate helix turns) is shown in Fig. II-10 for the frequency range 860 to 4000 megacycles. The general configuration of bands having greater and less

attenuation is evident; bands of relatively low attenuation occur in the UHF and lower L-band frequency ranges, and a narrow band of very low attenuation occurs near 3000 megacycles. This latter band matches a band of very low VSWR predicted by the VSWR measurement. A relatively high insertion loss of greater than 20 decibels was measured in the 2200- to 2300-megacycle band where a very low input VSWR was observed.

The attenuation curve of a diode-loaded helix shown in Fig. II-10 provides an important key to the understanding of the helix parametric amplifier. The particular periodic loading used results in a relatively narrow passband of low insertion loss at approximately 3000 megacycles and at 6000 megacycles (not shown in Fig. II-10). These passbands have been found experimentally to present an excellent load to signals applied to the helix at 3000 megacycles, with the result that such signals develop considerable voltages across each of the diodes. In fact, sparks have been observed between the diodes and helix turns in very dim light (when the contacts between these elements were broken) with r-f power of several hundred milliwatts applied to the helix in the band. Considerable radiation has been detected at a distance from the unshielded helix. The dissipative qualities of the structure are indicated by the fact that less than 10 milliwatts of r-f power was detected at the output of the helix when almost one watt of net power was applied to the input of the helix. The diode-loaded helix also acted as a harmonic generator at these frequencies with an input signal at 3000 megacycles delivering power at 6000 megacycles in the output with good conversion efficiency.

It has been determined experimentally that, at high gain, parametric amplification is possible when the pump signal is passed through the highest-frequency passband and the signal and idler frequencies are approximately 70 and 30 per cent, respectively, of the pump frequency provided that suitable passbands are developed by the diode-loaded helix at these frequencies. The location of the highest passband and the passbands used for the signal and idler frequencies can be controlled by (1) variation of the spacing between diode (and thus of  $a$ ), (2) use of an asymmetrical spacing if the helix diameter and pitch are maintained constant, or (3) adjustment of the helix parameters to provide a mechanical means for adjusting the frequency of operation over a range comprising a substantial portion of an octave.

Substantial insertion loss has been encountered in the frequency bands used for the signal frequency, but considerably less at the idler frequencies. Even in favorable transmission bands, the diode-loaded helix, unlike the shunt-loaded transmission line, provides a complex coupled bandpass-filter type of circuit in each passband. The diode-loaded turns present series components of high impedance in cascade to the signals traveling along the helix. This arrangement provides improved impedance matching to each diode

over wide frequency ranges because the helix turn shunting each element is a broadband circuit which enhances the signal development to the diodes at the principal frequencies. As a result, high gain is achieved with a very small number of diodes and circuit elements.

The circuit aspects of the helix parametric amplifier are based on a straightforward requirement. Because both input and pump signals are applied to the inputs of the amplifier, an amplified input signal, a pump signal of reduced intensity, and an idler signal are produced in the output of the amplifier. These three output signals must be terminated in proper impedances.

Figure II-11 shows the basic circuits and components of a test arrangement for gain measurement over the 2200-2300-megacycle frequency band. The input signal is applied from a tunable signal generator through a low-loss pump-rejection filter to the amplifier input. The pump signal is supplied to the amplifier by a tunable signal generator which drives a traveling-wave tube and provides pump power of up to one watt variable over the 2000- to 4000-megacycle frequency band.

The output circuit in Fig. II-11 is a triplexer type arrangement. The output of the parametric amplifier feeds into a power divider having three output circuits. One output circuit couples to a bandpass filter which passes the amplified band of frequencies to the mixer of a receiver. The second output is coupled to a high-pass filter which rejects both the amplified input signal and idler signal power and couples the remaining power at the pump frequency to a matched termination. The third output is coupled to a low-pass filter having a cutoff frequency between the low-frequency of the idler signal and high frequency of the input signal; a matched termination is provided at the output of the low-pass filter as a termination for the idler signal.

The receiver includes the mixer mentioned above, a local oscillator, a calibrated step attenuator, a 30-megacycle i-f strip, and a detector. Gain is measured by a comparison technique; the detector is first calibrated without the parametric amplifier between the input-signal generator and the power divider and then with the parametric amplifier in the circuit. The calibrated attenuator in the receiver is used to measure power gain.

Several precautions were adopted to assure the validity of gain measurements. First the detector was calibrated while pump power of up to one watt was fed into the triplexer to eliminate spurious mixer responses caused by pump-power leak-throughs; in addition, the filters in the triplexer arrangement were arranged to provide at least 80 decibels isolation between the mixer and the pump termination at pump frequency to prevent pump power from effecting the receiver.

Noise figure was measured at S-band with essentially the same circuit. The output of an AIL-70A noise source was applied to the pump-rejection filter, and a calibrated receiver and Hewlett-Packard 304B noise-figure meter (which also powers the noise source) were substituted for the receiver used in the gain measurements.

For evaluation of the helix parametric amplifier as a wide-band amplifier with respect to structure, circuit, and performance characteristics, a signal-frequency in the 2200- to 2300-megacycle band was chosen, and extensive measurements of electrical performance were made. The following discussion of pertinent performance characteristics is derived from these measurements. It must be emphasized, however, that these performance characteristics are intended only to illustrate the basic electrical behavior of the helix parametric amplifier and the relationship between the circuit structure and performance, and not to establish the design of a particular amplifier.

Operation in the 2200- to 2300-megacycle frequency band is consistent with the existence of a passband in that region, a higher-frequency passband for the pump in the 3000-megacycle range and a passband of relatively low insertion loss in the idler-frequency band of 800 to 900 megacycles. Figure II-10 shows the pass- and stop-band characteristics of a helix structure, when it is loaded by 3 diodes.

In the circuit shown in Fig. II-11, the band-pass filter in the output circuit passes only the desired 2200- to 2300-megacycle band. The high-pass filter in the output pump circuit has a cutoff frequency of 2600 megacycles, and the low-pass filter in the idler output circuit has a cutoff frequency of 1500 megacycles.

Signal connections to the helix parametric amplifier consist of the input signal and the pump signal which are applied to the input helical coupler and the input direct connection to the helix, respectively. The triplexer output circuit is coupled to the output helical coupler, which was specially designed to couple to the helix at all three principal frequencies. The output direct connection to the helix is coupled to a circuit arrangement which permits a wide choice of match and mismatch terminations at the idler frequency. One advantage of the use of pump and idler signals located in relative proximity to the principal signal frequency is that helical couplers have sufficiently wide frequency-coupling characteristics to couple to the helix at all three of these signals, thereby simplifying the coupling problem.

Gain in the 2200- to 2300-megacycle band is a function of several parameters if the helix characteristics remain fixed. These parameters include pump frequency, pump power, and diode spacing where the latter is defined by  $\alpha$ , the ratio of the electrical angle of the diode-loaded helix turn to the electrical angle of the entire unit cell in each

period. For example, when  $\alpha = 0.5$ , the diodes are in a row between alternate helix turns.

The gains achieved were very stable for long periods of time with frequent turning on and off of the equipment. The broad peak of the curve provides for peak gains with small change over a substantial range of pump power.

Figure II-12 shows gain characteristics with respect to various values of pump power for values of 0.55, 0.57, and 0.6. These curves do not establish optimum or maximum bandwidth values, but indicate that for a pump power of 500 milliwatts, peak values of more than 20 decibels of gain may be obtained. The gain peaks which are located in various parts of the 2200- to 2300-megacycle frequency band are dependent on the periodic diode-spacing parameter  $\alpha$ . No value of  $\alpha$  shown provides for gain across the entire 100-megacycle band at any value of pump power.

In measuring the noise figure, a 2200-2300 megacycle band-pass filter was used in the output circuit. The measurement was made with the amplifier adjusted to give a gain in excess of 25 decibels at the center frequency (2250 megacycles). The representative curve of gain as a function of pump power shown in Fig. II-13 was produced at a pump frequency of 3135 megacycles.

The pump rejection filter at the amplifier input stopped noise components at frequencies equal to the pump frequency and at those higher frequencies which beat with the pump signal and produce noise components at 2250 megacycles. In the output circuit, the local oscillator of a receiver driving the noise-figure meter was adjusted to 2280 megacycles. This produced a 30-megacycle component from 2250-megacycles noise which was amplified in the 30-megacycle receiver i-f strip. However, the image noise of the midband noise at 2310 megacycles was prevented from reaching the mixer by the sharp band edge characteristics of the 2200- to 2300-megacycle filter.

The curves of noise figure as a function of pump power and gain as a function of pump power for the operating frequencies mentioned above are shown in Fig. II-13. In regions of low pump power, the noise figure is high; the figure decreases as the pump power is increased to maximum gain. In the maximum-gain region the terminal noise figure passes through a minimum having a measured value of 4.5 decibels. This terminal noise figure includes approximately 1.5 decibels insertion loss due to the input helical coupler and the pump-rejection filter.

## D. MILLIMETER WAVE GENERATION BY PARAMETRIC METHODS

### Introduction

One of the most dependable methods of generating coherent millimeter wave radiation has been the multiplication of some lower frequency by means of the nonlinear resistance of a semiconductor diode. This technique has been used successfully by many workers in the field of molecular spectroscopy. Some fairly typical results are those published by Johnson, Slager, and Kiney<sup>7</sup> in which a conversion loss of -18 db was obtained for the second harmonic (6.25 mm) of a 24 kMc/s (12.5 mm) fundamental.

Manley and Rowe<sup>8</sup> have derived a power relation for three linear circuits which are resonant individually at frequencies  $\omega_1$ ,  $\omega_2$  and  $\omega_1 + \omega_2$ , and coupled by means of a nonlinear reactance.

This power relation states that

$$\frac{P_{12}}{\omega_1 + \omega_2} = -\frac{P_1}{\omega_1} = -\frac{P_2}{\omega_2} \quad (\text{II-19})$$

where  $P_{12}$ ,  $P_1$ ,  $P_2$  are the average powers flowing into the nonlinear reactor at the frequencies  $\omega_1 + \omega_2$ ,  $\omega_1$  and  $\omega_2$ . The fact that power flows from the reactor at the lower frequencies,  $\omega_1$  and  $\omega_2$ , at the expense of the higher frequency pumping power is indicated by the minus signs.

The above power relations can also be written as

$$\frac{-P_{12}}{\omega_1 + \omega_2} = \frac{P_1}{\omega_1} = \frac{P_2}{\omega_2} \quad (\text{II-20})$$

This suggests that if the reactor is pumped at the two lower frequencies, power will flow from the reactor at the higher frequency  $\omega_1 + \omega_2$ . It is easily appreciated that the two lower frequency pumps can have the same frequencies making harmonic generation possible from this scheme. Since the nonlinear reactance is essentially lossless, the conversion efficiency should be high compared to efficiencies obtained with nonlinear resistances.

Using the nonlinear (voltage-dependent) capacitance of a back biased semiconductor diode in a coaxial circuit, Chang<sup>9</sup> has obtained a conversion efficiency of 21 per cent (-6.8 db) for doubling from 3300 to 6600 megacycles. The extension of this principle to the millimeter region is not an easy one. Indeed, the only published result is that of Kita<sup>10</sup> who obtained a minimum conversion loss of -15.8 db in doubling from 24,000 to 48,000

megacycles. The main problems are those of obtaining materials suitable for operation in the millimeter region and a microwave system capable of high performance at these frequencies.

This section describes some recent experiments in the generation of millimeter waves using the nonlinear capacitance of a back-biased point contact semiconductor diode and compares these results with those obtained from point contact silicon and germanium nonlinear resistance diodes.

### **Experimental Methods and Results**

The experimental setup employed in our experiments is shown schematically in Fig. II-14. The modulated input signal was obtained from a 2K33 klystron and power measurements were made with calibrated crystals. Adequate matching was obtained using E-H tuners and short circuiting plungers.

The harmonic generator is shown in Fig. II-15. It consisted of a K band fundamental waveguide (operating range 18-26 kMc/s) crossed by an RG98U harmonic guide (operating range 45-75 kMc). The fundamental guide is tapered in height over a few wavelengths so that a smooth transition can be made to the height of the smaller guide. The harmonic guide acts as a high pass filter with a cutoff above the frequency of the fundamental radiation. In all cases, the crystal of interest is mounted, flush with the bottom, at the junction of the two guides, on a copper stud which could be easily rotated for optimum results. An r.f. by-pass is provided so that a d.c. bias can be employed. A differential screw mounted on the top of the guide with an effective pitch of 364 turns per inch permitted extremely low pressure contacts to be made to the crystals. The point material in all cases was electrolytically etched, silver plated platinum.

Measurements were made on some germanium and silicon crystals as a means of evaluating the performance of the microwave system by comparison with the fairly typical results of workers in the field<sup>7</sup>. The experimental data for harmonic generation using the nonlinear resistance is shown in Table II-4 and compares favorably with published work on these materials.

The results obtained with an n-type germanium point contact nonlinear capacitor are to be contrasted to the nonlinear resistance case. The conversion loss of -14.7 db represents a 1.7 db improvement over the nonlinear resistance case. The conclusion that the conversion mechanism was the nonlinear reactance was based on the fact that the bias was negative. In this region, the nonlinearity of the resistance was very small hence extremely poor efficiency would be expected by this mechanism. Figure II-16 shows a very

TABLE II-4  
EXPERIMENTAL RESULTS OF A MILLIMETER WAVE HARMONIC GENERATOR

	NONLINEAR RESISTANCE		NONLINEAR CAPACITANCE	
	Silicon	Germanium	Germanium	Gallium Arsenide
Pump Frequency $f_o$	24 kMc	24 kMc	24 kMc	24 kMc
Output Frequency $2f_o$	48 kMc	48 kMc	48 kMc	48 kMc
Pump Power $f_o$	.20 mw	.19.6 mw	.20 mw	.24 mw
Output Power $2f_o$	.36 mw	.45 mw	.68 mw	.3 mw
Bias	+3V	-2.0V	-8V	Zero Bias
Conversion Efficiency	-16.6 db	-16.38 db	-14.7 db	-9 db

interesting effect. As the bias was shifted to the forward direction from -.8V the conversion efficiency decreased then increased slightly to -20.8 at a forward bias of +1 volt before falling off rapidly with further increase in bias. The behavior in the forward region is attributed to the nonlinear resistance mechanism. Thus, both conversion mechanisms were observed in the same crystal, and the nonlinear reactance proved to be superior. The germanium crystals employed in these experiments had a resistivity of .013 ohm/cm and the points used were electrolytically etched, silver plated platinum.

By far the most interesting results were obtained with magnesium doped n-type gallium arsenide crystals of .003 ohm/cm resistivity. These results are shown in the Table II-4. A conversion efficiency of -9 db was obtained for the second harmonic of a 24,000 Mc/s input (6.25 mm). It was found to be extremely important to form the point immediately after etching the crystal in order to obtain favorable results. This behavior is attributed to the formation of a stable oxide of gallium on the surface. The best results were obtained under self-bias conditions or a small negative voltage. It is felt that, because the conversion efficiency was relatively insensitive to small bias shifts about the optimum values, both nonlinear reactance and resistance mechanisms were acting.

The characteristics of a typical gallium arsenide point contact diode are shown in Fig. II-17. The diode is seen to have a back current of less than 1 microampere in the region of interest where the diode exhibits a nonlinear capacitance. The nonlinear capacitance at zero bias had a value of approximately  $.58 \mu\text{f}$  and increased rapidly as the bias approached +1 volt.

The superiority of point-contact gallium arsenide nonlinear capacitance diodes over the germanium variety can be explained as follows. The higher electron mobility of gallium

arsenide gives rise to a lower spreading resistance. This, together with the lower capacitance due to a lower dielectric constant, yields a higher value of cutoff frequency than germanium or silicon units. Cutoff frequency for the back-biased diode is defined as that frequency at which the  $Q$  falls to one. The higher band gap of gallium arsenide gives rise to a voltage-current characteristic which increases more slowly in the forward direction than that for germanium. This permits wider voltage excursions into the forward direction where the capacitance nonlinearity is greatest before appreciable diode current is drawn and the  $Q$  deteriorates.

It is of interest to investigate the first order effect of crystal thickness on high frequency performance. If the point is assumed to form a hemispherical junction on the crystal surface the simple model shown in Fig. II-18 can be used to calculate the RC product,  $w$  is the depletion layer thickness,  $t$  is the crystal thickness and  $r$  is the assumed radius. The capacitance is given by the well-known relation

$$C = \frac{KA}{w} = \frac{2\pi r^2 K}{w}$$

The resistance is given by the familiar integral shown in the same figure where all parameters are defined as before.

Since  $r$  will be the controlling geometrical factor and usually quite small, the thickness of the crystal,  $t$ , will not be of primary importance in the subsequent R-C product.

In general a small capacitance is desirable for broad-band, high frequency operation. However, a small capacitance means high impedance and hence higher voltages across its terminals for a given pump power. D.C. conduction will thus occur to a greater extent with an accompanying loss of power in the shunt and series resistances of the diode.

Efficiency is known to drop at high input power levels in nonlinear capacitance diodes because of excursions into the forward bias region, breakdown over part of the cycle, and loss of power in higher harmonics. The ideal scheme then should possess high harmonic rejection, a high breakdown voltage diode, and a slowly increasing current characteristic in the forward directions.

In conclusion the feasibility of generating millimeter waves by means of the nonlinear capacitance of a back-biased semiconductor diode has been demonstrated and found to be superior to the nonlinear resistance multiplier at 6.25 millimeters.

### III TUNNEL DIODE AMPLIFIERS

#### A TUNNEL DIODE CHARACTERISTICS

The tunnel diode is an abrupt junction diode made from materials so heavily doped as to be degenerate in both the n and p regions. Because of this construction, the current-voltage characteristic no longer resembles that of a normal rectifying diode but has the shape of Fig. III-1. Near zero bias voltage and at all back biases, the diode is highly conducting. For small forward bias, the current increases with voltage, reaches a sharp maximum, and then increases exponentially with further bias. The dotted line indicates how a junction diode of similar composition but with a broad rather than an abrupt junction would behave. In the reverse direction it would be blocking until breakdown, while in the forward direction injection would become large at the same voltage where the tunnel diode goes over into the exponential response.

For a tunnel diode of germanium, the voltage of the maximum current occurs at about 50 mv and of the minimum at about 350 mv, roughly independently of the fabrication details. The current scale however, can be arbitrarily changed by changing either the junction area or the depletion layer thickness (i.e. the doping). Representative values of current range from 50  $\mu$ a to 500 ma, the ratio of current maximum to minimum is around 10/1 for good units. The negative conductance, given by the slope of the I-V characteristic in the negative region, may be as high as a mho or more.

Figure III-2, the energy band picture of a tunnel diode, gives the physical nature of the Esaki effect.<sup>11</sup> Here the energy of a carrier in the crystal is plotted as a function of its position in the crystal. The very high doping has made both sides of the junction degenerate and the electrons in the n region on one side of the junction have the same energy as holes in the p region on the other side. Quantum-mechanics states that under this condition there is a non-vanishing probability that an electron originally on one side of the junction can appear on the other at the same energy by tunneling through the barrier. Because the junction is abrupt the thickness of the barrier is only 100  $\text{\AA}$  and the tunneling is a first order effect, making the junction highly conducting with zero applied voltage. There is of course no net tunnel current with zero bias, since in thermal equilibrium the tunneling of electrons from the n to the p region is identically cancelled by the inverse tunneling from the p to the n.

Application of reverse bias displaces the relative energy of the bands on opposite sides of the junction by an amount equal to the bias, as shown in Fig. III-2b. The back current is increased because an increased number of electrons in the p region see equal-energy states in the n side that are accessible for tunneling. For small forward bias, Fig. III-2c, fewer electrons in the p region find sites to tunnel to, and the forward current results from a decrease in the inverse tunneling. With increase in forward bias, the reverse tunneling drops to zero, which roughly corresponds to the maximum in the forward current, and then the forward component starts to drop as the biasing brings the forbidden region of the p side opposite the conduction electrons on the n side. The minimum is reached when minority carrier injection becomes important, the exponential rise being due to the normal forward conduction of a diode.

The negative conductance of the diode, normalized to unit area, can be controlled by controlling the tunneling probability. Since this is extremely sensitive to the thickness of the junction, and since the thickness of an abrupt junction is dependent on the free carrier concentration, the negative conductance can be directly controlled through the doping of the p and n sides of the crystal.

### B. TUNNEL DIODE AMPLIFIER

Since Hull first disclosed the dynatron,<sup>12</sup> negative-conductance amplifiers have received sporadic attention. As early as 1935, E.W. Herold pointed out the possibility of using negative conductance for amplification.<sup>13</sup> However, lack of convenient negative-conductance elements made such amplifiers unattractive. The successful development of the tunnel diode<sup>14</sup> had made possible a new solid-state negative-conductance amplifier.

The amplifier circuit is shown in Fig. III-3. The negative-conductance tunnel diode  $D_1$  having a capacitance  $C_d$ , is energized by a battery  $V_o$  through a dc load resistance  $r_o$ . The resistance  $r_o$  should be smaller than the negative resistance so that stable biasing is possible. The biasing point at which the negative conductance is realized is defined by the combined adjustment of the series resistance  $r_o$  and the supply  $V_o$ . As shown in Fig. III-3 the negative conductance is shunted by an rf tank which determines the amplifier resonant frequency  $f$ . For stability, the rf load conductance presented by the combination of the generator conductance  $G_g$  and the load conductance  $G_L$  through a tap transformation should be larger than the negative conductance  $G$  of the diode. Stable amplification can be achieved only when both the dc and rf load conditions are fulfilled.

Expressions for power gains ( $\kappa_p$ ), bandwidth ( $\Delta f$ ), and noise factor ( $F$ ) of Fig. III-3 have been calculated they are

$$g_p = \frac{4G_g G_L}{\left[ G_T - \left( \frac{n_1}{n_2} \right)^2 G \right]^2} \quad (\text{III-1})$$

$$B = \frac{1}{Q_L \sqrt{g_p}} \left[ 1 + \sqrt{1 + 4Q_L^2 g_p} \right] - 2 \quad (\text{III-2})$$

$$\approx \frac{1}{Q_L \sqrt{g_p}} \left[ 1 + \frac{1}{4Q_L \sqrt{g_p}} \right] \text{ if } Q_L \sqrt{g_p} \gg 1$$

$$F = 1 + \frac{T}{T_o} \left[ \frac{G_L}{G_g} + \frac{G_L}{G_g} + \frac{G_e}{G_g} \right] \quad (\text{III-3})$$

where

$$G_T = G_L + G_g + G_L \quad (\text{III-4})$$

$$Q_L = \frac{\omega_L c_d}{2\sqrt{G_g G_L}} \left( \frac{n_1}{n_2} \right)^2 \quad (\text{III-5})$$

$$G_e = \frac{eI_o}{2kT} \left( \frac{n_1}{n_2} \right)^2 \quad (\text{III-6})$$

$$B = 2 \frac{\Delta f}{f_L} \quad (\text{III-7})$$

Measurements by W.H. Fonger of these Laboratories have shown that the primary noise in the tunnel diode is shot effect.  $G_e$  is the equivalent transformed noise conductance due to the shot effect of the diode, which has a dc current  $I_o$ .  $T_o$  is the reference temperature of the generator conductance ( $G_g$ ) and  $T$  is the ambient temperature.

An experimental lumped circuit based on Fig. III-3 has been built. The operating frequencies were 80 mc, 66 mc, and 30 mc. They all gave stable gains of about 20 db.

Representative experimental results at 30 mc are shown in the following table.

TABLE III-1  
EXPERIMENTAL RESULTS FOR CIRCUIT OF FIGURE III-3

$I_d$	G	$G_L$	$g_p$		$2\Delta f$		N.F.	
			NEGATIVE CONDUCTANCE (mho)	LOAD CONDUCTANCE (mho)	POWER GAIN (db)		BANDWIDTH (mc)	
DIODE CURRENT ( $\mu A$ )	Meas.	Comp.	Meas.	Comp.	Meas.	Comp.	Meas.	Comp.
250	$-\frac{1}{375}$	$\frac{1}{1000}$	20	.23	2	.3	4.5	4.7
300	$-\frac{1}{310}$	$\frac{1}{200}$	40	.36	.19	.16	6.3	5.5
350	$-\frac{1}{206}$	$\frac{1}{50}$	27	.26	.8	1.05	8.0	6.8

The computed gains, bandwidths, and noise factors are based on Eqs.(III-1) to (III-3) using values of  $G_g = 0.02$  mhos,  $C_d = 40 \mu\text{f}$  and  $(n_1/n_2)^2 = 7.65$ . These values were used in the experimental amplifier. It is noted that these computed results agree reasonably well with those measured.

The amplifier has much broader bandwidth at low gains. For instance, typical measured bandwidths at 10 db gain are of the order of 3 or 4 mc. According to Eq. (III-2) the bandwidth varies inversely as the voltage gain at high values of circuit Q's.

It is interesting to note that the negative-conductance tunnel diode amplifier has a striking resemblance to the nonlinear-susceptance amplifier<sup>2</sup> as far as the gain, bandwidth and noise factor are concerned.

For the nonlinear-susceptance amplifier, it has been shown that

$$g_p = \frac{4G_R G_L}{(G_T - G)^2} \quad (\text{III-8})$$

$$B = \frac{\omega_2}{\omega_1} \frac{1}{\sqrt{g_p}} \frac{1}{Q_2} \quad (\text{III-9})$$

$$F = 1 + \frac{T}{T_0} \left( \frac{G_L}{G_g} + \frac{G_L}{G_g} + \frac{\omega_L}{\omega_2} - \frac{G}{G_g} \right) \quad (\text{III-10})$$

By comparing Eqs. (III-8) to (III-9) with Eqs. (III-1) to (III-3) it follows that

1. Both amplifiers achieve gain through a negative conductance. In the nonlinear susceptance amplifier, the negative conductance is derived from an rf pump through a nonlinear interaction, while in the negative conductance amplifier, the negative conductance is intrinsic and is directly realized from a dc source.

2. By lowering the idling circuits  $Q$ 's of a nonlinear susceptance amplifier, one can increase the bandwidth, as shown by Eq. (III-9). However, the increase of bandwidth in this way is accompanied by an increase in the pumping power. This limitation is not present in the negative conductance amplifier where the loaded  $Q_L$  is not subject to any limitation.

3. At first thought, one might well assume that the tunnel diode amplifier, because of the shot noise, will generate more noise than the nonlinear susceptance amplifier. This is not necessarily so, according to Eq. (III-3). While the tunnel diode amplifier has noise originating from shot effect, the nonlinear susceptance amplifier has an equivalent noise due to the presence of the idling circuit. In practice, the idling circuit noise in the latter case can be minimized by choosing a very high idling frequency ( $\omega_2$ ) compared to the signal frequency. Analogously, the shot-effect noise in the former case can also be reduced by using a source conductance ( $G_g$ ) which is higher than the equivalent noise conductance ( $G_e$ ) (see Eq. (III-3)). However, the negative conductance amplifier has the advantage of using a dc source, and design of a high conductance source seems quite feasible.

The diodes which were used in the experimental amplifier happen to be low negative conductance diodes. According to Eq. (III-3) low negative conductance will give high noise factors. It is quite conceivable that a diode can be made with a negative conductance of 0.02 mho, at a diode current  $I_o = 200 \mu\text{a}$ , giving a conductance ratio  $G_e/G_g = 0.20$  and hence a noise factor of the order of a few tenths of a db regardless of the operating frequency.

The present experiments have demonstrated the principle of low noise amplification using the new tunnel diodes. While the results obtained are for the 30-100 megacycle range, there seems to be no reason why this principle cannot be used to obtain low noise amplification in the microwave region. Diodes for this purpose should have the properties of low conduction current and high negative conductance.

In addition, while the tunnel diode is employed in the amplifier as an intrinsic negative resistance as described above, the tunnel diode can also be used in a converter by utilizing the nonlinearity of the intrinsic negative resistance. A down converter can be realized with performance superior to the nonlinear positive-resistance case. An analysis has been made concerning general amplification and frequency conversion (with gain) produced by means of a nonlinear negative resistance.

### C. NOISE THEORY

The noise in a tunnel diode<sup>14, 15</sup> has been found to be essentially of the shot effect type. The magnitude of the excess noise factor, which is defined as the noise factor  $F$  minus unity, is

$$F - 1 \approx \left( \frac{G_n}{G_g} + \frac{G_d}{G_g} \right) \frac{T}{T_o} \quad (\text{III-11})$$

where  $G_g$  is the source conductance at a reference temperature  $T_o$ ,  $G_n$  is the loss conductance which contributes thermal noise and  $G_d$  is the equivalent shot noise conductance of the diode at the ambient temperature  $T$ .

If  $R$  is the negative resistance of the diode corresponding to the operating diode current  $I$ ,  $G_L$  is the load conductance and  $G_p$  is the power gain, it follows that

$$(A)(F-1) = \left( G_n R + \frac{eI}{2kT} R \right) \quad (\text{III-12})$$

where

$$A = (RG_g) \frac{T_o}{T} = \left\{ I \cdot \frac{G_L}{G_g} + \frac{G_n}{G_g} + \frac{2}{\sqrt{G_g}} \sqrt{\frac{G_L}{G_g}} \right\}^2 \frac{T_o}{T} \quad (\text{III-13})$$

Here  $A(F-1)$ , the product of the excess noise and a constant depending on gain, is a "figure of merit" of the noise behavior of the tunnel diode amplifier. A small value of  $A(F-1)$  means small noise factor and/or large power gain,  $G_p$ .

The purpose of this discussion is to show analytically that with a given I-V characteristic of a tunnel diode, a minimum figure of merit exists at a unique point on the characteristic. A further objective is to suggest an ideal I-V characteristic which can be a guide for the design of tunnel diode devices with low noise factors.

The I-V characteristic of a typical tunnel diode is shown in Fig. III-4a. The negative slope portion of the curve lies between  $V = V_1$ , and  $V = V_2$ , where the slopes are zero. An inflection point  $P_o(V_o, I_o)$  exists between these two points.

Suppose that the negative slope portion of the curve be represented by the following function.

$$I = I_o + f(V - V_o) \quad (\text{III-14})$$

Then its derivative with respect to  $V$  is

$$I' = \frac{dI}{dV} = f'(V - V_o) = \frac{I}{R} \quad (\text{III-15})$$

Where  $R$ , the reciprocal of the slope, is the negative resistance of the diode. Consider first the case in which the thermal noise term  $G_n R$  in Eq. (III-12) is negligible. The IR product  $= A(F-1) \frac{2kT}{e}$  is

$$IR = \frac{f(V - V_o) + I_o}{f'(V - V_o)} \quad (\text{III-16})$$

$IR$  is a maximum or a minimum at the point  $(V_m, I_m)$  where

$$\left. \frac{d(IR)}{d(V - V_o)} \right|_{\begin{array}{l} V = V_m \\ I = I_m \end{array}} = 0 \quad (\text{III-17})$$

that is

$$\frac{[f'(V_m - V_o)]^2 - f(V_m - V_o) + I_o f''(V - V_o)}{[f'(V_m - V_o)]^2} = 0 \quad (\text{III-18})$$

Since

$$V_1 < V_m < V_2 \quad (\text{III-19})$$

by Fig. III-4a

$$f'(V_m - V_o) \neq 0 \quad (\text{III-20})$$

Eq. (III-18) thus becomes

$$[f'(V_m - V_o)]^2 - [f(V_m - V_o) + I_o] f''(V_m - V_o) \quad (III-21)$$

It follows from Eq. (III-16) that

$$IR \begin{cases} \max. & \frac{f(V_m - V_o)}{f''(V_m - V_o)} \\ \text{or} \\ \min. & \end{cases} \quad (III-22)$$

Since  $f(V_m - V_o) + I_o$  is always positive,  $f''(V_m - V_o)$  is positive according to Eq. (III-21). Thus by the graph of  $f''(V_m - V_o)$  (Fig. III-4c)  $V_m$  must be greater than  $V_o$ ; that is, the maximum or minimum  $IR$  product occurs beyond the inflection point  $(V_o, I_o)$ .

From the graph of Fig. III-4, the  $IR$  product has a positive infinite value at both the peak and the valley points, it follows immediately that if the  $IR$  product is continuous and finite between  $V_1$  and  $V_2$ , the product will have at least one minimum in that range. It is possible that the product may also have maximum points. But the positive statement one can make on tunnel diode amplifiers is that the tunnel diode will exhibit a minimum noise beyond the inflection point.

The solutions of Eq. (III-22) represent all the maximum and minimum points for the  $IR$  product, one of which will yield an optimum minimum noise factor. By making use of Eq. (III-21), the second derivative of Eq. (III-16) at the optimum minimum noise point  $(V_m, I_m)$  is

$$\left( \frac{d^2(IR)}{dV^2} \right)_{V = V_m} = \frac{f'(V_m - V_o) f''(V_m - V_o) - [f(V_m - V_o) + I_o] f'''(V_m - V_o)}{[f'(V_m - V_o)]^2} \quad (III-23)$$

A minimum  $IR$  requires that Eq. (III-23) be negative. Since both  $f(V_m - V_o) + I_o$  and  $f''(V_m - V_o)$  are positive, and  $f'(V_m - V_o)$  is always negative between the peak point and the valley point, two cases are possible for a negative second derivative namely,

$$(1) \quad f'''(V_m - V_o) < 0$$

or

$$(2) \quad f'''(V_m - V_o) > 0$$

and

$$|f'''(V_m - V_o)[f(V_m - V_o) + I_o]| < |f'(V_m - V_o)f''(V_m - V_o)| \quad (III-24)$$

The I-V characteristic of a practical tunnel diode may satisfy either of these two cases, depending on the nature of the diode. Nevertheless, Eqs. (III-24) and (III-21) are the two necessary conditions for a minimum  $IR$  and a minimum value of  $A(F-1)$  does exist. This minimum point falls beyond the inflection point of the I-V characteristic.

## D SEMICONDUCTOR OSCILLATORS

Vacuum tubes as two-terminal negative-resistance oscillators are well known. Introduction of parametric and tunnel diodes has made possible similar solid-state oscillators. Since the characteristics of solid state devices are substantially different from those of vacuum tubes, the classic oscillation theory,<sup>16</sup> which is applied specifically to vacuum tubes, should be reinvestigated. The following modifies and extends the existing theory to solid-state negative-resistance oscillators.

### Theory

Consider a simple oscillation circuit as shown by Fig. III-5. The oscillation circuit comprises a LC tank, a loss conductance  $G_o$ , a load conductance  $G_L$ , and an active solid-state negative conductance device  $D$  shown by a dotted box. For a first approximation, assume the negative conductance device to satisfy the following ac I-V relationship.

$$I = [G_o] V + \frac{1}{k_1} V^2 + \frac{1}{k_2} V^3 \quad (\text{III-25})$$

which consists of a linear term, a quadratic term and a cubic term. Equation (III-25), which is typically represented by Fig. III-6a, has two zero-slope points  $V_1$  and  $V_2$  and one inflection point  $V_i$  between them. If the origin is taken at any arbitrary point between  $V_1$  and  $V_2$ , it can be shown that  $k_2$  must be positive. Furthermore, the sign of  $k_1$  is determined by the position of the origin with respect to the inflection point. In general, it follows

$$\begin{aligned} k_1 &> 0 & \text{if } V_i < 0 \\ k_1 &< 0 & \text{if } V_i > 0 \\ k_1 &= 0 & \text{if } V_i = 0 \end{aligned} \quad (\text{III-26})$$

The differential equation of free oscillation for Fig. III-5 can be written as

$$\frac{d^2\bar{V}}{dt^2} - \frac{G_o}{C} \frac{d\bar{V}}{dt} + \frac{G_L V_L}{C} - \frac{d\bar{V}^2}{dt} - \frac{k_2 V_L^2}{C} - \frac{d\bar{V}^3}{dt} + \omega_0^2 \bar{V} = 0 \quad (\text{III-27})$$

where

$$V = V/V_I \quad (\text{III-28})$$

$$\omega_o^2 = 1/(LC)^{1/2} \quad (\text{III-29})$$

$$G_e = |G_o| - (G_I + G_L) \quad (\text{III-30})$$

$$V_I = V_i \left[ 1 + \sqrt{1 + (3Q_2/G_I^2)G_o} \right] \quad (\text{III-31})$$

$$V_i = -\frac{G_I}{3Q_2} \quad (\text{III-32})$$

Equation (III-27) is the Van Der Pol differential equation. The approximate solution is known to be<sup>17</sup>

$$V = \sqrt{\frac{G_o}{3Q_2 V_I^2}} \cdot \frac{A_o e^{1/2Q_o t} \sin \omega_o t}{[1 + L/4 A_o^2 (\epsilon t/Q_o - 1)]^{1/2}} \quad (\text{III-33})$$

where

$$Q_o = \frac{\omega C}{G_o} \quad (\text{III-34})$$

At steady state; i.e.,  $t \rightarrow \infty$

$$V = 2 \left( \frac{G_o}{3Q_2 V_I^2} \right)^{1/2} \sin \omega_o t \quad (\text{III-35})$$

When the effective  $Q_o$  is large, the oscillation will no longer be a simple sinusoidal function, but in general consists of distorted harmonic waves, which are to be ignored in the present analysis.

### Power Output and Efficiency

The steady state power output  $P_o$  into the load conductance  $G_L$  is

$$P_o = V^2 G_L + 2/3 \cdot \frac{|G_o|}{Q_2} \left[ 1 - \frac{G_I + G_L}{|G_o|} \right] G_L \quad (\text{III-36})$$

Apparently, Eq. (III-36) has a maximum when

$$G_L = \frac{|G_o| - G_I}{2} \quad (\text{III-37})$$

and the maximum power is

$$(P_o)_{\max} = \frac{(G_o - G_L)^2}{6G_2} \quad (\text{III-38})$$

Eq. (III-38) gives the maximum power output at a given biasing point. That this maximum power output can again be optimized by shifting the bias will now be shown.

On shifting the origin of Fig. III-6 to any arbitrary point  $V = V_a$ ,  $I = I_a$ , Eq. (III-25) becomes

$$I - I_a = (-G_o'V + G_1' - 3V_a G_2')V^2 + (G_2')V^3 \quad (\text{III-39})$$

where

$$[G_o'] = G_o - [3G_2 V_a^2 G_1'] \quad (\text{III-40})$$

The maximum power is then

$$(P_o)'_{\max} = \frac{(G_o' - G_L)^2}{6G_2} \quad (\text{III-41})$$

Eq. (III-41) has a maximum value when

$$V_a = \frac{-G_1'}{3G_2} \quad (\text{III-42})$$

according to Eq. (III-32),  $V_a = V_I$ , thus at the inflection point, the power output is a maximum.

The efficiency ( $\eta$ ) is defined as the ratio of the power output ( $P_o$ ) to the power input ( $P_i$ ), that is

$$\eta = \frac{P_o}{P_i} \quad (\text{III-43})$$

The power input may be a d.c. source in the tunnel diode oscillator or an a.c. pump in the parametric oscillator.

### Tunnel Diode Oscillator

The typical I-V characteristic of a tunnel diode is shown by the solid curve in Fig. III-6. For a crude but simple approximation, assume that the characteristic in the negative slope region follows Eq. (III-25). This assumed characteristic is represented by the dotted

curve. As shown, between the point  $V = V_1$  and the point  $V = V_2$ , the assumed curve does match reasonably well with the experimental one.

To determine the rf loss conductance  $G_L$ , the series resistance of the tunnel diode should also be taken into account. Figure III-7 shows a practical tunnel diode oscillator circuit in which  $r_s$  is the series resistance,  $r_L$  is the coupled load resistance,  $L$  is the tank inductance and  $C$  is the diode capacitance. By a simple circuit transformation, Fig. III-7 can be reduced to a parallel circuit Fig. III-8 similar to Fig. III-5. This modified tunnel diode oscillator circuit will yield at resonance a power output  $P_{oT}$

$$P_{oT} = \frac{2G_{eT}}{3Q_2} \bar{G}_T \left( \frac{G_T}{G_L} \right) \quad (\text{III-44})$$

where

$$G_{eT} = |G_o| - \bar{G}_T \quad (\text{III-45})$$

$$G_T = \frac{1}{r_L + r_s} \quad (\text{III-46})$$

$$\bar{G}_T = \frac{G_T}{1 + Q^2} = \frac{\omega C}{Q} \quad (\text{III-47})$$

$$G_L = \frac{1}{r_L} \quad (\text{III-48})$$

$$Q = (\omega L) G_T \quad (\text{III-49})$$

Denoting  $\frac{\omega C}{G_o} = Q_o$  and  $r_s |G_o| = R_o$  and assuming  $r_s$  to be small, Eq. (III-44) has a maximum when

$$G_T = \frac{G_o}{2} \left[ \frac{1 + R_o Q_o}{(1 + R_o)} \right]^2 \quad (\text{III-50})$$

and

$$(P_{oT})_{\max} = \left\{ \frac{2G_o^2}{3Q_2} \left[ 1 - \frac{1}{2} \left[ \frac{1 + R_o Q_o^2}{1 + R_o} \right] \right] \right\} \cdot \left\{ \frac{1 + R_o Q_o^2}{2(1 + R_o)} - R_o \left[ \frac{(1 + R_o Q_o^2) + Q_o^2(1 + R_o)^2}{4(1 + R_o)^2} \right] \right\} \quad (\text{III-51})$$

If the d.c. voltage and current at the biasing point are  $V = V_o$  and  $I = I_o$ , by letting

$$Q_2 = \frac{2k_1 |G_o|}{3V_p^2} = \frac{2(|G_o| - Q_1 V_p)}{3V_p^2} \quad \text{and} \quad \frac{I_o}{G_o} = k_2 V_p$$

the maximum efficiency is

$$(\eta_T)_{max} = \frac{I}{k_1 k_2} \left( \frac{V_p}{V_o} \right)^2 \left\{ 1 - \frac{1}{2} \left[ \frac{1 + R_o Q_o^2}{1 + R_o} \right] \left\{ \frac{1 + R_o Q_o^2}{2(1 + R_o)} - \frac{R_o[(1 + R_o Q_o^2)^2 + 4Q_o^2(1 + R_o)^2]}{4(1 + R_o)} \right\} \right\} \quad (\text{III-52})$$

*Example:*

Given

From Figure III-6 and Figure III-7

$$G_o = -.0545 \text{ mho}$$

$$G_I = .1735 \text{ mho/V}$$

$$G_2 = 6.07 \text{ mho/V}^2$$

$$V_p = 56 \text{ mV}$$

$$V_o = 125 \text{ mV}$$

$$I_o = 3 \text{ ma}$$

$$\omega = 2\pi \times 2900$$

$$C = 7.5 \mu\text{f}$$

$$r_s = .38$$

The maximum power output is computed to be .065 mw at an efficiency of 17.3%. The measured power outputs<sup>18</sup> were in the range of .024 to .050 mw.

## IV TUNNEL DIODE CONVERTER

### A. SMALL PUMP THEORY

The purpose of this study is to investigate a down converter using a tunnel diode (Esaki diode) as the nonlinear resistance element. The fact that the negative resistance characteristic of a tunnel diode can be utilized to achieve low noise amplification has already been demonstrated.<sup>15</sup> It is now shown that the nonlinearity of this negative resistance characteristic can be used for frequency conversion. Since the nonlinearity of a resistance, is utilized for frequency conversion, the noise factor is independent of the ratio of the input frequency to the output frequency. Thus by using a tunnel diode, a low noise down converter with conversion gain has been achieved.<sup>20</sup>

#### Analysis

The converter circuit to be analyzed is shown in Fig. IV-1 which also establishes the notation to be used in the following analysis. The three tank circuits which resonate at  $\omega_1$ , the input signal frequency,  $\omega_2$ , the difference frequency, and  $\omega_3 = \omega_1 + \omega_2$ , the local oscillator frequency, are coupled together by the tunnel diode.

The analysis proceeds in a manner entirely similar to that for the small-signal nonlinear reactance case.<sup>2</sup> The I-V characteristic of the tunnel diode (Fig. IV-2) at the operating point "P" can be represented by a quadratic relation

$$I = G_o V - \frac{1}{2} V^2 \quad (\text{IV-1})$$

An operating point in the positive resistance region is chosen for reasons to be discussed later. The currents at the three frequencies are

$$\begin{aligned} I_1 &= V_1 (\bar{G}_1 - j\bar{B}_1) - \frac{1}{2} V_2 V_3 \\ I_2 &= V_2 (\bar{G}_2 + j\bar{B}_2) - \frac{1}{2} V_1 V_3 \\ I_3 &= V_3 (\bar{G}_3) - \frac{1}{2} V_1 V_2 \end{aligned} \quad (\text{IV-2})$$

where

$$\begin{aligned} \bar{G}_1 &= G_f + G_g + G_o \\ \bar{G}_2 &= G_2 + G_L + G_o \end{aligned}$$

$$\overline{G}_3 = G_3 + G_o$$

$$\overline{B}_1 = \omega_1 C_1 \frac{\omega}{\omega_1} - \frac{\omega_1}{\omega}$$

$$\overline{B}_2 = \omega_2 C_2 \frac{\omega_3 - \omega}{\omega_2} - \frac{\omega_2}{\omega_3 - \omega} \quad (\text{IV-3})$$

The small signal analysis neglects the effect of the nonlinear interaction on the local oscillator current. Hence,  $\frac{1}{2} V_1 V_2$  is neglected in the third of Equations (IV-2).

In Eqs. (IV-3),  $G_1$ ,  $G_2$  and  $G_3$  are the loss conductances of the respective circuits. These loss conductances consist of the circuit and the tunnel diode ohmic losses. The capacitances,  $C_1$  and  $C_2$  similarly consist of the circuit and tunnel diode capacitance,  $C_D$ .

### Conversion Power Gain

The conversion power ratio under matched conditions is defined as

$$g_c = \frac{\frac{V_2^2 G_L}{I_1^2}}{\frac{4 G_o}{4 G_o}} \quad (\text{IV-4})$$

Solving Eq. (IV-2) one obtains

$$g_c = \frac{4(\frac{1}{2} V_3^2 G_o G_L)}{[\overline{G}_1 \overline{G}_2 - (\frac{1}{2} V_3^2)^2]} \quad (\text{IV-5})$$

Equation (IV-5) is a general expression for the conversion power ratio. When  $G_o$  is positive, the ratio can be either greater or less than unity, depending on the I-V characteristic of the nonlinear conductance. In order to obtain a conversion gain (i.e.  $\sqrt{g_c} > 1$ ) with a positive  $G_o$ , it follows from Eq. (IV-5) that

$$g_c = \frac{2 \frac{(\frac{1}{2} V_3^2)}{G_o}}{\sqrt{G_o} \sqrt{G_L} \left\{ \frac{(G_R + G_L)(G_L + G_2)}{G_o} + G_1 + G_2 + G_o \left( 1 - \frac{(\frac{1}{2} V_3^2)}{G_o} \right) \right\} \sqrt{\frac{G_L}{G_o}} + \sqrt{\frac{G_R}{G_L}}} > 1 \quad (\text{IV-6})$$

Since

$$\sqrt{\frac{G_L}{G_o}} + \sqrt{\frac{G_R}{G_L}} > 2 \quad (\text{IV-7})$$

when  $G_o$  is positive, Eq. (IV-6) is satisfied if

$$\frac{G_0 V_3}{G_0} > I \quad (IV-8)$$

Equation (IV-8) is the necessary condition for gain. This equation shows, together with Eq. (IV-1), that the I-V characteristic whose origin is at the operating point (such as "P" in Fig. IV-2) must exhibit a maximum value, and that the local oscillator voltage,  $V_3$ , must be sufficiently large so that it swings the current below the value of the current at the operating point. In the case of an ordinary crystal detector, the I-V characteristic exhibits no such maximum and Eqs. (IV-1) and (IV-8) can never be satisfied simultaneously. It is important to note that Eq. (IV-8) can be satisfied when the operating point is chosen in the region where  $V < V_A$  and where  $G_0$  is positive.

For the region  $V > V_B$ , Eq. (IV-8) still applies. In this region, however, the diode current is due to minority carriers and so it is probably not suitable for high frequency conversion.

For the region  $V_A < V < V_B$ , the  $G_0$  is negative and stable biasing becomes critical. It is difficult to find a stable operating point without having the device break into spurious oscillations, because of the voltage swing of the local oscillator.

In order to normalize the conversion power ratio Eq. (IV-5) let

$$\lambda = \frac{G_0^2 V_3^2}{G_1 G_2} \quad (IV-9)$$

$$Q_g = \frac{\omega_1 C_1}{G_g} \quad (IV-10)$$

$$Q_L = \frac{\omega_2 C_2}{G_L} \quad (IV-11)$$

$$\bar{Q}_1 = \frac{\omega_1 C_1}{G_1} \quad (IV-12)$$

$$\bar{Q}_2 = \frac{\omega_2 C_2}{G_2} \quad (IV-13)$$

$$\bar{g}_c = \frac{Q_g}{Q_1} \cdot \frac{Q_L}{Q_2} \cdot g_c \quad (IV-14)$$

Equation (IV-5) then becomes

$$\bar{g}_c = \frac{4\lambda}{(1-\lambda)^2} \quad (\text{IV-15})$$

This equation is shown in graphical form in Fig. IV-3.

### Bandwidth

Assuming that the half-power frequencies are near the resonant frequency, the following approximation can be made

$$\bar{B}_1 = \omega_1 C_1 \left( \frac{\omega}{\omega_1} - \frac{\omega_1}{\omega} \right) \approx 2(\omega - \omega_1) C_1 \quad (\text{IV-16})$$

$$\bar{B}_2 = \omega_2 C_2 \left( \frac{\omega_3 - \omega}{\omega_2} - \frac{\omega_2}{\omega_3 - \omega} \right) = 2(\omega_1 - \omega) C_2 \quad (\text{IV-17})$$

By defining the relative bandwidth as  $B_1 = \frac{\Delta f_1}{f_1}$  and defining

$$S_1 = 2\bar{Q}_1 B_1 \quad (\text{IV-18})$$

and

$$C = \frac{\bar{Q}_2}{\bar{Q}_1} \cdot \frac{\omega_1}{\omega_2} \quad (\text{IV-19})$$

one obtains

$$S_1^2 = \frac{[2c(1-\lambda) - (1+c)^2] + \sqrt{[2c(1-\lambda) - (1+c)^2]^2 + 4c^2(1-\lambda)^2}}{2c^2} \quad (\text{IV-20})$$

For the case of high gain, i.e.  $\lambda \ll 1$ , Eq. (IV-20) becomes

$$S_1 = \frac{1-\lambda}{1+c} \approx \frac{1}{1+c} = \frac{2\sqrt{1+\bar{g}_c}-1}{\bar{g}_c} \quad (\text{IV-21})$$

and the voltage gain-bandwidth product is

$$\sqrt{\bar{g}_c} B_1 \approx \frac{1}{1+c} = \frac{1}{\bar{Q}_1} \quad (\text{IV-22})$$

This equation is shown in graphical form in Fig. IV-4.

## Noise Figure

The noise figure can be found by considering the currents in Eq. (IV-2) to be due to the thermal noise sources of the circuits

$$|\delta_1|^2 = 4k\Delta f(G_g T_o + G_L T + G_e T)$$

$$|\delta_2|^2 = 4k\Delta f(G_L T + G_2 T + G_e T) \quad (IV-23)$$

where  $k$  = Boltzman's constant

$T_o$  = Reference temperature ( $290^\circ K$ )

$T$  = Ambient temperature

$G_e$  = Equivalent shot noise conductance of the tunnel diode

$G_e = \frac{eI_o}{2kT}$ ,  $I_o$  = DC current of the tunnel diode

$|\delta|$  = Equivalent noise currents

Equation (IV-2) can then be written as:

$$|\delta_1|^2 = |V_1 \bar{G}_1 - \frac{1}{2} V_2^* V_3|^2$$

$$|\delta_2|^2 = |V_2 \bar{G}_2 - \frac{1}{2} V_1^* V_3|^2 \quad (IV-24)$$

$$|\delta_3|^2 = |V_3 \bar{G}_3 - \frac{1}{2} V_1 V_2|^2$$

From the definition for the noise figure one obtains

$$F = \frac{P_{in}}{P_{out}} = \frac{N_{out}}{N_{in}} = \frac{1}{g_e} N_{out} = \frac{1}{kT_o \Delta f} \frac{|\delta_2|^2}{G_L} = \frac{1}{g_e kT_o \Delta f} \quad (IV-25)$$

After solving Eq. (IV-24) for  $V$  and substituting g, Eq. (IV-25) becomes

$$F = 1 + \frac{T}{T_o} \left[ \frac{G_e}{G_g} + \frac{G_L}{G_g} + \frac{(G_L + G_2 + G_e) G_L}{G_g G_2} \frac{1}{1 - \frac{2(\sqrt{1+g_e}-1)}{g_e}} \right] \quad (IV-26)$$

In Eq. (IV-26), a compensation noise term<sup>19</sup> has been ignored. It can be shown that this term is comparatively small particularly when the pump voltage is small and  $G_g$  is chosen to be much larger than  $G_e$ . A simplified expression of this equation is shown in graphical form in Fig. IV-5.

## B. COAXIAL LINE CIRCUIT FOR UHF DOWN CONVERTER

Various experimental set ups have been built in an effort to prove the above developed theory and to investigate the feasibility of certain circuit configurations.

The first circuit to be build used coaxial lines and double stub tuners. This method offered the advantage of ready availability and flexibility which was an important factor for early experiments. It did, however, impose the disadvantage of sharp and narrow tuning, which in turn contributed to narrow bandwidth. It also involved considerable space demands, which became quite awkward at frequencies below 1000 mc. A block diagram of this "coaxial line" circuit is shown in Fig. IV-6. The operating frequencies were  $f_1 \sim 210$  mc,  $f_2 = 30$  mc, and  $f_3 \sim 240$  mc.

Figures IV-7 and IV-8 show typical curves of the I-V characteristic of the germanium and gallium arsenide\* tunnel diodes that were used in the above experiments. The germanium diode has a peak current of 25 ma at 62 mv, its operating point was chosen at 18 ma and 29 mv yielding a positive  $G_o = .42$  mhos. The gallium arsenide diode had a peak current of 23.6 ma at 100 mv, the operating point was at 20 ma and 60 mv with a positive  $G_o = .21$  mhos.

To complete the calculations according to Eqs. IV-15, IV-22, and IV-26, it is necessary to know the values of certain circuit parameters. For the case of the experimental circuit of Fig. IV-6, the following values were measured. The values of  $\lambda$  were chosen to give agreement with measured gain ratios.

TABLE IV-1

Germanium Diodes	$\lambda = .43$	$C = .1$	$\bar{Q}_I = 1000$	$G_g = 4$ mhos, $G_L = \frac{1}{4}$ mhos,
	$G_1 = G_2 = 0$	$G_e = 20$	$I_o = .36$ mhos	$G_o = .42$ mhos
Gallium Arsenide	$\lambda = .88$	$C = .1$	$\bar{Q}_I = 100$	$G_g = 4$ mhos, $G_L = \frac{1}{4}$ mhos
	$G_1 = G_2 = 0$	$G_e = .40$ mhos		$G_o = .21$ mhos

Representative results are shown in the following Table, and compared with computed values.

\*The gallium arsenide diode is an experimental sample developed by the Advanced Development Group of RCA Semiconductor Division, Somerville, New Jersey.

TABLE IV-2

DIODE	POWER GAIN		BANDWIDTH		CONVERTER NOISE FIGURE		SENS
	Meas.	Comp.	Meas.	Comp.	Meas.	Comp.	
Germanium	6 db	6 db	.9 mc	.6 mc	5.2 db	4.4 db	1.5 $\mu$ v
Gallium Arsenide	22.7 db	22.7 db	.15 mc	.26 mc	2.8 db	3.8 db	0.25 $\mu$ v

It is noted from Figures IV-7 and IV-8 that the operating points for the diodes were chosen at a region where the slope of the I-V characteristic is positive. These operating points were established by the initial DC current from the bias supply and the rectified RF current of the local oscillator.

Conversion gain will result for positive  $G_o$  when the requirements of Eqs. (IV-1) and (IV-8) are met simultaneously (see Fig. IV-3). If  $V_3$  will be larger than  $G_o$  when the RF voltage swing of the local oscillator is large enough to drive across the peak of the I-V curve and into the negative slope region until the instantaneous values of the current are smaller than the DC current at the operating point.

However, any appreciable voltage swing into the negative slope portion will make the system unstable, particularly when the negative slope is very steep. For this reason it is more difficult to obtain high gain with germanium diodes, where the negative slope is much steeper, than for gallium arsenide. Had it not been for this stability problem, the germanium diodes would have yielded the same low noise factor as the gallium arsenide diodes.

Further consideration of Eqs. (IV-22) and (IV-26) will show the approach to optimum bandwidth and noise factor, (see Figs. IV-4 and IV-5). For improved bandwidth the parameter  $c$  should be made small and the circuit  $Q$  values should also be made small. Since  $\bar{Q}_1 = \frac{\omega_1 C_1}{G_1}$ , this immediately suggests that the circuit capacitances and especially the diode capacitance  $C_D$  should be made as small as possible. For improved noise factor  $G_g$  should be made larger than  $G_e$ .

The possibility of obtaining conversion using a lower pump frequency is to be noted. In this case the nonlinearity of the diode characteristic could be used to produce the desired harmonic of the lower pump frequency for mixing. It is also noted that the possibility of making the diode-pump circuit self oscillatory exists. Thus direct down conversion can be obtained without a separate local oscillator.

Both these possibilities were reduced to practice and demonstrated in the above circuit. For the first case a signal of 400 mc was pumped with a local oscillator of 185 mc (instead of 370 mc) and the desired intermediate frequency of 30 mc was obtained with comparable results for gain, bandwidth and noise. In the second case a diode with low series resistance and relatively low capacitance was used in the converter circuit and biased at an operating point near its peak current. With only signal voltage applied (at 210 mc) the intermediate frequency of 30 mc was obtained. The diode thus acted as its own local oscillator. However, the pumping in this particular case was not strong enough to obtain conversion gain, and the noise figure was only comparable to that of ordinary crystal diodes.

### C. S-BAND-DOWN CONVERTER

While previous experiments had worked with signal frequencies at 200 and 400 mc, efforts were also made to extend the frequency range of the tunnel diode down converter into the kMc range.

One experiment was carried out in the "S" band range and used a signal frequency of 2800 mc, a local oscillator of 2830 mc, and an intermediate frequency of 30 mc. The tunnel diode chosen for this experiment was especially prepared by the Semiconductor Group of the RCA Laboratories. A directional coupler was utilized to feed both the signal and the local oscillator frequencies to the tunnel diode (see Fig. IV-9 for a block diagram of this circuit). The high directivity of the coupler prevented the signal generator from being loaded by the local oscillator. The tunnel diode itself was mounted inside a coaxial "T" connector, as shown in the detail of Fig. IV-9.

The results obtained from this test were very promising as far as the noise factor was concerned (approx. 5 db), but the bandwidth was less than 1 mc. A study of the equation for the gain-bandwidth product

$$\sqrt{g_e} B_I \approx \frac{I}{(1+c) Q_I}$$

shows that for a high value of  $c$  the bandwidth would be narrow. The factor  $c$  is proportional to the ratio of signal frequency to intermediate frequency, and in this particular case was  $2800/30 = 93$ . Thus the narrow bandwidth was the direct result of this ambitious down-conversion ratio. A more conservative ratio should result in broader bandwidth. Unfortunately, this part of the test could not be made, as the diode became inoperative when the junction lead wire connection opened up. Subsequent measurements with other diodes built with larger and less fragile junctions did not yield as good results.

For good results in the kMc range it is necessary that the cutoff frequency of the diode be sufficiently higher than the required operating frequency. This frequency limitation of the diode comes mainly from the capacitance and series resistance of the diode itself. The capacitance especially should be as low as possible. At the moment (and probably until new materials become available) low capacitance can only be achieved by making the area of the junction as small as possible. Severe fabrication problems will have to be overcome before stable junction of fractions of one mil in diameter can be produced.

#### D. LUMPED PARAMETER CIRCUIT FOR UHF DOWN CONVERTER

Still another problem that exists with the application of tunnel diodes in down-converters is related to the proper choice of generator and load admittances. The equation for the noise figure shows that for low-noise performance the ratios of  $G_o/G_g$ ,  $G_e/G_g$  and  $G_e/G_o$  should be made small. Since for a certain diode the values of  $G_o$  and  $G_e$  at the operating point are more or less given, the only recourse left is to make  $G_g$  large. Thus values  $G_g = 1$  mho or more become desirable. This obviously calls for low impedance circuitry, and since most of the conventional microwave equipment is terminated in 50 ohms, considerable impedance transformation is necessary.

Early experiments accomplished this impedance transformation by means of a double stub tuner. But, as mentioned before, the disadvantage of narrow tuning together with the space demands of the coaxial lines, called for a more practical solution.

Based on these considerations, a tuned circuit, consisting of lumped parameters was built, which is capable of transforming the output impedance of the signal generator from 50 ohms down to 1 ohm. The complete circuit of this down-converter from 400 to 30 mc is shown in Fig. IV-10. The input circuit of the converter is broad enough to accept not only the signal frequency but the local oscillator with sufficient amplitude. For this reason it is possible to use the directional coupler as a common input and injection point. Figure IV-11 shows a photograph of the actual converter.

For the final evaluation of the tunnel diode converter the test set-up shown in Fig. IV-12 was selected. Noise factors were measured with the help of the "AIL-70A" noise source (which is essentially an argon discharge lamp giving white noise from 200 to 2600 mc, with an excess noise of 15.2 db), and its companion equipment, the "AIL-74" Automatic Noise-Figure Indicator. The "automatic" feature of this equipment was used to adjust the tunnel diode converter to its optimum operating condition. The actual test readings were then obtained by "manual" control.

The remaining equipment can be divided into functional units. A signal generator for single sideband noise measurements, and for accurate determination of bandwidth and tangential sensitivity, as well as for image and spurious frequency responses. A sweep signal generator, covering both the RF and IF range, for quick optimization of converter and IF bandwidths. Both generators are coupled to the noise source through a 20 db pad, which also serves as 50 ohm termination for the source. The noise source feeds the signal to the converter input through a 10 db pad, an adjustable coaxial transmission line and a directional coupler. The reason for using the directional coupler is to decouple the local oscillator from the signal generator when making single sideband noise factor measurements. The output of the converter is connected to a "pre" IF amplifier, operating at 30 mc. This amplifier has a bandwidth of 6 mc, and a noise factor of 3 db. The "pre" IF amplifier is coupled to the Automatic Noise-Figure Indicator through a "precision" adjustable attenuator. The "ANFI" consists of a square-wave modulator for the noise source, a gain controlled "post" IF amplifier, detector and differential output circuits, and a meter calibrated directly in decibels of noise factor. In addition a Tektronic 545A oscilloscope was used to monitor the wave shape of the modulated noise source. The oscilloscope gives an excellent visual comparison of the noise power output with the noise generator on and off. Any circuit instability can be quickly noticed, and misadjustments in tuning or biasing, which might cause erroneous results, can be avoided. Figure IV-13 shows a picture of the scope tracings of the IF bandwidth, and the noise output with the noise generator modulated.

The tunnel diodes used in this work were germanium diodes with a peak current of .9 ma at 55 mv, a valley current of 0.1 ma and a capacitance of approximately  $10 \mu\text{f}$ .

Figure IV-14 shows the behavior of the noise factor of the converter (including the IF amplifier) as a function of bias voltage. A brief explanation of the test procedure will help in understanding the results

First the diode was biased at an operating point near the peak current, then the input network was tuned, and the local oscillator voltage varied until a low noise factor was obtained. Next the coaxial line and IF amplifier were adjusted to give a minimum noise factor. With the operating conditions of the converter established at this point a system noise factor of 3.0 db, a bandwidth of 1.0 mc and a conversion power gain of 27 db were measured. Finally the diode bias was varied and the resulting changes in noise factor were observed.

As can be seen from Fig. IV-14, the noise factor under the described tuning conditions is very critical to bias voltage. Obviously the circuit parameter directly responsible

for this behavior is the diode conductance  $G_o$ , which changes as the bias is varied. At the same time the ratio of diode conductance to signal generator conductance  $G_o/G_g$  changes drastically. How this in turn effects the noise factor can be seen from the following considerations:

From Eq. (IV-2)

$$I_1 = V_1 \bar{G}_1 - \frac{Q}{4} V_3 V_2^*$$

$$0 = V_2 \bar{G}_2 - \frac{Q}{4} V_3 V_1^*$$

$$\text{one finds } I_1 = V_1 \bar{G}_1 - \frac{(\frac{Q}{4} V_3)^2}{\bar{G}_2} V_1$$

$$\text{and using the gain parameter } \lambda = \frac{(\frac{Q}{4} V_3)^2}{\bar{G}_1 \bar{G}_2}$$

$$I_1 = V_1 \bar{G}_1 (1 - \lambda) \quad (\text{IV-27})$$

Then

$$Y_1 = \frac{I_1}{V_1} = G_1 (1 - \lambda) \quad (\text{IV-28})$$

$$\text{and from Fig. IV-10 it follows that } Y_1 = G_g + G_{in} \quad (\text{IV-29})$$

thus

$$G_{in} = \bar{G}_1 (1 - \lambda) = \bar{G}_g + k_1 G_g \quad (\text{IV-30})$$

where  $k_1$  is a coupling coefficient, such that for matched input, i.e.,  $G_{in} = G_g$ , the coupling coefficient  $k_1 = 1$ .

Solving Eq. (IV-30) for  $G_g$  one obtains

$$G_g = G_o \frac{1 - \lambda}{k_1 + \lambda} \quad (\text{IV-31})$$

and substituting into the noise factor Eq. (IV-26) one can write approximately (with  $\frac{T}{T_o} = 1$  and  $\frac{G_e}{G_g}$  assumed small)

$$F \approx 1 + \frac{1 + k_1}{(1 - \lambda)\lambda} \quad (\text{IV-32})$$

A qualitative analysis of Eq. (IV-32) shows that for  $-1 < k_l < 0$  and for large gains ( $\lambda \rightarrow 1$ ) the noise factor can be made very low. However, Eq. (IV-30) also shows that for these conditions  $G_{in} = G_g$ , that is to say that the input of the converter circuit will be mismatched, and its stability critical to changes.

The stability can be improved if one is willing to accept a higher noise factor and lower conversion gain. For values of positive  $k_l$  ( $0 < k_l < 1$ ) and approaching unity, and low  $\lambda$ , the input admittance becomes matched and the circuit is input stable. An evaluation of Eq. (IV-32) for  $k_l = 1$  gives

$$F = 1 + \frac{2}{(1-\lambda)\lambda}$$

which has a minimum point for  $\lambda = .5$ , yielding a minimum noise factor under matched conditions of  $F = 9.5$  db. Experimentally, with reasonable good stability and matching ( $k_l \approx 1.0$ ), a system-noise factor of 8.5 db, a bandwidth of 6 mc and a conversion gain of 1 db were found. The effect of spurious responses, principally the image response was negligible, since the image rejection was greater than 10 db.

Another important characteristic of a first stage converter is its capability of handling large input signals without overloading. The maximum usable input signal can then be defined as the highest level of input signal for which the converter gives acceptable performance. The test procedure is simple and straightforward. With the converter controls remaining fixed at the optimum performance positions the input level of the converter is gradually increased, and the highest input signal for which the distortion is trivial is recorded. This test was repeated for various values of modulation from 30% to 90% with the frequency of modulation 400 cps. The detector output was carefully observed on an oscilloscope, and the r.f. input voltage noted when distortion in the sinusoidal output waveform appeared.

The results of these tests demonstrated that the tunnel diode converter is capable of receiving input signals of at least 100 millivolts before overloading. This held for modulations from 30 to 70%, and only at 90% was a reduction to 80 millivolts observed. At an input impedance of 50 ohms this corresponds to a 7 dbm power handling capability. While this is a very respectable performance, it was *not* the real limitation of the converter itself, but a value imposed by the overloading of the IF amplifier which followed it.

An interesting experiment was performed in conjunction with the present converter circuit, when an attempt was made to operate the tunnel diode without any external D.C. bias supply. Figure IV-15 shows the circuit of the self bias scheme. The diode establishes its own operating point through the rectification of the pump voltage from the local oscillator.

Optimum results were obtained with a series resistance of 100K and an average D.C. diode current of 1 microamp, yielding a bias of 100 mv, which is near the inflection point of the negative conductance region. At this point a noise figure of 7.5 db, a bandwidth of 1 mc and unity gain were measured. These results are not as good as the best obtained with external d.c. bias, yet the obvious simplification and cost reduction achieved through the elimination of the d.c. bias supply might make a compromise in performance attractive for certain applications.

Previous theoretical considerations have shown that the tunnel diode down converter is capable of yielding high conversion gains and low noise factors. However, it was noticed that the operating conditions required for low noise factors also made the circuit sensitive to changes in the input impedance. This sensitivity with respect to the input impedance is due to the fact that the input for a low-noise high-gain operation is far from matched. This is shown in Eqs. (IV-30) to (IV-32). In order to operate at a matched condition the tunnel diode can be biased at the positive slope side of the I-V characteristic and the conversion gain be reduced. The noise factor in the matched case will, of course, be degraded. However, the stability will be improved and the bandwidth increased. These features have been verified in the second mode of operation.

#### a) Mismatched Case

The mismatched case is quite difficult to evaluate, since some of the circuit parameters are not readily available for measurement, but must be estimated.

It has been demonstrated before that low noise factors can be obtained with high gain (i.e., high  $\lambda$ ). Furthermore, Eq. (IV-26) points out additional means for achieving low noise factors. Obviously the shot noise contribution ( $G_o + 20 I_o$ ) should be made as small as possible. It is also desirable to make the conductance of the signal generator,  $G_g$ , large as this helps to reduce the ratio of  $G_o/G_g$ . With these considerations in mind the following is believed to be a reasonable description of the mismatched case. For a mismatch of  $k_1 = .9$  and a high gain  $\lambda = .9$  the required  $G_g = G_o \frac{1-\lambda}{k_1 - \lambda} = 50 G_o$ . With the operating point near the peak current,  $G_o = .001$  mhos and with  $G_g = .050$  mhos  $G_1$  becomes .051 mhos.  $G_L$  is .020 mhos and  $\bar{G}_2 = .021$  mhos.  $G_e$  the equivalent shot noise conductance  $\approx 20 I_o = 20 \times .9 \text{ ma} = .018$  mhos. The noise factor for the mismatched case then is:

$$F = 1 + \frac{.018}{.050} = \frac{(.020 + .018(.051))}{(.050)(.021)} = 1.1 = 1 + .36 + 2.04 = 3.4 \text{ or } 5.3 \text{ db;}$$

The normalized conversion gain  $g' = \frac{4\lambda}{(1-\lambda)^2} = 360$  and the conversion gain  $g_c = g_e \cdot \frac{G_g G_L}{G_1 G_2} = 336$ , or 25.3 db.

The bandwidth is obtained through the parameters  $\bar{Q}_1$ ,  $\bar{Q}_2$ ,  $C$ ,  $\lambda$ ,  $S_1$ , and  $B_1$ . Thus  $\bar{Q}_1 = 1.5$ ,  $\bar{Q}_2 = 1.33$ ,  $c = 11.8$ ,  $S_1 = .0078$ ,  $B_1 = .0052$  and finally the bandwidth  $2\Delta f_1 = 2.0$  mc.

*b) Matched Case*

At a different bias point (somewhat below the peak current) the tunnel diode conductance  $G_o = .014$  mhos and the equivalent shot noise conductance  $G_e \doteq 20I_o = .014$  mhos. For matched condition, i.e., for  $k_f = 1$  and  $\lambda = .5$ ,  $G_g = G_o \frac{1-\lambda}{k_f+\lambda} = .33 G_o \doteq .005$  mhos, and therefore  $\bar{G}_1 = G_g + G_o = .019$  mhos. With a load conductance of  $G_L = .020$  mhos presented by the input of the IF amplifier  $\bar{G}_2 = G_L + G_o = .034$  mhos. The noise factor of

$$F = 1 + \frac{.014}{.005} \frac{(.020 + .014)(.019)}{(.005)(.034)} 2 = 1 + 2.8 + 7.6 = 11.4 \text{ or } 10.6 \text{ db}$$

The normalized conversion gain  $\bar{g}_c = \frac{4\lambda}{(1-\lambda)^2} = 8$ , or 9 db and from it a conversion gain

$$g_c = \bar{g}_c \frac{G_R G_L}{G_1 G_2} = 1.24, \text{ or } 1 \text{ db can be calculated. The bandwidth is again obtained with the}$$

help of the parameters  $\bar{Q}_1$ ,  $\bar{Q}_2$ ,  $C$ ,  $\lambda$ ,  $S_1$ , and  $B_1$ . Thus  $\bar{Q}_1 \doteq 4$ ,  $\bar{Q}_2 \doteq .83$ ,  $c \doteq 2.76$ ,  $S_1 = .132$ ,  $B_1 = .032$  and finally the bandwidth  $2\Delta f_1 = B_1 f_1 = 13.2$  mc. The measured bandwidth of 6 mc seems to be limited by the IF amplifier, which at best had a 6 mc bandwidth by itself.

To summarize the effects of various operating conditions on the overall performance of the converter, it is possible to make use of a "figure of merit." Performance characteristics such as gain, bandwidth and noise factor should be included in this figure of merit, which consequently would be defined as

$$F_M = \frac{2\Delta f \times \sqrt{g_c}}{F} \quad (\text{IV-33})$$

For the above mentioned cases one obtains.

	$2\Delta f$	$\sqrt{g_c}$	$F$	$F_M$
Matched Case	13.2 mc	1.12	11.4	1.3
Mismatched Case	2.1	18.30	3.4	11.3

It should be noted that the bandwidth  $2\Delta f$  is a measure of the stability. When the bandwidth becomes zero, the converter is self-oscillatory.

## E. METHOD OF OPTIMIZATION OF NOISE FACTOR

The expression for the noise factor of the tunnel diode down converter can be written for the loss-less case as:

$$F = 1 + \frac{T}{T_o} \left[ \frac{G_e}{G_g} \frac{(G_L + G_e)(G_e + G_b)^2}{G_g (G_b V_3)^2} \right] \quad (\text{IV-34})$$

Several attempts have been made to derive from this expression the conditions that would yield a minimum noise factor. A rigorous optimization through partial differentiation with respect to  $G_L$ ,  $G_g$ ,  $G_e$  and  $V_3$  is much too complex to be of any practical help to the circuit designer. Instead, a series of numerical calculations has been made in the Laboratories' 650 computer to give at least a useful approximation. The following procedure was used to program this problem:

First the  $I$  vs.  $V$  and then the  $\frac{\partial I}{\partial I}$  vs.  $V$  characteristics of a certain tunnel diode with approximately 1 ma peak current were measured. An equation was fitted to the latter curve. In the range of interest where the pump voltage is small this curve resembled a parabola and the equation

$$G_o = (V_B - .26)^2 - .0423 \quad (\text{IV-35})$$

(where  $V_B$  is the applied d.c. bias voltage) gave a good description. This expression for  $G_o$  together with the following values

$$G_g = k G_L$$

$$G_e = .020 \text{ mhos (for } I_e = 1 \text{ ma} = \text{const.})$$

$$(G_b = .2 \text{ (from } I \text{ vs. } V \text{ curve)})$$

$$F = 1 + \frac{.020}{k G_L} \frac{(G_L + .020) k G_L + (V_B - .26)^2 - .0423^2}{.04 k G_L V_3^2} \quad (\text{IV-36})$$

This equation was then given to the computer with the request to calculate  $F$  vs.  $V_B$  for  $V_B$  ranging from .040 to .060 volts, with various values of  $G_L$  ranging from .0022 to .100 mhos, various values of  $k$ , and various values of  $V_3$  from .080 to .125 volts. The numerical results obtained from the computer were plotted as shown in a representative graph of Figure IV-16.

For the given diode, with its peak current occurring at 55 mv, the important range of bias voltage is around that value. As can be observed from the graphs the noise factor is decreasing as the peak bias voltage is approached. The noise factor also decreases

with increased pump voltage  $V_3$ . It can be further noticed that the choice of a low  $G_L$  is more favorable in obtaining low noise factors. Similarly,  $G_g$  should be made low, but a compromise has to be reached here, in order to keep the term  $\frac{G_g}{G_o}$  of the noise factor equation from getting too large.

Only the solidly drawn portions of these curves can be used for practical purposes. The dashed lines do not represent realizable conditions because additional considerations and requirements such as circuit stability and freedom from oscillations, limit the validity of these calculations to a range of operation for which the gain parameter  $\lambda < 1$ . From the equation

$$\lambda = \frac{(\frac{1}{2} V_3)^2}{(G_g + G_o)(G_L + G_o)} \leq 1$$

one finds the limiting value of  $G_o$  (and consequently bias voltage  $V_B$ ) for any given range of  $\frac{1}{2} V_3$ ,  $G_g$  and  $G_L$ . The dot-dashed line denotes this limitation of  $\lambda \leq 1$ .

As a further extension of the search for a *practical* optimization of the noise factor, that is to say an optimization which not only looks for a low noise factor by itself, but also considers the effects on the gain and bandwidth performance of the system, the curves of Fig. IV-17 have been calculated. These curves show the relation between noise factor and the gain  $\times$  bandwidth product for various operating conditions. Of the variables involved,  $G_o$ ,  $G_g$  and  $\frac{1}{2} V_3$  are determined by the diode itself, and are here represented by the bias voltage  $V_B$ , which appears as one of the parameters. The parameters  $G_g$  and  $G_L$ , as well as the local oscillator voltage  $V_3$  are given as independent circuit parameters. Together, these device and circuit variables determine the gain, the bandwidth and the noise factor of the down converter. The final choice of operating conditions is, of course, settled by the requirements of the overall system.

#### F. LARGE PUMP THEORY

In the first paper on tunnel diode down converters<sup>20</sup> the possibilities of low noise factors and high gain were noticed and analyzed. Since then work has been continued to achieve further improvements, such as wider bandwidth and more stable performance under various operating conditions such as may be encountered in UHF television and microwave communication. The results of many of these tests have shown that low noise factors can indeed be obtained by biasing the tunnel diode in the negative slope region. However, this operating condition may lead to instabilities because of mismatching of the impedance at the input termination.

More recent measurements have shown that low noise factors and stability can be achieved through the application of relatively large pump voltages. To explore these possibilities, the previous "small-pump" analysis of the tunnel diode down converter is now being extended to include the effects of large pump voltages. As will be shown in the following derivation, the high pump voltage causes first an appreciable increase in the effective diode conductance which helps to improve the input stability, and second, due to an accompanying increase in the nonlinearity term  $\frac{1}{4}V_3$ , it causes a reduction in noise contribution from the converter circuit. Also shown is the effect of partial noise compensation due to correlation<sup>19</sup> between the RF and IF shot noises. The necessary conditions for this type of noise reduction are fulfilled by a tunnel diode which is biased in region No. 2 of the I-V characteristic given in Fig. IV-18.

### Power Series Representation

In the previous analysis, which was based on small-pump theory, the tunnel diode I-V characteristic at the operating point  $P_1$  was represented by a quadratic relation.

$$I = G_o V - \frac{1}{4} V^2$$

This was sufficient for the small-pump theory, however, for large pump voltages it becomes necessary to use a polynomial expansion including higher order terms. Let the current of the tunnel diode be given by the following relation

$$I = I_o + \alpha(V - V_o) + \frac{\beta}{2!}(V - V_o)^2 + \frac{\gamma}{3!}(V - V_o)^3 + \frac{\delta}{4!}(V - V_o)^4 + \frac{\epsilon}{5!}(V - V_o)^5 + \frac{\zeta}{6!}(V - V_o)^6 + \dots \quad (IV-37)$$

where  $I_o$  and  $V_o$  are the current and the voltage at the bias point. The conductance at this point is the derivative of the I-V characteristic.

$$G = \frac{dI}{dV} = \alpha + \beta(V - V_o) + \frac{\gamma}{2!}(V - V_o)^2 + \frac{\delta}{3!}(V - V_o)^3 + \frac{\epsilon}{4!}(V - V_o)^4 + \frac{\zeta}{5!}(V - V_o)^5 + \dots \quad (IV-38)$$

On application of a sinusoidal local oscillator voltage with the angular frequency  $\omega$  the conversion conductance becomes:

$$G_n = \frac{1}{2\pi} \int_0^{2\pi} [\alpha + \beta V \cos \omega t + \frac{\gamma}{2!} V^2 \cos^2 \omega t + \frac{\delta}{3!} V^3 \cos^3 \omega t + \frac{\epsilon}{4!} V^4 \cos^4 \omega t + \frac{\zeta}{5!} V^5 \cos^5 \omega t + \dots] \cos n \omega t d(\omega t) \quad (IV-39)$$

and after further manipulation and collection of terms:

$$G_n = \frac{1}{2\pi} \int_0^{2\pi} [(\alpha + \frac{\gamma}{4} V^2 + \frac{\epsilon}{64} V^4) + (\beta V + \frac{\delta}{8} V^3 + \frac{\zeta}{192} V^5) \cos \omega t + \dots] \cos n\omega t d(\omega t) \quad (IV-40)$$

From this relation it can be seen that the linear term of the previous parabolic representation  $G_o$  now has a new value

$$G'_o = \alpha + \frac{\gamma}{4} V_3^2 + \frac{\epsilon}{64} V_3^4 \quad (IV-41)$$

and the nonlinearity term  $\frac{1}{4} V_3$  becomes

$$\frac{1}{4} V_3 = - \left( \frac{\beta}{2} V_3 + \frac{\delta}{16} V_3^3 + \frac{\zeta}{384} V_3^5 \right) \quad (IV-42)$$

The I-V characteristic of a tunnel diode (see Fig. IV-18) may be considered to consist of two regions. Region No. 1 comprises that part of the curve that turns downward from the peak current  $I_A$ , while in region No. 2 the curve turns upward from the valley current  $I_B$ . The curves of these two regions can be represented by separate power series. The following table gives a summary of the expansion coefficients in both regions for a typical tunnel diode ( $I_A = 1 \text{ mA}$ ) used in recent experiments. It is to be noted that the signs of the coefficients pertaining to the nonlinearity term  $\frac{1}{4} V$  are opposite for the two regions.

The significance of the difference in signs will be considered in the discussion of the noise factor expression.

TABLE IV-3

REGION	$V_o$ ma	$I_b$ ma	$\alpha$	$\beta$	$\gamma$	$\delta$	$\epsilon$	$\zeta$
No. 1 at $P_1$	50	.96	$4.60 \times 10^{-3}$	$-416 \times 10^{-6}$	$9.12 \times 10^{-6}$	$-81.6 \times 10^{-9}$	$2.98 \times 10^{-11}$	$-1.18 \times 10^{-12}$
No. 2 at $P_2$	360	.15	$1.30 \times 10^{-3}$	$9.20 \times 10^{-6}$	$.060 \times 10^{-6}$	$37.0 \times 10^{-9}$	$1.00 \times 10^{-9}$	$13.5 \times 10^{-12}$

How well a power series with the above coefficients describes the I-V characteristic of the tunnel diode is shown in Fig. IV-19, where both the calculated and measured values are given. Also shown are the reverse and forward components of the actually measurable diode current  $I$ , and the equivalent shot noise current  $I_o$ . The relation of these currents has been established as follows.

$$\text{Forward current } I_F = \frac{I}{1 - \exp(-qV/kT)} \quad (\text{IV-43})$$

$$\text{Reverse Current } I_R = I_F \times \exp(-qV/kT) \quad (\text{IV-44})$$

$$\text{Measurable Diode Current } I = |I_F| - |I_R| \quad (\text{IV-45})$$

$$\text{Equivalent Shot Noise Current } I_e = |I_F| + |I_R| \quad (\text{IV-46})$$

### Noise Factor with Correlation Term

The derivation of the extended noise factor expression for the converter circuit (see Fig. IV-1) follows closely the analysis presented in the paper of Reference No. 1, except that the effect of the correlation term is no longer negligible.

There are two sources of noise present in the converter circuit. The first is due to the *thermal noise sources* in the individual RF and IF circuits

$$|\delta_{1T}|^2 = 4K\Delta/(G_1 T_o + G_1 T) \quad (\text{IV-47})$$

$$|\delta_{2T}|^2 = 4K\Delta/(G_2 T_o + G_2 T)$$

These currents are uncorrelated with one another. The second type of noise is due to the *shot effect* in the diode itself which produces correlated RF and IF currents. The reason for this can be shown briefly as follows:

The shot noise current of the diode is the sum of the current pulses due to individual electrons traversing the diode. The elementary current pulse can be represented by a delta function that is

$$i(t) = e \sum_k \Delta(t - t_k) \quad (\text{IV-48})$$

where  $e$  is the electron charge and  $t_k$  is the time at which the event occurs. The Fourier transform pair of the current are

$$i(t) = e \sum_k \frac{1}{2\pi} \int_0^\infty \cos \omega(t - t_k) d\omega \quad (\text{IV-49})$$

$$I(\omega) = \int_{-\infty}^{+\infty} i(t) e^{-j\omega t} dt$$

Thus at the time  $t = t_k$  a continuous frequency spectrum of sinusoidal waves is generated in the converter circuit. However, b. cause of the circuit resonances, only current waves of a passband  $\Delta\omega$  centered at the input frequency  $\omega_1$  and at the IF frequency  $\omega_2$  excite the circuit. The current waves of interest are.

$$i_1(t) = e \sum_k \frac{1}{\pi} \int_{\omega_1}^{\omega_1 + \Delta\omega} \cos \omega(t - t_k) d\omega \quad (\text{IV-50})$$

$$i_2(t) = e \sum_k \frac{1}{\pi} \int_{\omega_2}^{\omega_2 + \Delta\omega} \cos \omega(t - t_k) d\omega$$

At the particular instant  $t = t_k$ , the nonlinearity of the diode gives rise to a second IF current resulting from the interaction of the input circuit voltage and the local oscillator voltage. Since all of these noise current components originate from the same delta function at the same instant, the primary IF noise current is fully correlated with the second IF noise current which results from conversion of the primary RF noise current. At the time  $t = t_k$  the noise currents at the RF and IF are

$$\delta_{1S} = e \frac{1}{\pi} \int_{\omega_1}^{\omega_1 + \Delta\omega} \cos \omega(t - t_k) d\omega \quad (\text{IV-51})$$

$$\delta_{2S} = e \frac{1}{\pi} \int_{\omega_2}^{\omega_2 + \Delta\omega} \cos \omega(t - t_k) d\omega$$

For the thermal noise currents ( $\delta_{IT}$ ,  $\delta_{2T}$ ) and the shot noise currents ( $\delta_{IS}$ ,  $\delta_{2S}$ ) one can write the following equations from the converter network

$$\delta_{IT} + \delta_{IS} = V_1 \bar{G}_1 - (\frac{1}{2} V_2^* V_3) \quad (\text{IV-52})$$

$$\delta_{2T} + \delta_{2S} = V_2 \bar{G}_2 - (\frac{1}{2} V_1^* V_3)$$

and solving one finds

$$V_2 = \frac{(\delta_{2T} + \delta_{2S}) + \frac{1}{2} V_3}{\bar{G}_2 - \frac{(\frac{1}{2} V_3)^2}{\bar{G}_1}} (\delta_{IT} + \delta_{IS}) \quad (\text{IV-53})$$

The absolute value squared is

$$|V_2|^2 = |V_2| |V_2| = \frac{|\delta_{2T}|^2 + |\delta_{2S}|^2 + \frac{(\frac{1}{2} V_3)^2}{\bar{G}_1^2} (|\delta_{IT}|^2 + |\delta_{IS}|^2) + \frac{1}{2} V_3 \left( \delta_{IS} \delta_{2S} + \delta_{IS}^* \delta_{2S}^* \right)}{\left( \bar{G}_2 - \frac{(\frac{1}{2} V_3)^2}{\bar{G}_1} \right)^2} \quad (\text{IV-54})$$

which averaged over the time distribution becomes

$$|V_2|^2 = \frac{|\overline{\delta_{2T}}|^2 + |\overline{\delta_{2S}}|^2 + \frac{(\frac{Q}{4}V_3)^2}{G_1^2} (\overline{|\delta_{IS}|^2} + \overline{|\delta_{2S}|^2}) + \frac{QV_3}{G_1} (\overline{\delta_{IS}\delta_{2S}} + \overline{\delta_{IS}\delta_{2S}^*})}{\left(\frac{G_2}{G_1} - \frac{(\frac{Q}{4}V_3)^2}{G_1}\right)^2} \quad (IV-55)$$

In these equations  $\delta_{IS}$  and  $\delta_{2S}$  are the original shot noise currents and  $\frac{QV_3}{G_1} \times (\overline{\delta_{IS}\delta_{2S}} + \overline{\delta_{IS}^*\delta_{2S}^*})$  is the cross-product of these two correlated currents. The averages of the mean square currents over the time distribution are

$$|\overline{\delta_{IS}}|^2 = |\overline{\delta_{2S}}|^2 = 2I(\omega)^2df = 2eI_e df = 4KTG_e df \quad (IV-56)$$

and thus one can write

$$\frac{QV_3}{G_1} (\overline{\delta_{IS}\delta_{2S}} + \overline{\delta_{IS}^*\delta_{2S}^*}) = 2 \frac{QV_3}{G_1} 4KTG_e \Delta f \quad (IV-57)$$

where  $G_e$  is the equivalent noise conductance. The noise correlation term can be either additive or subtractive, depending on the sign of the factor  $\frac{QV_3}{G_1}$ . This in turn depends on the shape of the IV characteristic of the tunnel diode and the bias point. Thus the significance of large pump voltages and the sign of the coefficients shown in Table I becomes apparent.

A further comment has to be made about the value of  $G_e$ . In region No. 1, where the tunneling noise is predominant,  $G_e = \frac{el_e}{2KT}$ , where  $I_e$  is equivalent diode shot noise current and equals the sum of the averages  $|I_F| + |I_R|$ . In region No. 2 beyond the valley point, the thermal noise becomes important and  $G_e$  is merely equal to the linear term of the conversion conductance.

Substituting these terms into the expression for the noise factor

$$F = \frac{V_2^2 G_L}{g_c K T_o \Delta f}$$

and using

$$g_c = \frac{4(\frac{Q}{4}V_3^2 G_R G_L)}{[G_1 G_2 - (\frac{Q}{4}V_3)^2]^2}$$

one obtains:

$$F = \frac{G_L}{g_c K T_o \Delta f} \times \frac{g_c G_L^2}{4(\frac{Q}{4}V_3^2 G_R G_L)} \times 4K\Delta f \left[ (G_R T_o + G_1 T + G_e T) \frac{(\frac{Q}{4}V_3^2)^2}{G_1^2} + 2 \frac{QV_3^2}{G_1} G_e T + (G_L T + G_2 T + G_e T) \right] \quad (IV-58)$$

which reduces to.

$$F = 1 + \frac{T}{T_o} \left[ \frac{G_1}{G_g} + \frac{G_e}{G_g} + \frac{\bar{G}_1^2}{G_g^2 V_3^2} \left\{ G_L + G_2 + \left| G_e \left( 1 + 2 \frac{G_e V_3}{\bar{G}_1} \right) \right| \right\} \right] \quad (\text{IV-59})$$

This equation is similar to the one derived for the "small-pump" analysis except that now the noise correlation  $2 \frac{G_e V_3}{\bar{G}_1}$  is included, and the values  $G_o$  and  $G_e V_3$  are replaced with the newly found  $G'_e$  and  $G'e V_3$ . As further refinement one can also calculate a new dynamic  $G'_e$  that will represent the equivalent shot noise conductance of the tunnel diode under large pump voltage conditions.

### Reduction of Noise Factor

To minimize the noise factor one can consider the following conditions:

- 1) Obviously the shunt admittances  $G_1$  and  $G_2$ , that is the losses of the RF and IF circuit, should be made as low as possible.
- 2) The load admittance  $G_L$  should be made small.
- 3) The term  $\frac{G_e}{G_g}$  should be made as small as possible. This can be done by making  $G_e$  small and/or  $G_g$  large. However, there are certain limitations.  $G_g$  cannot be made too large because of its interaction with another term in the equation that contains  $\bar{G}_1^2 = (G_g + G_o)^2$  in the numerator.
- 4) Rearranging the noise factor equation (in the manner used in Fig. IV-5 where a lossless converter with high gain is assumed) leads to a simplified form

$$F = 1 + a K_o + (K_L + a K_o) \frac{1 + K_o}{K_L + K_o}$$

where

$$K_L = \frac{G_L}{G_g}, \quad K = \frac{G_e}{G_g}, \quad a = \frac{K_e}{K_o} = \frac{G_e}{G_o} - \frac{T}{T_o} = 1$$

Certainly this noise factor expression can be made small if  $a \cdot \frac{G_e}{G_o}$  can be made small. Several attempts have been made to produce special diodes to meet this requirement. But this proved to be a difficult task for the "device" man. However, the value of  $G_o$  can be increased without increasing  $G_e$  at the same time through the use of large pump voltages, when  $G_o$  becomes  $G'_o$ . This situation exists for example when the tunnel diode is biased in region No. 1 at point  $P_1$  and pumped with large voltages.

- 5) Another possibility can be found in the term  $\bar{G}_1^2 = (G_g + G_o)^2$ . This term should be made as low as possible. This could be accomplished by making  $G_o$  negative and letting

it approach  $G_g$ ; then  $\bar{G}_I^2 = (G_g - G_o)^2$  will approach zero. This condition can be fulfilled by biasing the tunnel diode in the negative slope region. But this leads to instability because it seriously effects the input termination of the converter, which then becomes mismatched to the antenna.

6) Finally, considering the factor  $|G \left(1 + 2 \frac{Q' V_3}{G_I}\right)|$  which contains the newly discussed correlation term, one finds still another possibility of obtaining a low noise factor. This can be done when the nonlinearity term  $Q'$  is made negative, and the pump voltage  $V_3$  is sufficiently large so that  $|1 + 2 \frac{Q' V_3}{G_I}|$  approaches zero. As has been shown in Table IV-3 this situation exists when the tunnel diode is biased in region No. 2, as for instance at point  $P_2$  and pumped with large voltages.

There is still another important feature resulting from the large pump voltage operation. When  $Q' V_3$  becomes larger than  $G_o$  the last term of the noise factor becomes less sensitive to the change of the input impedance. Therefore, low noise factor and stable operation are possible with either a matched or a mismatched input condition. This is indeed a very desirable feature for practical applications. In the experimental test set-up the input to the converter could be opened or shortened without causing the circuit to break into oscillation.

### System Noise Factor

The above theory gives the noise factor of the converter stage by itself, but neglects the effect of the noise factor of the IF amplifier on the total or system noise factor of a receiver. If one considers the noise factor of a diode converter plus the IF amplifier one finds the well known equation

$$F_{\text{Total}} = F_{\text{conv.}} + \frac{F_{\text{IF}} - 1}{g_c} \quad (\text{IV-60})$$

where  $g_c$  is the power conversion ratio of the converter stage.

In ordinary "crystal" diode mixers this ratio  $g_c$  is less than unity, and  $\frac{1}{g_c}$  is called the conversion loss of the mixer. Figure IV-20 is a graphical illustration of the I-V characteristic of a crystal diode similar to the 1N21. Since the slope of this curve is always positive it is apparent that such a diode can never have gain. Typical values for conversion losses are in the order of 4 to 8 db.

In the tunnel diode, however,  $g_c$  can be made larger than unity as long as the condition  $\frac{Q' V_3}{G_o} > 1$  is satisfied. The significance of this was discussed in more detail in reference No. 1. Since  $Q'$  in region No. 2 of the I-V characteristic is relatively small, large pump

voltage is required to drive the current from the bias point  $P_2$  sufficiently deep into the region of negative I-V slope. Because the tunnel diode exhibits this negative I-V slope, it can produce conversion gain. Consequently, the tunnel diode is capable of further reducing the total system noise factor.

To demonstrate this effect consider that both the tunnel diode and the "crystal" diode yield the same noise factor for the converter part of the two receiver systems under comparison. Let this noise factor  $F_{Conv}$  be 3.2 db (power ratio 2.09) as will be shown later. Also let the noise factor of the following broad-band IF amplifier  $F_{IF}$  be 3.0 db (p.r. = 2.0). Then with a typical conversion loss of the crystal as  $\frac{1}{g_c} = -6$  db (p.r. = .25) and the conversion gain of the tunnel diode  $g_c = 5.0$  db (p.r. = 3.16), and the total system noise factor for the "Crystal" System

$$F_{Total} = 2.09 + \frac{2-1}{.25} = 6.09 \text{ or } 7.85 \text{ db and for the Tunnel Diode System}$$

$$F_{Total} = 2.09 + \frac{2-1}{3.16} = 2.40 \text{ or } 3.82 \text{ db.}$$

This represents an improvement of 4 db, and shows that even with a modest gain the tunnel diode converter is effective in reducing the system noise factor.

### Results

A few simple calculations will illustrate the reduction of the noise factor according to the scheme outlined in IV-4 above. For the specific diode under consideration the power series coefficients at the bias point  $P_1$  ( $V_o = 50$  mv,  $I_o = .95$  ma) are given in the previous Table. They allow the calculation of the terms  $G_o$  and  $Q/V_3$  for various values of pump voltage  $V_3$ . Figure IV-21 shows the results of this calculation for pump voltages up to 250 mv. With these terms established one can then calculate the noise factor  $F$  and the conversion ratio  $g_c$  for various parameters of  $G_g$  and  $G_L$ . Figure IV-22 shows the results of such calculations. In these curves  $G_g$  ranges from 20 to 180 millimhos,  $G_L$  is chosen at a typical value of 3 millimhos, and  $G_1$  and  $G_2$  are assumed to be negligible.  $G_g$  is determined by the shot noise current at the bias point and is  $G_g = 20 \times I_s = 20 \times 1.3 \times 10^{-3} = 26$  millimhos. Two values of pump voltage,  $V_3 = 200$  mv and 225 mv, have been plotted.

Since a low noise converter can be used to full advantage, only if it does not introduce a conversion loss by itself, values for the total noise factor of a system have also been calculated. In this calculation a noise factor of 3 db has been assumed for a broad-band IF amplifier following the converter stage. A reasonable compromise solution for low noise factor and stable gain seems to be reached at a pump voltage of 225 mv and a  $G_g$  of

120 millimhos. This yields a calculated converter noise factor of 3.2 db, and a total system noise factor of 3.9 db.

These calculated results are in good agreement with experimental results. The tunnel diode down converter used for the test set-up was a lumped parameter circuit operating at a signal frequency of 440 mc, a pump of 470 mc and an IF of 30 mc. One of the features of this circuit was a double-tuned input transformer which allowed the R.F. impedance of the signal as seen by the diode ( $G_g$ ) to be changed and optimized as predicted by the theoretical curves of Figure 6. A total system, single sideband noise factor of 5.3 db was measured with a pump voltage of 200 mv.

Another important feature of this circuit was the use of a self bias scheme for the tunnel diode. No external D.C. bias source was supplied, and the diode established its own bias voltage through the rectification of the pump voltage. The measured bias voltage across the diode was about 50 mv when operated at the above mentioned conditions.

A similar calculation can also be performed to explore the possibilities of noise reduction due to IV-6. For this case the diode is biased in region 2 at  $B_2$  ( $V_o = 360$  mv,  $I_o = .15$  ma), and the corresponding power series coefficients can again be found in Table 1. After calculating a new series of terms for  $G_o$  and  $\frac{1}{2}V_3$  for various pump voltages, one can then determine the noise factor and gain as a function of  $G_g$  and  $V_3$ . Figure IV-23 shows the results of these calculations. It should be noted that the minimum converter noise factor occurs at the point where the correlation term  $2 \frac{1}{2}V_3$  reaches the value of -1. This is possible because of the negative sign for  $\frac{1}{2}V_3$  together with a  $V_3$  large enough for their product to cancel out the effective diode noise contribution in the last part of the noise factor equation.

The minimum total system noise factor in this case occurs at a pump voltage of 225 mv and a  $G_g$  of about 32 millimhos. The converter noise factor is 4.2 db, the conversion gain about unity and the total noise factor 5.55 db. As might be expected the conversion gain is rather low at this bias point because the I-V characteristic near the valley point is considerably flat.

Experimental results which were instrumental in establishing and proving the "large-pump" voltage theory, were obtained with the same tunnel diode converter described above. A single sideband noise factor of 5 db was measured for the total system consisting of input filter, converter and IF amplifier. The diode bias voltage was 360 mv and the pump voltage as measured across the diode was 250 mv.

## G. MILLIMETER WAVE TUNNEL DIODE DOWN CONVERTER

Results on UHF tunnel-diode down converters have proven so successful that they have encouraged an attempt to develop a millimeter wave tunnel-diode down converter. The noise factor of present millimeter wave detectors is poor. It is expected that the noise factor will be improved considerably through use of a tunnel diode down converter.

A line of attack has been agreed upon and the necessary equipment has been ordered or borrowed. Some equipment is being made for this project by the various Laboratory organizations.

The diode is to be electrically formed in a tapered section of RG-98/u waveguide. The waveguide section and mounts for placing the semiconductor and point in the waveguide are being made.

The diode for this experiment is to be of gallium-antimonide with a zinc point. The process of forming the diode has been tried with preliminary results of current ratios of the order of 2 to 1. An improved sample of Gallium Antimonide #55 has recently been used and has given better results. Diode fabrication is in progress.

## V. SOLID-STATE MICROWAVE DEVICES

### A. NEGATIVE-RESISTANCE TRANSMISSION LINE-AMPLIFIER

#### Introduction

Present negative-resistance devices, such as parametric diodes<sup>21</sup> and tunnel diodes, because of their one port property, are narrow-banded and require auxiliary isolators for low-noise applications. To convert them from one-port to two-port operation, traveling-wave circuitry<sup>5</sup> has been suggested. Previous circuit analyses, however, have been limited to the lossless case and the circuit has been assumed free from any distributed Johnson noise or shot-effect noise, and also any input or output reflection.

The purpose of the present work is to treat a transmission line with distributed negative-resistances in a more general way. First, the line is considered to be lossy, with both series resistances and shunt conductances. Secondly, distributed noise voltages and currents are introduced. These noise voltages and currents may be due, not only to thermal noise in the lossy elements, but also to shot noise in the active elements. Gain and noise factor are then derived as a function of the input and output conditions.

#### Transmission Line

The transmission line under investigation is shown in Fig. V-1. The line has the following distributed parameters

$R$  = net series resistance per unit length

$L$  = series inductance per unit length

$G$  = net shunt conductance per unit length

$C$  = Shunt capacitance per unit length

$|\hat{v}_n|^2$  = noise voltage squared per unit length

$|\hat{i}_n|^2$  = noise current squared per unit length

These parameters are either smoothly distributed or are made of lumped constants so closely spaced (preferably less than 1/8 wavelength) that a smoothline approach is still valid. In addition, both  $R$  and  $G$  are generalized to include negative values. It is when  $R$  and/or  $G$  are negative that the line behaves as the active device, which is of main interest here.

## Basic Equations

The usual transmission line equations in voltage  $V$  and current  $I$  are:

$$-\frac{\partial V}{\partial z} = (R + j\omega L) I \quad (V-1)$$

$$-\frac{\partial I}{\partial z} = (G + j\omega C) V \quad (V-2)$$

However, because the problem of essential interest involves uncorrelated noise sources, the square of the voltage  $|V|^2$  and the power  $P$ , instead of the voltage ( $V$ ) and the current ( $I$ ), are chosen as the working electrical parameters. Let

$$VI^* + V^*I = 2P_r \quad (V-3)$$

$$VI^* - V^*I = 2jP_x \quad (V-4)$$

where  $P_r$  is the real power and  $P_x$  is the reactive power.

Ignoring the distributed noise, a set of four working equations is derived from V-1 and V-2:

$$-\frac{\partial}{\partial z} |V|^2 = 2R P_r + 2\omega L P_x \quad (V-5)$$

$$-\frac{\partial}{\partial z} |V|^2 = 2G P_r - 2\omega C P_x \quad (V-6)$$

$$-\frac{\partial}{\partial z} P_r = R |I|^2 + G |V|^2 \quad (V-7)$$

$$-\frac{\partial}{\partial z} P_x = (\omega L) |I|^2 - (\omega C) |V|^2 \quad (V-8)$$

These equations are quite similar to the noise equations which were treated in the electron stream of traveling wave tubes.<sup>22</sup>

Equations (V-5), (V-6), (V-7), and (V-8) can be transformed into the following common equation:

$$\left[ \frac{\partial^4}{\partial z^4} + 4(\omega^2 L C - R G) \frac{\partial^2}{\partial z^2} - 4(\omega L G + \omega C R)^2 \right] (|V|^2, |I|^2, P_r \text{ or } P_x) = 0 \quad (V-9)$$

Equation (V-9) is the differential equation of  $|V|^2$ ,  $|I|^2$ ,  $P_r$  or  $P_x$  for an ordinary transmission line in the absence of distributed noise. If the line, which is of length  $D$ , with a

characteristic impedance  $Z_o (= R_o + jX_o)$  is terminated by an impedance  $Z_D (= R_D + jX_D)$  and is driven by a signal voltage source  $|E|^2$  with a generator impedance  $Z_g$ , the solution of Eq. (V-9) can be readily determined<sup>23</sup>, it is

$$|V|^2 = \frac{P_o}{R_o} |Z_o|^2 \left[ \frac{a_z + b_z}{a_o + b_o} \right] \quad (\text{V-10})$$

$$|I|^2 = \frac{P_o}{R_o} \left[ \frac{a_z - b_z}{a_o + b_o} \right] \quad (\text{V-11})$$

$$P_r = \frac{P_o}{2R_o(a_o + b_o)} [Z_o(\bar{a}_z + j\bar{b}_z) + Z_o^*(\bar{a}_z - j\bar{b}_z)] \quad (\text{V-12})$$

$$P_x = \frac{P_o}{2R_o(a_o + b_o)} [Z_o(\bar{a}_z + j\bar{b}_x) - Z_o^*(\bar{a}_z - j\bar{b}_x)] \quad (\text{V-13})$$

where

$$P_o = \frac{|E|^2}{|Z_o + Z_g|^2} R_o \quad (\text{V-14})$$

$$\frac{a_z}{a_o} = e^{-a_1 z} + |N|^2 e^{a_1(z+D)} \quad (\text{V-15})$$

$$\frac{b_z}{a_o} = -2e^{-D a_1} |N| \frac{\sin[(|a_2|(z+D) + \theta_2)]}{\cos[(|a_2|(z+D) + \theta_2)]} \quad (\text{V-16})$$

$$a_o = 1 + |MN|^2 e^{-2D a_1} \quad (\text{V-17})$$

$$b_o = -2e^{-D a_1} |MN| \cos[\theta_1 + \theta_2 - D|a_2|] \quad (\text{V-18})$$

$$a_1 = \omega \sqrt{2LC} [(XY - 1) + \sqrt{(1+X^2)(1+Y^2)}]^{\frac{1}{2}} \quad (\text{V-19})$$

$$a_2 = \omega \sqrt{2LC} [(XY - 1) - \sqrt{(1+X^2)(1+Y^2)}]^{\frac{1}{2}} \quad (\text{V-20})$$

$$X = \frac{R}{\omega L} \quad (\text{V-21})$$

$$Y = \frac{G}{\omega C} \quad (V-22)$$

$$Z_o = \frac{L}{C} \frac{X+j}{Y+j} \quad (V-23)$$

$$M = \frac{Z_o - Z_R}{Z_o + Z_R} = M e^{j\theta_1} \quad (V-25)$$

$$N = \frac{Z_o - Z_D}{Z_o + Z_D} = N e^{j\theta_1} \quad (V-25)$$

In Eq. (V-19),  $a_1$  has a positive sign if the line is passive (i.e., if both  $R$  and  $G$  are positive). For an active line, (i.e., the case where  $R$  and/or  $G$  is negative), it is noted from Eq. (V-20), that  $a_2$  is always a pure imaginary number. Thus  $a_1$  is either an amplification constant or an attenuation constant, while  $a_2$  is a phase constant.

$M$  and  $N$  are coefficients of reflection respectively for the input and for the output end respectively. Because the denominators of Eqs. (V-10), (V-11), (V-12), and (V-13) contain these two reflection coefficients, they can be expanded into a power series in  $|MN|$  when  $|MNe^{D\alpha_1}| < 1$  or in  $|MN|^{-1}$  when  $|MNe^{D\alpha_1}| > 1$ . The successive terms of these series are the contributions due to multiple reflections back and forth from the ends of the line.

#### Transmission Line with Distributed Noise Generators

Now assume that a noise mean square voltage  $|\hat{V}_n|^2$  and a noise mean square current  $|\hat{I}_n|^2$  are distributed along the line. Equations (V-5), (V-6), (V-7), and (V-8) can be then written, for noise alone, as:

$$-\frac{\partial}{\partial z} |\hat{V}|^2 + 2R\hat{P}_r + 2\omega C\hat{P}_x - |\hat{V}_n|^2 \quad (V-26)$$

$$-\frac{\partial}{\partial z} |\hat{I}|^2 + 2G\hat{P}_r - 2\omega C\hat{P}_x - |\hat{I}_n|^2 \quad (V-27)$$

$$-\frac{\partial}{\partial z} \hat{P}_r = R |\hat{I}|^2 + G |\hat{V}|^2 \quad (V-28)$$

$$-\frac{\partial}{\partial z} \hat{P}_x = (\omega L) |\hat{I}|^2 - (\omega C) |\hat{V}|^2 \quad (V-29)$$

where the crowns designate the noise case. The noise sources  $|\hat{v}_n|^2$  and  $|\hat{i}_n|^2$  can be, for instance, the Johnson noise due to the losses of the line, and whatever noise the negative-resistance devices contribute.  $|\hat{v}_n|^2$  and  $|\hat{i}_n|^2$  are assumed not to be functions of the line distance  $z$ . Equations (V-26), (V-27), (V-28), and (V-29) have almost the same form as Eqs. (V-5), (V-6), (V-7), and (V-8) except for the presence of the noise generator terms. By making the following substitutions:

$$|\hat{V}|^2 = |\hat{V}|^2 \quad (V-30)$$

$$|\hat{I}|^2 = |\hat{I}|^2 \quad (V-31)$$

$$\hat{P}_r = \hat{P}_r - \hat{p}_r \quad (V-32)$$

$$\hat{P}_x = \hat{P}_x - \hat{p}_x \quad (V-33)$$

$$\hat{p}_r = \frac{1}{X+Y} \left[ \frac{|\hat{v}_n|^2}{2\omega L} + \frac{|\hat{i}_n|^2}{2\omega C} \right] \quad (V-34)$$

$$\hat{p}_x = \frac{1}{X+Y} \left[ Y \frac{|\hat{v}_n|^2}{2\omega L} - X \frac{|\hat{i}_n|^2}{2\omega C} \right] \quad (V-35)$$

one arrives at the same differential equation as (V-9) for  $|\hat{V}|^2$ ,  $|\hat{I}|^2$ ,  $\hat{P}_r$ , or  $\hat{P}_x$ . A set of solutions similar to Eqs. (V-10), (V-11), (V-12), and (V-13) will be obtained in the noise case provided  $Z_D$  and  $N$  are respectively replaced by  $\hat{Z}_D$  and  $\hat{N}$  where

$$\hat{Z}_D = R_D + j\hat{X}_D \quad (V-36)$$

$$\hat{R}_D = R_D \left( 1 - \frac{\hat{p}_r}{\hat{p}_{xD}} \right) \quad (V-37)$$

$$\hat{X}_D = X_D \left( 1 - \frac{\hat{p}_x}{\hat{p}_{xD}} \right) \quad (V-38)$$

$$N = \frac{Z_o - \hat{Z}_D}{Z_o + \hat{Z}_D} = |\hat{N}| e^{j\theta_2} \quad (V-39)$$

Here  $\hat{p}_{xD}$  and  $\hat{p}_{xD}$  denote, respectively, the real noise power and the reactive noise power at the termination. Equations (V-36), (V-37), (V-38), and (V-39), have an important physical

meaning; namely, as far as the electrical performance is concerned, a line with distributed noise generators and a passive terminating impedance  $Z_D$  is equivalent to the same line without such noise generators but with a fictitious termination  $Z_D$ , which is a function of the driving powers  $\hat{P}_{rD}$  and  $\hat{P}_{xD}$ .

### Gain and Noise Factor

The real signal and noise powers,  $P_r$  and  $\hat{P}_r$ , which have been derived as Eq. (V-12), are now used for the computation of the gain and noise factor.

Using Eq. (V-12), the power gain  $G_p$ , which is defined as the ratio of the output power  $P_r$  to the available input power  $P_a$ , is

$$G_p = \frac{P_{rD}}{P_a} = \frac{P_o}{P_a(a_o + b_o)} \left[ \bar{a}_D - \frac{x_o}{R_o} \bar{b}_D \right] \quad (V-40)$$

where

$$P_a = \frac{|E|^2}{4R_g}$$

$$\bar{a}_D = (\bar{a}_z) | z=D \quad (V-41)$$

$$\bar{b}_D = (\bar{b}_z) | z=D$$

The equation for the output noise power  $\hat{P}_{rD}$  is

$$\hat{P}_{rD} = P_o \left( \frac{1}{\bar{a}_o + \bar{b}_o} \right) \left[ \hat{a}_D - \frac{x_o}{R_o} \hat{b}_D \right] \quad (V-42)$$

Here  $\hat{a}_o$ ,  $\hat{b}_o$ ,  $\bar{a}_D$  and  $\hat{b}_D$  are derived from Eqs. (V-17), (V-18), and (V-41) by substituting  $|\hat{N}|$  for  $N$ . Since  $|\hat{N}|$  is a function of  $P_{rD}$ , Eq. (V-42) is a polynominal equation in  $\hat{P}_{rD}$ . The solution is rather involved. Only a few special cases are illustrated in the examples to be shown.

Using the solution of  $\hat{P}_{rD}$  from Eq. (V-42), the noise factor  $F$  is

$$F = \frac{\hat{P}_{rD}}{\hat{P}_a G_p} \quad (V-43)$$

*Examples:*

To show the noise performance of an active transmission line distributed with noise generators, three simple cases are illustrated in Table V-1. They are a matched line, a mismatched input line and a mismatched output line. The lines are distortionless (i.e.,  $X = Y$ ). An isolated load is assumed for the termination in all three cases.

TABLE V-1

CASE	MATCHED INPUT & OUTPUT $X = Y = \text{NEG}$	MISMATCHED INPUT $X = Y = \text{NEG}$	MISMATCHED OUTPUT $X = Y = \text{NEG}$
GIVEN	$R_g = R_0 = R_D$ $X_g = X_0 = X_D = 0$ $\hat{P}_x = 0$	$R_g \neq R_0, R_0 = R_D$ $X_g = X_0 = X_D = 0$ $\hat{P}_x = 0$	$R_g = R_0, R_0 \neq R_D$ $X_g = X_0 = X_D = 0$ $\hat{P}_x = 0$
$a_0$	1	1	1
$b_0$	0	0	0
$\hat{a}_D$	$e^{-\alpha_0 D}$	$e^{-\alpha_0 D}$	$(1 - INI^2)e^{-\alpha_0 D}$
$\hat{a}_0$	1	$1 + IMNI^2 e^{-\alpha_0 D}$	1
$\hat{b}_0$	0	$\pm 2e^{-0.5IMNI} \text{, ASSUME } DI(\alpha_2) = n\pi$	0
$\hat{a}_D$	$(1 - INI^2)e^{-\alpha_0 D}$	$(1 - INI^2)e^{-\alpha_0 D}$	$(1 - INI^2)e^{-\alpha_0 D}$
$G_p$	$e^{-\alpha_0 D}$	$(1 - M^2)e^{-\alpha_0 D}$	$(1 - INI^2)e^{-\alpha_0 D}$
$\hat{P}_{RD}$	$\frac{1}{2}[\hat{P}_r + G_p \hat{P}_D] \cdot$ $[1 + \sqrt{1 - (\frac{\hat{P}_r}{\hat{P}_r + G_p \hat{P}_D})^2}]$	$\frac{1}{2}[\hat{P}_r + \frac{G_p}{1-M^2}(\hat{P}_0 + M \hat{P}_r)] \cdot$ $[1 + \sqrt{1 - (\frac{\hat{P}_r(1 + \frac{1-M^2}{M} G_p)}{\hat{P}_r + \frac{G_p}{1-M^2}(\hat{P}_0 + M \hat{P}_r)})^2}]$	$\frac{1}{2}[\hat{P}_r + G_p \frac{\hat{P}_D}{1-N^2}] \cdot$ $[1 + \sqrt{1 - (\frac{\hat{P}_r}{\hat{P}_r + G_p \frac{\hat{P}_D}{1-N^2}})^2}]$
$F$	$\frac{1}{2}\left[1 + \frac{\hat{P}_r}{P_0 G_p}\right] \cdot$ $[1 + \sqrt{1 - (\frac{\hat{P}_r / \hat{P}_D}{\hat{P}_r / P_0 + G_p})^2}]$	$\frac{1}{2}\left[1 + \frac{\hat{P}_r}{P_0 G_p} (1 - M^2) \pm \frac{\hat{P}_r}{P_0} M\right] \cdot$ $[1 + \sqrt{1 - (\frac{(1 \pm MG_p / 1 - M^2)^2}{1 + \frac{G_p}{1 - M^2}(\frac{\hat{P}_0}{\hat{P}_r} \pm M)})^2}]$	$\frac{1}{2}\left[1 + \frac{\hat{P}_r}{P_0} \frac{1 - N^2}{G_p}\right] \cdot$ $[1 + \sqrt{1 - (\frac{\hat{P}_r / \hat{P}_D}{\hat{P}_r / P_0 + G_p / 1 - N^2})^2}]$

The case of a non-isolated bilateral transmission line with both mismatched input and output is rather complex. The output noise would be the sum of the noises resulting from multiple reflections at the input and output plus the distributed noise. Consider the special case where the load is matched to the line (i.e.,  $N = 0$ ). Then the input noise power originating from the non-isolated load which generates a noise power  $\hat{P}_l$  is

$$\hat{P}_L = \hat{P}_l \hat{M}^2 e^{+D\alpha_l} = \hat{P}_l \frac{\hat{M}^2}{1 - M^2} G_p \quad (V-50)$$

The new input noise power now becomes

$$\hat{P}'_o = \hat{P}_o + \hat{P}_I \frac{\hat{M}^2}{1 - \hat{M}^2} G_p \quad (V-51)$$

Therefore, the actual values of the noise factor are the same as those obtained by Eq. (V-43) provided  $\hat{P}_o$  is replaced by  $\hat{P}'_o$ .

Equations (V-47) and (V-49) are plotted in Fig. V-2 for the case  $M = 0$ . Equation (V-48) is plotted for two cases,  $N = 0, M = .2$ , (Fig. V-3) and  $N = 0, M = .5$  (Fig. V-4). As expected, the curves all indicate that the noise factor tends to increase at high gains, and at high reflection coefficients. The magnitude of  $\hat{p}_r/\hat{p}_o$  used in these curves can be easily computed from Eqs. (V-34) and (V-35). For a distortionless transmission line, that is  $X = Y$

$$\frac{\hat{p}_r}{\hat{p}_o} = \left[ \frac{R_d + R_n}{| | R_a - R_d | |} + \frac{G_d + G_n}{| | G - G_d | |} \right] \quad \begin{array}{l} R_a > R_d \\ G_a > G_d \end{array} \quad (V-52)$$

where  $R_d, G_d$  = line positive resistance, conductance per unit length

$R_a, G_a$  = introduced negative resistance, conductance per unit length

$R_n, G_n$  = equivalent noise resistance, conductance per unit length.

Equation (V-52) reveals that low negative resistances and conductances per unit length would result in relatively high noise powers on the line and thus high noise factors according to Figs. V-3 and V-4. In cases where the distributed negative resistance just overcomes the distributed positive resistance, the noise factor becomes extremely large. In addition, since the gain per unit length is small, because of the small net negative resistance, a large total gain is possible only when the line is long.

### Distributed Tunnel Diode Amplifier

To test the validity of the above theory, an experimental amplifier was built. A picture of this amplifier is shown in the attached photograph (Fig. V-5). The amplifier, similar to a low pass filter of the coaxial line type was built. Fifteen tunnel diodes are "distributed" in a series circuit along the "inner" conductor of the coaxial line. Alternately arranged between the diodes are small disc shaped capacitors, which are held in place by polystyrene spacers. The d.c. bias for the diodes is provided by a single external source in such a manner that all of the diodes are connected in series. While this circuit greatly simplified the bias problem it necessitated the selection of matched diodes. In this experiment it was advantageous to choose diodes with a peak current of 25 ma at approximately 75 mv. Transmission line measurements of the passive line, that is, before

any diode was inserted, showed that its cut-off frequency was 1500 mc, and that the passive insertion loss was 3 db.

Two basic experiments were conducted with this device. The first one was designed to demonstrate its feasibility as a microwave amplifier. At 900 mc a gain of 3 to 4 db was measured. It was observed that the bandwidth was very broad, but final results have to await further measurements.

The second experiment consisted of exploring the performance of the device as a microwave traveling-wave down-converter. In the manner of a superheterodyne converter, the following frequencies were supplied: signal frequency = 900 mc, local oscillator frequency = 930 mc, which yield a difference frequency of 30 mc. A conversion power gain of 15 db was obtained.

No results are as yet available for the noise factor, because attempts to optimize the circuit conditions were thwarted by spurious oscillations. This instability is due to the inadequacy of the bias supply, and further efforts are needed to overcome these difficulties.

### B. TWO-PORT MICROWAVE DEVICES

Two-terminal negative-resistance devices, such as masers, parametric amplifiers and tunnel-diode amplifiers, require a circulator or other nonreciprocal device to minimize the noise and to stabilize the performance. There are many nonreciprocal devices in the prior art, for instance, vacuum tubes, transistors, ferrite gyrators, etc. However, most of these seem to be useful only at low frequencies. Ferrite gyrators are capable of microwave application, but they are passive and lossy. In the semiconductor field, a nonreciprocal device based on the Hall-effect is well known.

The nonreciprocal Hall-effect in solids has been known for several decades. In the past, very few Hall devices have been practical. Most of them have been limited to application at very low frequencies, i.e., a few hundred cycles.

A recent study shows that the limitation of present Hall devices is not basic but rather in the embodiments and materials involved. Hall-effect, being itself a majority-carrier phenomenon, should have response to very high frequencies. The practical problem is, however, the need for a semiconductor with a high carrier mobility together with a special circuit geometry to improve the overall efficiency. At the present time, an investigation is being carried out to develop such a practical device.

The concept for such a novel device may be seen in a simultaneous measurement of magneto resistance and Hall-effect of a semiconductor sample. In the past, magneto-resistance and Hall-effect were always measured separately and found to be insensitive to the magnetic field and to have low impedance levels. However, a novel effect is suggested that produces a much enhanced sensitivity and impedance. Theoretical predictions are substantiated by experimental results.

The new method utilizes a unique interaction between Hall-effect and magneto-resistance. The scheme consists of supplying a longitudinal electric field and a transverse current, both from a common source, to a semiconductor wafer so that in an orthogonal magnetic field the Hall field opposes the applied longitudinal field. Thus, if the Hall field and the applied field are varied together, the current in the longitudinal direction changes little and the impedance is, in effect, high. However, a change in magnetic field upsets the balance so that the longitudinal current becomes extremely sensitive to the magnetic field. It is conceivable that the effect would lead to important high-frequency applications.

Meanwhile, the nonreciprocal feature of such a Hall-effect device may be complemented by a tunnel diode to obtain sufficient gain. This combined high frequency unit will then have all of the desirable characteristics of an active, high gain, nonreciprocal device.

Two approaches are possible: the first approach is to use an r.f. magnetic field normal to the wafer face and to amplify the Hall voltage thereby produced. No d.c. magnetic field is required in this case. The energy supply is in a direction orthogonal to the magnetic field and the Hall field. The device consists of a semiconductor wafer and a built-in parametric or tunnel diode. It can be an amplifier, an oscillator, or a frequency converter.

The second approach is a combination of a Hall isolator and a tunnel diode. The idea hinges upon the fact that a Hall-effect semiconductor wafer immersed in a transverse uniform magnetic field may become a unidirectional 2-port device if properly combined with an external passive network, for a proper value of the externally applied field. Such a device, which is referred to as a Hall-effect isolator, is combined with a tunnel diode to form a 2-port active network. The network is characterized by unidirectional transmission with simultaneous amplification. Due to the inherent property of the Hall-effect isolator, unidirectional amplification can function stably in spite of drastic changes that may occur in the impedance on the output side of the isolator.

## Hall-Effect Magneto-Resistance Devices

In an attempt to produce a nonreciprocal solid-state device, a Hall-Effect magneto-resistance amplifier is being explored. Magneto-resistance and Hall-Effect arise from crossed electric and magnetic fields. Consider a wafer sample of a rectangular shape. Two sets of electrostatic potentials are applied orthogonally to the sample in the  $x$ - $y$  plane (Fig. V-6). Under the influence of a d.c. magnetic field  $B_z$  in the  $Z$  direction, the transport equations at steady-state conditions in a rectangular coordinate system are

$$\omega_z \dot{y} - \frac{1}{r_x} \dot{x} + n E_{x_0} = 0 \quad (V-53)$$

$$-\omega_z \dot{x} - \frac{1}{r_y} \dot{y} + n E_{y_0} = 0 \quad (V-54)$$

where

$$n = \frac{\rho}{m} \quad (V-55)$$

$$\omega_z = n B_z \quad (V-56)$$

$$r_x = r_{x_0} \left( 1 + \frac{R_x}{R_{x_0}} \right)^{-1} \quad (V-57)$$

$$r_y = r_{y_0} \left( 1 + \frac{R_y}{R_{y_0}} \right)^{-1} \quad (V-58)$$

$$E_{x_0} = \frac{V_x}{\lambda_x} \quad (V-59)$$

$$E_{y_0} = \frac{V_y}{\lambda_y} \quad (V-60)$$

A general anisotropic case has been considered here.  $r_{x_0}$  and  $r_{y_0}$  are the relaxation times of the sample respectively in the  $x$  and  $y$  direction.  $R_{x_0}$  and  $R_{y_0}$  are the corresponding resistances of the sample in the two directions.  $R_x$  and  $R_y$  are the external resistances. It is noted that the presence of the external resistance reduces the sample relaxation times  $r_{x_0}$  and  $r_{y_0}$  into the effective values  $r_x$  and  $r_y$  for a given external battery source. By solv-

ing Eqs. (V-53) and (V-54) and making use of the relation  $I_x = N e \dot{x} \ell_y \ell_z$ ,  $I_y = N e \dot{y} \ell_x \ell_z$  the solutions for the currents are

$$I_x = \frac{g_x V_x + g_y V_y \theta_x \left( \frac{\ell_y}{\ell_x} \right)}{I + \theta_x \theta_y} \quad (V-61)$$

$$I_y = \frac{g_y V_y - g_x V_x \theta_y \left( \frac{\ell_x}{\ell_y} \right)}{I + \theta_x \theta_y} \quad (V-62)$$

where  $\theta_x = \omega_x r_x$ ,  $\theta_y = \omega_x r_y$ ,  $g$  and  $g$  are the conductances in the  $x$  and  $y$  directions. Equations (V-61) and (V-62) can be written alternatively in terms of applied potentials  $V_z$  as

$$I_x = \frac{g_x V_x - g_y V_y \mu_x b V_z \left( \frac{\ell_y}{\ell_x} \right)}{I + \mu_x \mu_y b^2 V_z^2} \quad (V-63)$$

$$I_y = \frac{g_y V_y + g_x V_x \mu_y b V_z \left( \frac{\ell_x}{\ell_y} \right)}{I + \mu_x \mu_y b^2 V_z^2} \quad (V-64)$$

where

$$b V_z = B_z \quad (V-65)$$

$\mu$ 's are the mobilities and  $V_z$  is the potential which is responsible for producing a magnetic field in the  $z$ -direction.  $b$  is the linear "electromagnetic" coefficient which governs the relationship between the electric potential and the magnetic flux.

Assume now that  $V_x$  and  $V_y$  are derived from a common source (as shown by Fig. V-6) so they satisfy the relation

$$V_y = y V_x \quad (V-66)$$

Define

$$R_{xx} = \frac{\partial V_x}{\partial I_x} \Big|_{B = \text{constant}} \quad (V-67)$$

$$G_{xc} = b \frac{\partial I_x}{\partial B} \quad V_x = \text{constant} \quad (\text{V-68})$$

Thus, one obtains

$$R_{xx} = \frac{1 + \theta_x \theta_y}{g_x + y g_y \theta_x \frac{\ell_y}{\ell_x}} \quad (\text{V-69})$$

$$g_{xc} = \frac{\mu_x V_x}{b(1 + \theta_x \theta_y)^2} \left[ -g_x(2\theta_y) - g_y(\theta_x \theta_y - 1) \frac{\ell_y}{\ell_x} \right] \quad (\text{V-70})$$

The power gain can be defined as

$$G_p = \frac{\text{Maximum power output}}{\text{Available power input}}$$

$$\frac{I_x^2 R_p / 4}{V_x^2 / 4 R_z} = g \quad K \quad K = \frac{4P_x \theta_y^2 - 4P_{xy} \theta_y + P_y}{P_i} \quad (\text{V-71})$$

where

$$P_x = (g_x V_x^2) \phi \quad (\text{V-72})$$

$$P_{xy} = (g_x V_x V_y) \phi \quad (\text{V-73})$$

$$P_y = (g_y V_y^2) \phi \quad (\text{V-74})$$

$$\beta_i = \frac{V_x^2}{4 R_z} \quad (\text{V-75})$$

$$\phi = \frac{(\mu_x \hat{B}_z)^2}{(1 + \theta_x \theta_y)^4} \quad (\text{V-76})$$

The physical interpretation of Eqs. (V-71) to (V-76) has to be clarified before any power gain or loss is estimated.  $P_x$ ,  $P_{xy}$ , and  $P_y$  are the d.c. ohmic powers which are dissipated in the sample multiplier by a Hall factor  $\phi$ . This Hall factor, which is related to the mobility and the magnetic field, is the key parameter for determining the efficiency.

of converting the d.c. power into the useful r.f. power.  $P_i$  is the r.f. input power.  $V_z$  and  $B_z$  are the r.f. voltage and its corresponding magnetic field.  $V_z$  is related to  $B_y$  by a proportional constant  $b$ .

Equation (V-71) states that the power gain is proportional to the dissipated d.c. input power, and also depends upon the mobility of the sample. These are probably the two limiting factors for realizing such a Hall-effect magneto-resistance amplifier.

To check the new magneto-resistance ( $K_{xx}$ ) and transconductance ( $g_{xc}$ ), n type germanium wafers of rectangular shape were for the measurement. The wafer has the dimensions 1 cm  $\times$  1 cm  $\times$  .05 cm. The sample has a resistivity of  $25 \Omega$  cm. The electron mobility of the material is of the order of  $1400 \text{ cm}^2/\text{vs}$ . The plots of magneto-resistances and magneto-transconductances as functions of the electric potentials and the magnetic field are shown in Figs. V-7 and V-8. For comparison, measured magneto-resistances and computed ones are plotted together. The agreement is good except at high magneto resistances, which, with the Hall modulation almost equal but opposite to the magneto-resistance modulation, are very sensitive to any change of the field and the potential.

Thus, a combined mode of utilizing of Hall-Effect and magneto-resistance is achieved. The sensitivity and impedance level of this mode are much higher than that of the individual Hall-Effect and magneto-resistance. A magneto-resistance is defined as the change in the output current due to change in magnetic field divided by the input voltage which produces the change in field. The DC dependence of this magneto-transconductance and Hall-Effect resistance are reminiscent of that of the plate resistance and the transconductance of a vacuum triode.

To test the above theory of amplification, experiments are being carried out at two frequencies

(a) *A 2mc. Hall-Effect Device*

Early experiments provided the first experimental verification of this scheme. These measurements were made with two basic circuits. One as an amplifier at 2 mc the other as a down converter in the same frequency range. The results were quite encouraging, especially those of the converter case, since the presence of frequency conversion alone represents tangible and noteworthy substantiation of theoretical predictions. While considerable isolation and electronic gain were achieved the sensitivity of the circuit was still low and subject to appreciable experimental error. Consequently our present efforts are concerned with possible improvements in the experimental set-up. Several approaches are in the process of evaluation.

A new sample of InSb was prepared with the help of J. Briggs and R. Vannozzi of the Integrated Electronics Group. This sample was only .008" thick compared to the .020" of the first sample. Mounted on a thin ceramic wafer, it was inserted into a .025" gap in a ferrite ring. The d.c. resistance of the sample was improved, making the matching of the associated circuitry somewhat easier. New converter circuits were built and carefully measured to eliminate any possibility of conversion occurring in other than the desired mode, i.e., through the Magneto-Hall-Effect.

Several combinations of d.c. and a.c. auxiliary fields were explored, as well as various levels of permanent magnetic fields. These tests pointed up the need for further improvements in the design of the magnetic paths of the circuit. The ferrites which were available at the beginning of our tests imposed some definite limitations. New ferromagnetic materials with higher permeability, higher saturation flux densities, and lower losses at the desired frequency range have been obtained recently and are in the process of evaluation.

It is hoped that these ferrites, together with thinner samples of the order of .003" thickness, will eventually improve the device sensitivity.

(b) *A 4 kMc Hall-Effect Mixer*

A quarter-wavelength coaxial cavity was constructed having a .010" thick InSb sample mounted at the end of the reentrant post. The resonant frequency was 4060 MC with an air gap of .020". The measured cavity Q was of the order of 400.

Signal and local oscillator were introduced on a common loop at the low voltage end of the cavity. "IF" output was derived on a lead soldered to the center of the sample and brought out through the reentrant post.

Early measurements have indicated that the mixer has a sensitivity of -14 dbm with a L.O power of .5 watt. A piece of teflon was introduced in the cavity to fill the air gap. The resonant frequency was shifted to 3380 MC, and the sensitivity was improved by 10 db. This suggests a need to increase the coupling of the r.f. magnetic field to the sample.

**Unidirectional Tunnel Diode Amplifiers and Hall Isolators**

The purpose for which this project was undertaken was to investigate the feasibility of a nonreciprocal amplifier emerging from the combination of a tunnel diode and a Hall isolator.<sup>24</sup> Such a pursuit was justified by the fact that tunnel diode amplifiers cannot be cascaded directly due to their two-terminal bilateral nature and the instability problems associated with them as negative resistance devices. Toward this goal several Hall

isolators were constructed to be incorporated in the circuit of a typical tunnel diode amplifier intended to operate in the neighborhood of 30 MC/S. A schematic diagram of the combined circuit is shown in Fig. V-9. An overall forward gain of 2 db with an isolation of 10 db (that is, a difference in transmission between the two directions of 12 db) was recorded, but any attempt to improve these figures, especially the isolation, at higher frequencies of operation met with no success. On the contrary, the isolation demonstrated a rather rapid rate of decrease until, at about 50 MC/S, the circuit became almost bilateral. This type of behavior, not entirely unexpected, was found to be due to the isolator.

This determination started a second phase of the project, an undertaking to determine causes of isolator failure at higher frequencies to study them quantitatively and to propose possible remedies. Several more Hall isolators were constructed and after extensive testing, the following experimental evidence became available:

All of the isolators exhibited superlative isolation (as high as it could be measured with available instruments – better than 80 db) at DC and very low radio frequencies. At higher frequencies the isolation was found to deteriorate rapidly until in effect, the isolator became a bilateral network at frequencies in the neighborhood of 50 MC/S. This observation was reminiscent of the same type of failure witnessed during direct testing of the integrated tunnel diode – Hall isolator amplifier, as stated previously. Such a failure at those frequencies could not be attributed to the semiconductor of the isolators (Germanium or Indium Antimonide) but rather to the stray elements mainly capacitative inherent to the isolator by construction and coupling the input and output ports.

Figure V-10 represents the generalized form of the "practical" Hall-effect isolator which, for normal operation, is terminated in  $z_{11}$  and  $z_{22}$  at ports 11' and 22', respectively.  $z_1$ ,  $z_2$ ,  $z_3$  and  $z_4$  are the stray impedances and the rest of the circuit is what will be conventionally labeled as the "unperturbed" Hall isolator, possessing finite forward and infinite backward insertion loss.

Figure V-11 demonstrates the synthesis of the practical isolator of Fig. V-10 as parallel combination of three distinct 2-terminal-pair networks  $N_1$ , the unperturbed isolator,  $N_2$  and  $N_3$ , the stray impedance networks referred to as the "spoiling" circuits. The overall Y-matrix of the combination is the sum of the Y-matrices of the three separate component networks:

$$[Y]_{(NO)} = [Y]_{(N1)} + [Y]_{(N2)} + [Y]_{(N3)}$$

$$= \begin{bmatrix} Y_{11} & 0 \\ Y_{21} & Y_{22} \end{bmatrix}_{(N1)} + \begin{bmatrix} Y_{N2} & -Y_{N2} \\ Y_{N2} & Y_{N2} \end{bmatrix}_{(N2)} + \begin{bmatrix} Y_{N3} & Y_{N3} \\ Y_{N3} & Y_{N3} \end{bmatrix}_{(N3)}$$

$$= \begin{bmatrix} Y_{11} + (Y_{N2} + Y_{N3}) & (-Y_{N2} + Y_{N3}) \\ Y_{21} + (-Y_{N2} + Y_{N3}) & Y_{22} + (Y_{N2} + Y_{N3}) \end{bmatrix} = \begin{bmatrix} Y_{10} & Y_{20} \\ Y_{30} & Y_{40} \end{bmatrix} \dots (V-77)$$

where,  $Y_{11}$ ,  $Y_{22}$ ,  $Y_{21}$  are the driving point and transfer impedances respectively of NI,  
and  $Y_{N2} = \frac{1}{z_1 + z_2}$ ,  $Y_{N3} = \frac{1}{z_3 + z_4}$

The Z-matrix corresponding to  $[Y]_{(NO)}$  is

$$[Z]_{(NO)} = \begin{bmatrix} \frac{Y_{40}}{\det([Y]_{(NO)})} & \frac{Y_{20}}{\det([Y]_{(NO)})} \\ \frac{Y_{30}}{\det([Y]_{(NO)})} & \frac{Y_{10}}{\det([Y]_{(NO)})} \end{bmatrix} = \begin{bmatrix} Z_{10} & Z_{20} \\ Z_{30} & Z_{40} \end{bmatrix} \dots (V-78)$$

For the generalized isolator of Fig. V-11 the following expressions were derived:

1a) Input impedance as seen from port 11' with port 22' terminated,

$$z_{11} = \frac{Z_{10} z_{12} + \det([Y]_{(NO)})}{z_{12} + Z_{40}} \dots (V-79)$$

1b) Input impedance as seen from port 22' with port 11' terminated,

$$z_{12} = \frac{Z_{40} z_{11} + \det([Y]_{(NO)})}{z_{11} + Z_{10}} \dots (V-80)$$

Observe from Eqs. (V-79) and (V-80) that, for an ideal isolator (either  $Z_{20} = 0$ , or  $Z_{30} = 0$  – infinite insertion loss in either direction, finite, not necessarily zero, in the other),  $z_{11} = Z_{10}$  and  $z_{12} = Z_{40}$ , i.e., the input impedances are equal to their respective driving point impedances and are independent of  $z_{11}$  and  $z_{12}$ , even in cases when  $z_{11}$  and  $z_{12}$  are active (negative) impedances.

2a) Power Loss Ratio (PLR) in the  $1 \rightarrow 2$  direction, with port 22' terminated and port 11' driven by a source.

$$(PLR)_{1 \rightarrow 2} = \frac{\text{Power entering port 11'}}{\text{Power delivered to } z_{12}} = \left| \frac{z_{12} + Z_{40}^2}{Z_{30}} \right| \left\{ \frac{\text{Re}(z_{11})}{\text{Re}(z_{12})} \right\} \dots (V-81)$$

2b) Power Loss Ratio (PLR) in the 2+1 direction, with port 11' terminated and port 22' driven by a source.

$$(PLR)_{2+1} = \frac{\text{Power entering port } 22'}{\text{Power delivered to } z_{11}} = \left| \begin{array}{c|c} z_{11} + Z_{10}^2 & Re(z_{12}) \\ \hline Z_{20} & Re(z_{11}) \end{array} \right| \quad (V-82)$$

3) Isolation in db's

$$\text{Isol (db's)} = 10 \log_{10} \left\{ \left| \begin{array}{c|c} z_{11} + Z_{10}^2 & Re(z_{12}) \\ \hline Z_{20} & Re(z_{12}) \\ \hline z_{12} + Z_{40}^2 & Re(z_{11}) \\ \hline Z_{30} & Re(z_{12}) \end{array} \right| \right\} \quad (V-83)$$

The last expression is of importance. Its form can be simplified considerably under special conditions without invalidating the more basic conclusions to which the original expression Eq. (V-83) leads. For example, in the case of a symmetrical unperturbed isolator ( $Y_{11} = Y_{22}$ ), considering  $z_{11} = z_{12}$  (which would be the case if  $z_{11}$  and  $z_{12}$  were the image impedances of the 2-terminal-pair network of the said isolator), one obtains

$$\text{Isol (db's)} = 20 \log_{10} \frac{Z_{30}}{Z_{20}} = 20 \log_{10} \left| \frac{Y_{30}}{Y_{20}} \right| \quad (V-84)$$

But it is concluded from either Eq. (V-83) or (V-84) that the isolation becomes optimum (infinite) when  $Z_{20}$  or  $Y_{20}$  becomes zero. From Eq. (V-71), letting  $Y_{20} = 0$ , the following condition for optimum isolation is obtained.

$$\left. \begin{array}{l} Y_{N2} = Y_{N3} \\ \text{or} \\ z_1 + z_2 = z_3 + z_4 \end{array} \right\} \quad (V-85)$$

Therefore, the mere existence of stray impedances does not necessarily affect the isolation provided that condition Eq. (V-85) is satisfied. This condition has been simulated with lumped impedances  $z_n$  ( $n = 1 \dots 4$ ) for isolation measurements made around 30 Mc/s. Typical values of isolation measured are in the neighborhood of 40 db's.

At this point it was felt as quite appropriate to test the above conclusions with practical Hall isolators in the VHF domain by employing strip-line techniques. The purpose of this venture is two-fold: First, to the best of our knowledge, comparative work which has been done so far with practical Hall isolators is pretty well limited to the lower radio frequencies. Second, high efficiencies (low insertion loss in the order of 2 to 1 db's) are possible with multicontact Hall isolators<sup>25</sup>, and results to substantiate this are avail-

able at lower frequencies. On the other hand, condition Eq. (V-85) can be closely approximated in triplate structures due to the symmetrical placement of the semiconductor wafer with respect to the ground planes.

Figure V-12 represents a 4-Contact Hall isolator in strip line designed for operation at 600 Mc/s. The design is a tentative one, but the main ideas were incorporated in it. Because of the four-terminal nature of the isolator, the ordinary 2-ground-plane triplate geometry is not directly applicable. Instead, 3-ground-plane triplate lines are employed. The strip lines shown in the sketch are of such length and characteristic impedance as to effect proper impedance matching and phase relation. The construction of this isolator is presently under way. Meanwhile, the continuity performance of simple transitions between center strips of single triplate lines is being investigated, since knowledge about such transitions will be immediately employed in the construction of the isolator.

## VI. GERMANIUM AND GALLIUM ANTIMONIDE TUNNEL DIODES

### A. GERMANIUM TUNNEL DIODES

#### Introduction

In contrast to most alloyed pn junctions, the properties of tunnel diodes can depend greatly on the recrystallized region under the alloyed dot. Figures VI-1 and VI-2 illustrate why this is so. Figure VI-2 represents the densities of four components, germanium, gallium, arsenic and thallium as a function of distance from a previously molten alloy front. This front had been penetrating from a thallium-arsenic dot into a gallium-doped germanium wafer and consisted of these four ingredients in the concentrations depicted at the far right of the figure. Before a sudden or quench cooling cycle, a 1-second diffusion at 700°C was assumed to take place. The same doping profile, however, might also have arisen from longer times at lower temperatures.

The effect of diffusion during the cooling cycle was to move the pn junction back toward the recrystallized region. Consequently the metallurgical variables which control the doping profile in the recrystallized region take on increased importance. The effects of such variables as alloying phase composition, alloying ambients, time, and temperature will now be considered in turn.

#### Alloying Phase Composition

Some of the limitations and fabrication difficulties of tunnel diodes can be circumvented by alloying with doped thallium dots. Thallium is unique among the useful "carrier" metals in that it forms low melting point alloys with high dopant concentrations (above 10%). This property allows it to alloy to semiconductors and produce a junction region doped to the solubility limit of both thallium ( $10^{17}/\text{cc}$ ) and of the dopant it carries. The dopants (Mg, Zn, Cd, As, P, Sb, S, Se, Te) will far outnumber the larger less soluble thallium ions in the recrystallized semiconductor. (Figure VI-2). The electrical properties of this region (and any subsequently diffused junction) will depend on the dopant rather than the thallium.

Utilizing dopants alone, without carrier metal would sacrifice the reproducible alloying of a dot which melts while standard fluxes are still liquid and able to clean the surfaces during the initial spreading and wetting. Moreover, most of the dopants have

unfavorable melting points, vapor pressures, malleability, and surface films. Utilizing other carrier metals than thallium furnishes a much lower dopant concentration for a similarly low melting point, or a much higher melting point for the same concentration. While these are satisfactory for many purposes, thallium alloy junctions should have the advantage wherever the highest concentration is wanted in a recrystallized region. With thallium-arsenic dots even the most highly gallium doped crystal available ( $4 \times 10^{20}/\text{cc}$ ) has given peak to valley current ratios of better than 3 to 1. Under optimum alloying conditions these dots have given current ratios up to 7.5., and current-to-capacitance ratios greater than  $1 \text{ ma}/\mu\mu\text{f}$ . Since these latter measurements were on low doped crystals fired were on low doped crystals fired above  $600^\circ\text{C}$ , significant improvement may be anticipated.

A eutectic alloy of 30% antimony in thallium with a  $195^\circ\text{C}$  mp has given tunnel diodes on highly gallium-doped germanium ( $1-2 \times 10^{20}/\text{cc}$ ) when heated to  $760^\circ\text{C}$ . The antimony solubility apparently is greatly enhanced over its Ge:Sb equilibrium value. Another novel eutectic alloy of 27% gallium in bismuth has given tunnel diodes on the most highly arsenic-doped germanium ( $4 \cdot 10^{19}/\text{cc}$ ). Unfortunately, both this and the more standard 3% gallium in tin are too brittle to provide good dots. A ternary alloy of tin, bismuth and gallium of  $120^\circ\text{C}$  mp was found more malleable than the above, and also gave tunnel diodes. The presence of tin here and in most tunnel diode alloys seems to break up the semiconductor surface at lower temperatures than other alloys do.

### Alloying Ambients

The ambient or fluid in which alloying takes place can either serve to clean or to contaminate the recrystallized region. Ordinarily the alloy dot is given a liquid flux ambient which serves to remove films, such as solid oxides, that might interfere with spreading and wetting. Most of these evaporate before the final alloying temperature is attained and thus expose the dot to a gaseous ambient during the final stages.

With thallium-arsenic dots it has been found that notably poorer diodes have been obtained when divalent atoms such as Cu, Zn, or Mg are contained in the ambient. Both Divco fluxes #229 and 335 have been analyzed and found to contain Zn. It has been noticed that alloying in encapsulations containing copper yields poorer peak-to-valley current ratios than are obtained on unencapsulated diodes utilizing no flux (or pure glycerin). Near the solubility limits of the dominant impurities we know that the solubility of these unfavorable impurities are enhanced.<sup>26</sup>

Above  $600^\circ\text{C}$  our thallium-arsenic dots were found to flux themselves by forming a second, clear yellow arsenic-rich phase which floats around the metallic phase. In pure

hydrogen, the formation of arsine ( $\text{AsH}_3$ ) gas prevents this, so that better diodes are obtained below  $550^\circ\text{C}$ . In nitrogen or argon, the best peak to valley current ratios are obtained between  $600^\circ\text{C}$  and  $800^\circ\text{C}$  and occur wherever this yellow coating is most noticeable. (Fig. VI-3). Spectroscopic analysis of this coating and the underlying dot, revealed them to be pure arsenic and the arsenic-thallium eutectic. (.81..19), respectively. This is the equilibrium expected from the phase diagram of Mansuri<sup>27</sup>.

### Temperature and Time Experiments

Once the choice of a favorable ambient and composition of alloy dots is made it remains to determine the desired alloying temperature and time. Heating cycles which give the best peak to valley current ratio are in general different from those giving maximum current density and hence frequency response (cf. Pt II).

Time effects were investigated by fabricating diodes at a constant temperature and measuring the same diodes after successive time increments. Temperature effects were similarly characterized for constant time intervals at sufficiently large temperature increments. Peak and valley current measurements have been performed in this manner. Although second order "history" effects are undoubtedly present, the relatively broad maxima obtained compared to the test intervals justified the procedure. These effects and deviations in area and doping would dominate all others if different junctions were used instead.

A single crystal of germanium doped with  $1.2 \times 10^{20} \text{ Ga/cc.}$  was sliced perpendicularly to the 111 axis. After sufficient etching to remove surface damage, a single slice was cut into 40 mil squares, and placed directly upon a tungsten foil heater strip above a welded thermocouple. Thallium-arsenic 5 mil cylinders were placed atop each unit and they were heated in a controlled atmosphere. Figures VI-3, VI-4, and VI-5 show the results obtained.

The diminution of peak current at long times and high temperatures is undoubtedly due to a diffusive broadening of the junction depletion layer. The well known exponential behavior of tunneling current may be restated in terms of the donor and acceptor doping levels,  $N_A$  and  $N_D$ , thru their effect on this depletion width

$$I \propto \exp - \text{Const} \frac{1}{N_A} + \frac{1}{N_D}^{\frac{1}{2}}$$

The increase of solubility into, and then later the increase of diffusion with higher temperature, apparently can produce the maxima in the curves of Figure VI-3 and VI-4.

A preliminary factorial design experiment was used to determine degradation of units fabricated in the low inductance "sandwich" structure (Fig. VI-5). Three variables were considered cooling time, orientation, (alloy dots atop or under the opposite-doped pellet) and pellet-preheating. (A private communication from E. Hockings of RCAL indicated that highly-doped samples would give fewer free electrons after annealing).

Cooling time changes gave the only significant results, indicating that quenching always produced the better units. Impurity segregation effects in addition to diffusion and reactions are important when the alloying time is comparable to the time to cool to approximate 40°K. below the maximum temperature<sup>28</sup>. In such a case the junction which has diffused slightly ahead of the metallurgical junction (Fig. VI-1) may diffuse back out and disappear entirely. Because of segregation effects during the cooling cycle, the high density liquid impurity source is replaced by an epitaxial layer of much lower density. (Fig. VI-2). The very thin indiffused layer apparently drops rapidly in density when it can diffuse in both directions. Several rough approximations can be used to estimate whether these conditions will be present. At the metallurgical junction there exists a planar diffusion source of constant density  $N_0$  equal to the solubility in the semiconductor. If the liquid alloy is only a fraction ( $f$ ) saturated, the epitaxial layer will be regrown with a lower density of  $fN_0$ . If this is far lower than the original base doping  $N_D$ , the junction can disappear entirely during a slow cooling cycle.

Observations on germanium tunnel diodes indicate that the valley current is increased more drastically than the peak current is decreased for the above-mentioned conditions. (Fig. VI-6). Since both currents are thought to tunnel across the same barrier, it must be assumed that somehow the density of valley tunneling sites is increased. If a reaction is assumed to take place between donors and acceptors this divergent behavior of peak and valley currents can be explained. (Appendix A). Experiments have been performed indicating that such sites are probably formed by a reaction between gallium and arsenic when they diffuse together in the depletion region of a tunnel diode as it is fabricated.

These experiments show that overcooking a tunnel diode at alloying temperatures initially decreases the peak current but increases the valley current (Fig. VI-6). Since both these tunneling currents vary monotonically with the width of the depletion layer and the band gap, we are forced to assume that the density of levels in the impurity band giving rise to excess current has increased near the junction by a diffusion mechanism. It seems a plausible hypothesis that the impurity band may be due to products of reactions of the form  $\ell + mD + nV \rightarrow A\ell D_m V_n$  where  $\ell$ ,  $m$ , and  $n$  may be 0, 1, 2...,  $A$ ,  $D$ , and  $V$  are acceptors, donors, and vacancies respectively. General continuity equations may be written for the density change of each species. For only one reaction and product these will be

the sum of a diffusion, a dissociation, and a recombination reaction term. Because of the slow diffusion of vacancies, and the low frequency factor for multiple collisions, a reasonable guess would be that a "simple collision" between one Ga and one As by diffusion populates the impurity band and would give a profile similar to the shaded region of Figure VI-2 (bottom left).

This figure shows conditions under which the junction may actually diffuse back into the distribution of impurity band levels. Here this would occur when the inflection point of the arsenic distribution passed through the gallium concentration (i.e., the junction) under the double in-then out-diffusion conditions of junction heating then cooling. Before cooling, an "infinite" arsenic source exists at  $x = 0$ , which corresponds to the inflection point until cooling. During cooling, the epitaxially recrystallized germanium would become an arsenic sink, probably with a larger diffusion constant because of vacancy inclusions.

An experiment designed to test the hypothetical diffusion gradients in Figure 4 vindicated these speculations as follows. Unmounted units were made by alloying the same 3% gallium dots (of Figure VI-6) to arsenic-doped germanium at 655°C for ten seconds, quenching and testing. These data were compared to data obtained after reheating the same units to 625°C for ten more seconds and quenching. The alloy interface under these latter conditions was shallower (since less germanium was soluble in the alloy) so that recrystallized germanium remained to provide a sink for out-diffusing gallium. Recycling a number of times gave the following correlation between the last equilibrium temperature and the peak to valley ratio.

TABLE VI-1

POSTULATED CONDITION AT $x=0$	TEMPERATURE	NORMALIZED AVERAGE CURRENTS			TOTAL TIME BEFORE TEST
		$I_p/I_v$	$I_v$	$I_p$	
Ga source	655°C	3.5	.29	1	10 sec
Ga sink	625°C	1.15	.87	1	20
Ga sink	625°C	1.1	.74	.81	30
Ga source	655°C	1.9	.31	.588	40
Ga source	655°C	1.6	.25	.4	50
Ga sink	625°C	1	.28	.28	60
Ga source	655°C	1.33	.30	.40	70
Ga source	655°C	1.25	.20	.25	80

The drop in the ratio whenever a gallium sink existed at  $x = 0$  seems to be due to jumps in the valley or excess current. This supports the contention that the junction is

moving back into an increasing distribution of impurity centers of the nature of a GaAs V complex, whenever a gallium sink appears at  $x = 0$ . The opposite movement is expected whenever a gallium source is brought to  $x = 0$ .

## B. GALLIUM ANTIMONIDE TUNNEL DIODES

### Introduction

A consideration of the tunnel diode equivalent circuit in Fig. VI-7 will show that the useful frequency range of tunnel diodes can be increased in either of two ways. First the diode conductance ( $G$ ) can be increased to exceed the shunt susceptance up to higher gain-bandwidth products ( $G/2\pi C$ ). Secondly, the series reactance can be decreased below the diode impedance to prevent excess power storage near the LC resonant frequency. These limitations are superimposed on the familiar LC impedance chart in Fig. VI-8. The diode capacitance on the abscissa is dependent mainly on the junction diameter within the small doping range illustrated. The gain bandwidth product (on the slant ordinate) is in one-to-one relation with the doping density for any given material. In gallium antimonide the relation favors higher frequencies than germanium. The two parameters of reduced junction area and higher doping are the ones which must be pushed to achieve better tunnel diode frequency response once the material is chosen.

A closer look at the tunnel diode equivalent circuit (Fig. VI-7) allows a more accurate calculation of the frequency behavior, which is seen to be closely related but not always equal to the two frequencies plotted in Fig. VI-8. When the tunnel diode is biased away from its peak or valley current into the negative resistance region its self-resonant frequency  $f_s$  decreases from  $f_s = \frac{1}{2\pi\sqrt{LC}}$  to

$$f_s = \sqrt{\frac{1 - \frac{LC}{(RC)^2}}{2\pi\sqrt{LC}}} = \sqrt{1 - \left(\frac{G}{2\pi f_s C}\right)^2} \quad (\text{VI-1})$$

in which  $f_s$  and  $G/2\pi C$ , the gain bandwidth produce are given on Fig. VI-8.

The cutoff frequency above which negative resistance disappears is a function of series resistance  $r_s$

$$f_{co} = \left( \frac{\frac{R}{r_s} - 1}{2\pi R C} \right)^{\frac{1}{2}} \quad (\text{VI-2})$$

For junctions of small radius  $R'$  compared to base thickness  $r_s$  will vary inversely with  $R'$ , while  $G = \frac{1}{R}$  and  $C$  will vary directly with  $R'^2$ . These considerations point to the fact

that the cutoff frequency will asymptotically improve as  $(1/R)^{1/2}$ . Hence, it is desirable to reduce the junction area for both high frequencies and for high impedances.

Welded-point junctions, and small dot etching and mounting techniques are suggested by this last consideration. Novel materials such as gallium antimonide will lead to lower noise as well as higher frequencies. These general considerations then outline the course pursued in this investigation.

### Procedure and Results

Tunnel diodes have been made on tellurium-doped antimonide ( $1.7 \times 10^{18}/\text{cc}$ ) by two methods:

1) Welding junctions by passing a capacitor discharge of known energy through a point contact.

2) Alloying small junctions in flowing hydrogen under controlled time and temperature cycles similar to germanium units. Low melting point eutectic alloys of tin with zinc or cadmium have been successful by both methods.

Figure VI-9 shows typical changes in peak and valley currents up reheating diodes made with tin-zinc eutectic alloy dots. (mp. 198°C). The heating and cooling cycles were similar to those shown in Fig. VI-10 in terms of thermocouple potential (roughly linear with respect to temperature). Probably because of the short heating times, the valley currents have risen comparatively high during the cooling cycle. Note that the maximum current densities (and hence gain-bandwidth products) occur at significantly lower temperatures than the best peak to valley ratios. On the basis of the maximum cross-sectional area of the alloy dot, significantly higher gain-bandwidth products have been calculated for these units (Fig. VI-8 right side). Welded zinc points have given almost as favorable results with ratios up to 3 to 1.

Poorer current densities but better ratios have been found so far using tin-cadmium (mp. 177°C) eutectic dots. Figure VI-11 shows how fast these are degraded even at a low alloying temperature. Peak to valley current ratios up to 7 have been obtained with momentary heating cycles at higher temperatures. Gain-bandwidth products near 5 kmc have been calculated on the basis of apparent junction cross-sectional area.

### Interpretation of Results

Degradation of valley current appears similar to that of germanium units. Faster diffusion and lower doping in this material may cause this. Less reproducibility of results is attributed to material which is single crystal only over small areas. Under slightly higher

tellurium doping, patches of gallium telluride are apparently formed to drive the material polycrystalline. Other n-type dopants experience similar difficulty. Mobility and hence cutoff frequency are therefore reduced in the latest higher-doped units.

### C. APPENDIX - A GENERAL MODEL FOR THE SOURCE OF TUNNEL DIODE VALLEY CURRENT

#### Introduction

Dissipation in the positive resistance in shunt or series with any semiconductor junction can mask its nonlinear characteristic. In most diodes, these resistances are not directly related to the primary nonlinear effect. However, in tunnel diodes, a close relationship does exist in that both the negative and positive resistance regions are produced by the tunneling phenomena.

In all junction diodes holes flowing toward the junction on the p-type side recombine with electrons flowing toward the junction on the n-type side. In an ordinary forward-biased diode these carriers diffuse an appreciable distance from the junction during their "lifetime" before recombining through various centers. In the tunnel diode, a similar recombination path can account for tunneling between electrons and holes held at different energy levels by an applied voltage beyond the valley region. The kinetics of the possible formation of any such centers under the usual fabrication conditions will be explored. The implications involved will be seen to bear light on the behavior of tunnel diode currents under operating conditions.

Tunnel diode alloy processes seek to dissolve germanium from a highly doped base wafer and recrystallize an epitaxial layer of the opposite type to form as abrupt a junction as possible, without introducing or creating valley current recombination centers. Such centers might be formed by reactions of the type,



in which  $l$ ,  $m$ , and  $n$  may each be 0, 1, 2/..., and  $D$ ,  $A$ , and  $V$  are donors, acceptors, and vacancies respectively. General continuity equations may be written for the density charge of each species. These will be given in general by the sum of diffusion, dissociation and recombination reaction terms.

$$\frac{dN_{DAVd}}{dt} = \nabla \cdot (D_{DAVd} \nabla N_{DAVd}) + k_r N_D^{l'} N_A^m N_V^n - k_d N_{DAVd} \quad (\text{VI-4})$$

$$\frac{dN_D}{dt} = \nabla \cdot (D_D \nabla N_D) - \sum_r l_r k_r N_D^{l,r} N_A^{m,r} N_V^{n,r} + \sum_d l_d k_d N_{DAVd} \quad (\text{VI-5})$$

$$\frac{dN_A}{dt} = \nabla \cdot (D_A \nabla N_A) - \sum_r m_r k_r N_D^{l,r} N_A^{m,r} N_V^{n,r} + \sum_d m_d k_d N_{DAVd} \quad (\text{VI-6})$$

$$\frac{dN_V}{dt} = \nabla \cdot (D_V \nabla N_V) - \sum_r n_r k_r N_D^{l,r} N_A^{m,r} N_V^{n,r} + \sum_d n_d k_d N_{DAVd} \quad (\text{VI-7})$$

in which  $N_{DAVd}$  is the concentration of species  $D_l r A_m r V_n r$ , with recombination rate constant  $k_r$ , and dissociation rate constant  $k_d$ ;  $N_D$ ,  $N_A$ , and  $N_V$  refer to the donor, acceptor, and vacancy densities respectively.

These equations can be simplified by a number of practical considerations. If a planar diffusion on source with negligible edge effects is assumed, the divergence and gradient reduce to simple derivatives. Moreover, the diffusion transport of compound species in a semiconductor lattice must be negligible in comparison to that of single atoms and vacancies. The diffusion of vacancies, on the other hand, is so fast, that their density will be given essentially by the solubility limit.<sup>26,29</sup>

Because of the smaller probability of multiple collisions and because of the repulsion of like ions, it can be assumed that only the reaction between a single donor and single acceptor are appreciable ( $\ell_r = m_r = n_r = 1$ ). If the reverse dissociation reaction is negligible because of a highly unfavorable activation energy, the density of the valley-current-carrying centers can be given by

$$N_{DAV}(x) = k_{r0} \int_0^t N_D N_A \exp\left(-\frac{\Delta H_r}{kT_i} dt\right) \quad (\text{VI-8})$$

in which  $k_{r0}$  is the collision frequency factor and  $\Delta H_r$  is the activation energy of the donor-acceptor pairing reaction. The increasing valley current of higher-doped diodes would be due to variation of  $N_{DAV}$  with the product of  $N_D$  and  $N_A$ .

For short times we might expect negligible perturbation of the standard diffusion profiles (Fig. VI-11 – Fig. VI-2). Initially diffusion is fast compared to the reaction. Then p-alloys on n-semiconductors would have  $N_D \approx N_{DO} \operatorname{erf} x/(4D_D t)^{1/2}$  and  $N_A \approx N_{AO} \operatorname{erfc} x/(4D_A t)^{1/2}$  within a factor of about two because of either ambipolar diffusion effects, as well as varying boundary conditions. Here  $N_{AO}$  is the acceptor solubility limit and  $N_{DO}$  the base doping. The case for n-alloys on p-material simply reverse the above subscripts.

*A* and *D*. For the small activation energies expected the exponential in Eq. (VI-1) approaches one and is easily calculable. Profiles with a maximum of  $N_{DAV}$  between the metallurgical and the stoichiometric junction are obtained under the boundary conditions of Fig. VI-2. Should a diffusion sink for both constituents be obtained at slightly lower than maximum temperatures, this maximum density of valley-current carrying centers might start to catch up with the tunneling barrier (Fig. VI-1). This mechanism could explain much of the observed behavior.

After long times diffusion profiles similar to Fig. VI-12 would be obtained to give an essentially heterogeneous reaction, occurring at plane  $x$ . The reaction ultimately becomes fast with respect to the diffusion. The base dopant is brought to the plane at a rate of  $\approx N_{DO} (D_D / t)^{1/2}$ , and the alloyed dopant must arrive at the equal rate  $N_{AO} D_A / x$ . The reaction plane therefore moves as  $x \approx t^{1/2}$ , finally leaving a constant density  $N_{DAV} = N_{DO}$  deposited behind this plane. The minimum  $N_{DAV}$  that exists somewhere between here and the initial maximum found in the first part would give a junction with maximum peak to valley ratio. Thus the behavior (Figs. VI-6, VI-11) of tunnel diode currents with alloying time can be understood.

## REFERENCES

1. S. Bloom and K.K.N. Chang, *Parametric Amplifiers Using Low-Frequency Pumping*, J. Appl. Phys., Vol. 29, p. 594, March 1958.
2. S. Bloom and K.K.N. Chang, *Theory of Parametric Amplifiers Using Non-Linear Reactances*, RCA Review, Vol. 18, pp. 578-593, Dec. 1957.
3. K.K.N. Chang, *Analysis of a Four-Terminal Parametric Amplifier*, RCA Review, Vol. 20, pp. 205-221, June 1959.
4. F.E. Terman, *Radio Engineers Handbook*, McGraw Hill Company, 1943, p. 196.
5. P.K. Tien, *Parametric Amplification and Frequency Mixing in Propagating Circuits*, J. Appl. Phys., Vol. 29, p. 1347, Sept. 1958.
6. C.L. Cuccia, K.K.N. Chang, *The Helix Parametric Amplifier - A Third Solid-State Microwave Amplifier*, RCA Review, Vol. 22, June 1951.
7. Johnson, Slager and Kiney, *Millimeter Waves from Harmonic Generators*, Rev. of Scientific Instruments, March 1954.
8. J.M. Manley and H.E. Rowe, *Some General Properties of Nonlinear Elements*, Proc. IRE, Vol. 44, p. 904.
9. K.K.N. Chang, *Harmonic Generation with Nonlinear Reactances*, RCA Review, Sept. 1958.
10. S. Kita, *A Harmonic Generator by Use of the Nonlinear Capacitance of Germanium Diode*, Proc. IRE, Vol. 46, June 1958.
11. L. Esaki, *New Phenomenon in Narrow Ge p-n Junctions*, Phys. Rev., Vol. 109, p. 603, 1958.
12. A.W. Hull, *Description of the Dynatron*, Proc. IRE 6, 5, (1918).
13. E.W. Herold, *Negative Resistance and Devices for Obtaining It*, Proc. IRE, 23, 1201, (1935).
14. H.S. Sommers, *Tunnel Diodes as High Frequency Devices*, Proc. IRE, July 1958.
15. K.K.N. Chang, *Low-Noise Tunnel-Diode Amplifier*, Proc. IRE, July 1959.
16. B. VanDerPol, *Non-Linear Theory of Electric Oscillations*, Proc. IRE, Vol. 22, p. 2051, Sept. 1934.
17. N.W. McLachlan, *Ordinary Non-Linear Differential Equations*, Oxford at the Clarendon Press, 1956.
18. D. Nelson, RCA Laboratories, private communication.
19. A. VanDerZiel, *Noise*, Prentice-Hall 1956, p. 249.
20. K.K.N. Chang, G.H. Heilmeier, H.J. Pruger, *Low-Noise Tunnel Diode Down Converter Having Conversion Gain*, Proc. IRE, Vol. 4, May 1960.
21. L.J. Giacopietto and J. O'Connell, *A Variable Capacitance Germanium Junction Diode for UHF*, RCA Review, Vol. 17, p. 68, March 1956.
22. J. Berghammer and S. Bloom, *On the Non-Conversion of Noise Parameters in Multi-Velocity Beams*, J. Appl. Phys. 32, 454 (1960).
23. S. Goldman, *Transformation Calculus and Electrical Transients*, Prentice-Hall, Inc., New York, pp. 396-415.
24. R.F. Wick, *Solution of the field Problem of the Germanium Gyrorator*, Jour. Appl. Phys., Vol. 25, p. 741, June, 1954.

25. G. Arlt, *Hall Effect - Vierpole Mit Hohen Wirkungsgrad*, Solid-State Electronics, Pergamon Press, 1960, Vol. 1, pp. 75 - 84, and also Digest of Technical Papers, 1961 International Solid-State Circuits Conference, pp. 8-9.
26. Shockley W. Moll, J. Appl. Phys. 119, 5, 1480, Sept. 1, 1960.
27. Q.A. Mansuri, J. I. Metals 28, 453, 1922.
28. Schover K. Pihl J. Electrochemistry Society 108, 6, 552, June 61.
29. Unfortunately, this is a function of doping as well as temperature. C.F. Valenta, and Ramsey M.W. Phys. Rev. 106, 1, 73, April 1, 1957, and R.A. Logan Phys. Rev. 145, 1454, 1956.

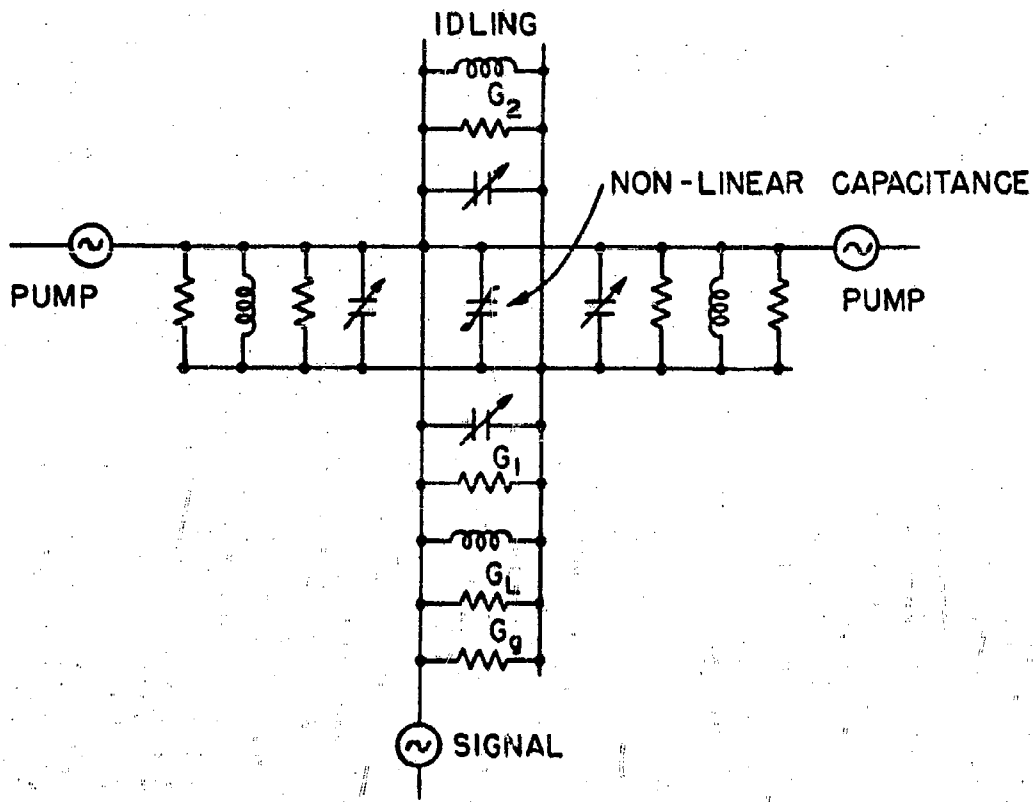


FIG.II-1. EQUIVALENT CIRCUIT OF A NONLINEAR-CAPACITANCE PARAMETRIC AMPLIFIER CONTAINING TWO PUMP CIRCUITS RESONANT AT  $\omega_3$  AND  $\omega_4$ , AN IDLING CIRCUIT AT  $\omega_2 = \omega_3 + \omega_4 - \omega_1$ , AND A SIGNAL CIRCUIT AT  $\omega_1 < \omega_3, \omega_4$ .

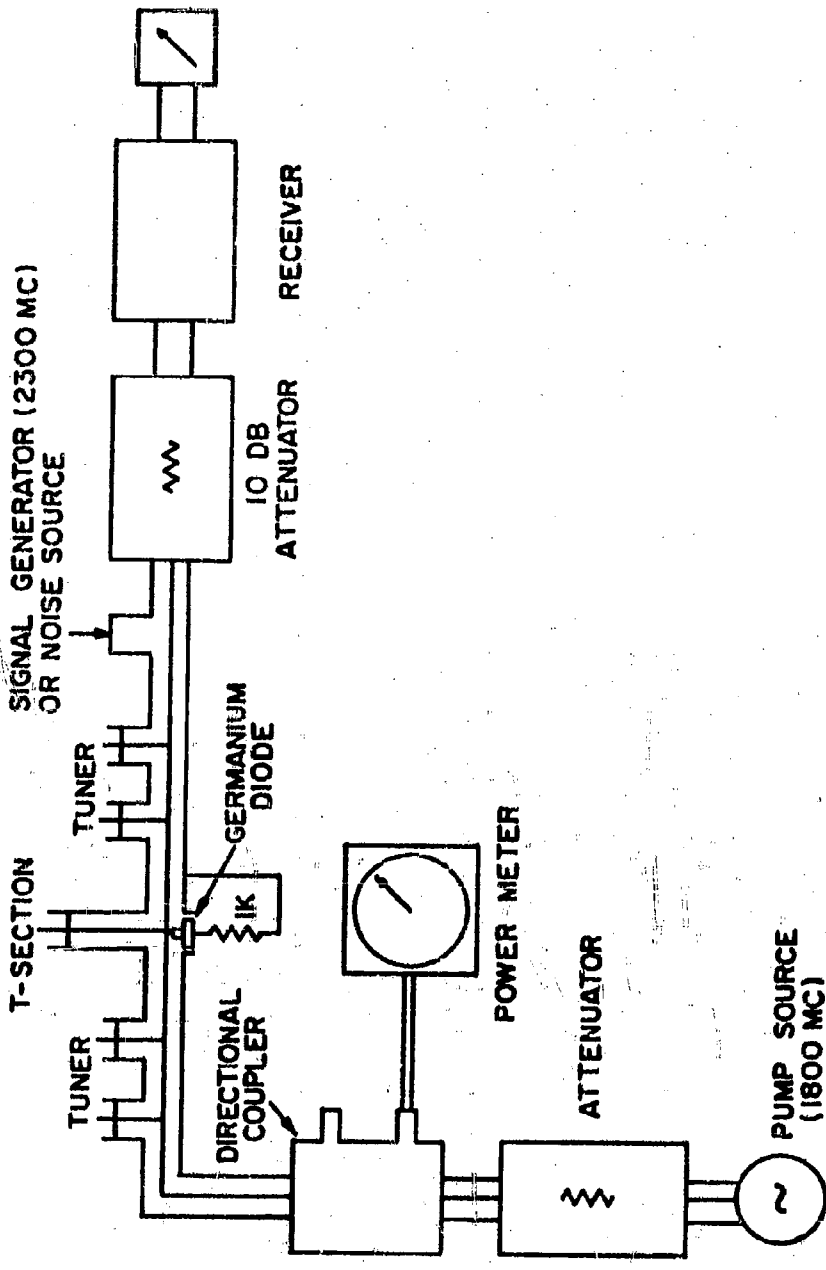
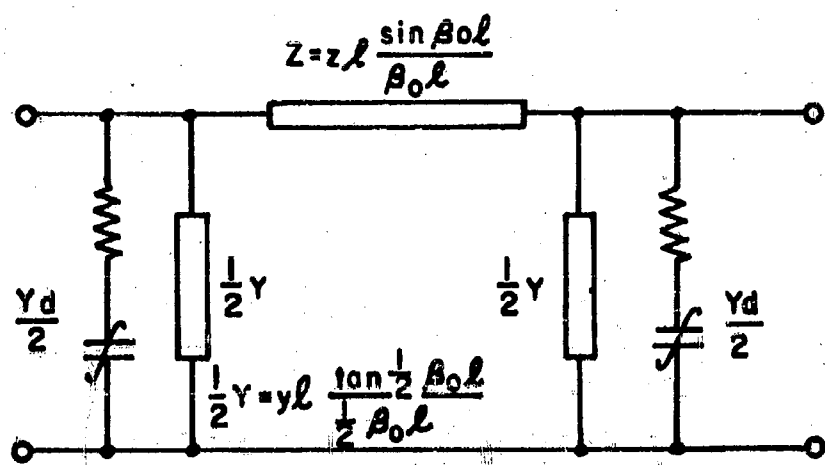
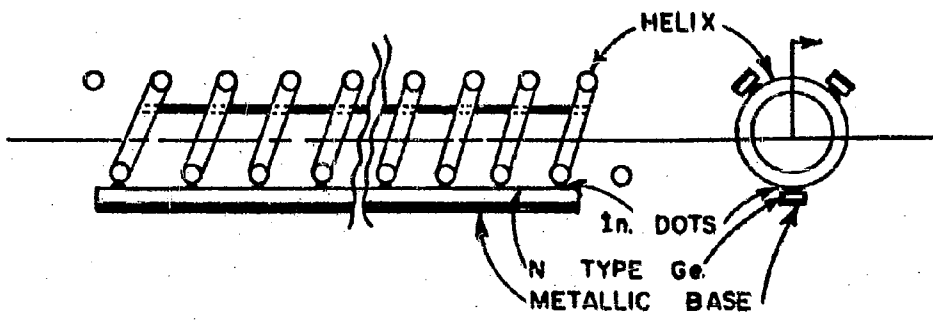


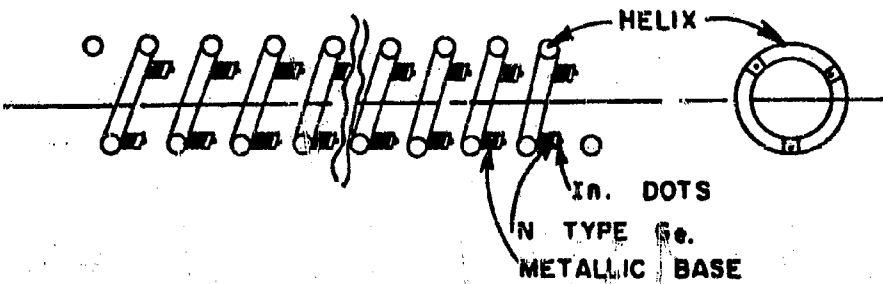
FIG. II - 2. NOISE FACTOR MEASUREMENT ON AN S-BAND PARAMETRIC AMPLIFIER USING LOWER FREQUENCY PUMPING.



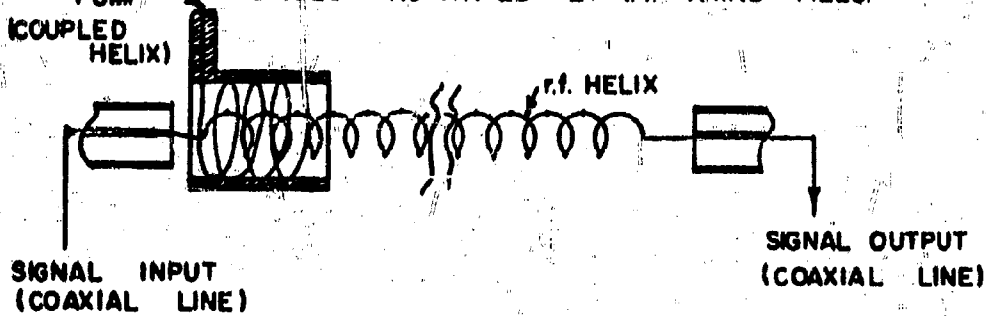
**FIG. II-3. EQUIVALENT NETWORK OF A SMOOTH TRANSMISSION LINE LOADED WITH SEMICONDUCTOR DIODES.**



(a.) HELIX LINE INCORPORATED WITH DISTRIBUTED JUNCTION DIODES ACTIVATED BY r.f. RADIAL FIELD



(b.) HELIX LINE INCORPORATED WITH DISTRIBUTED JUNCTION DIODES ACTIVATED BY r.f. AXIAL FIELD.



(c.) HELIX LINE INCORPORATED WITH r.f. INPUT AND OUTPUT CIRCUITS.

**FIG.II-4. HELICAL-LINE TRAVELING-WAVE PARAMETRIC AMPLIFIER**

44305

FIG. II-5 S-BAND HELIX - TYPE PARAMETRIC AMPLIFIER



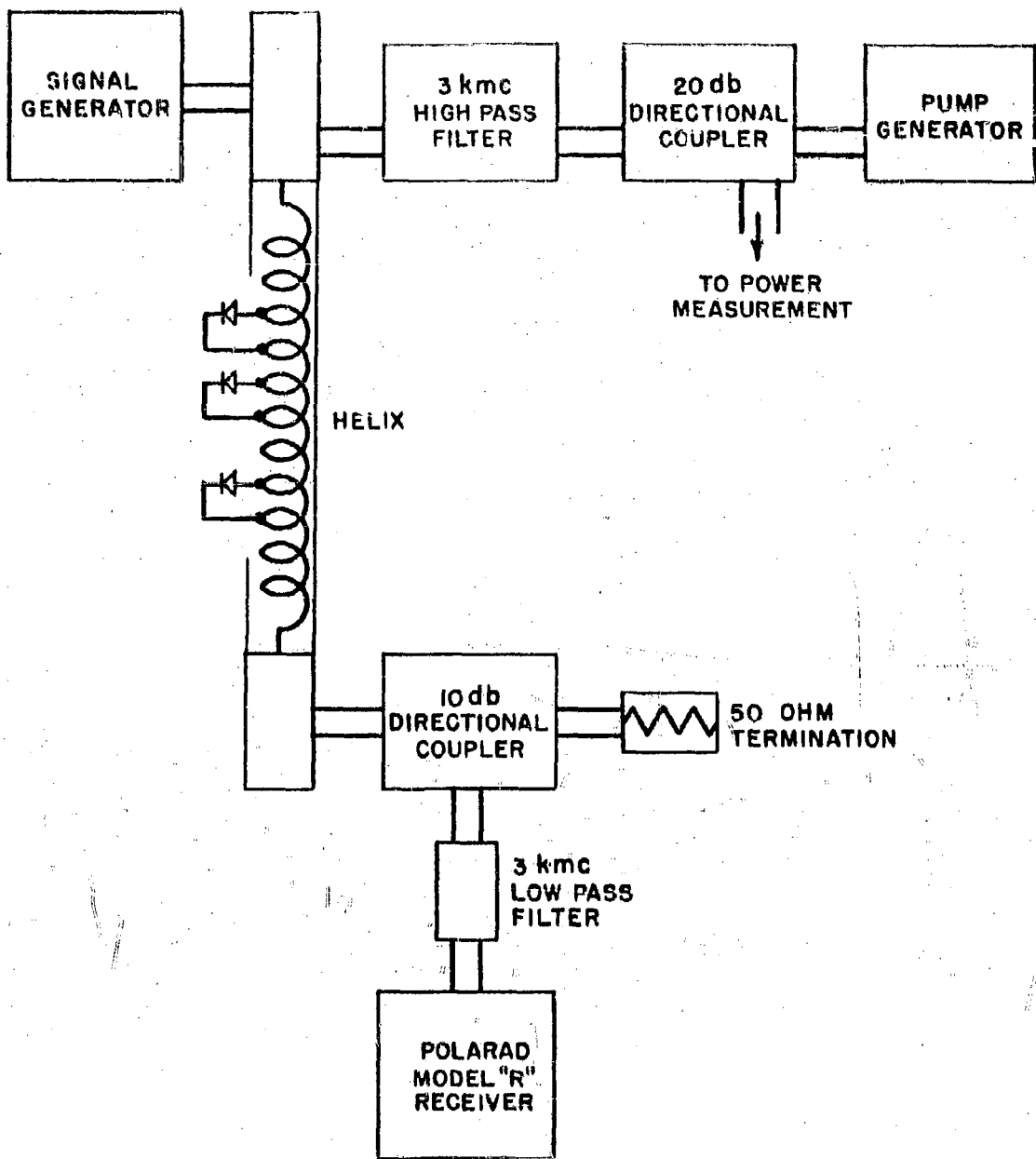
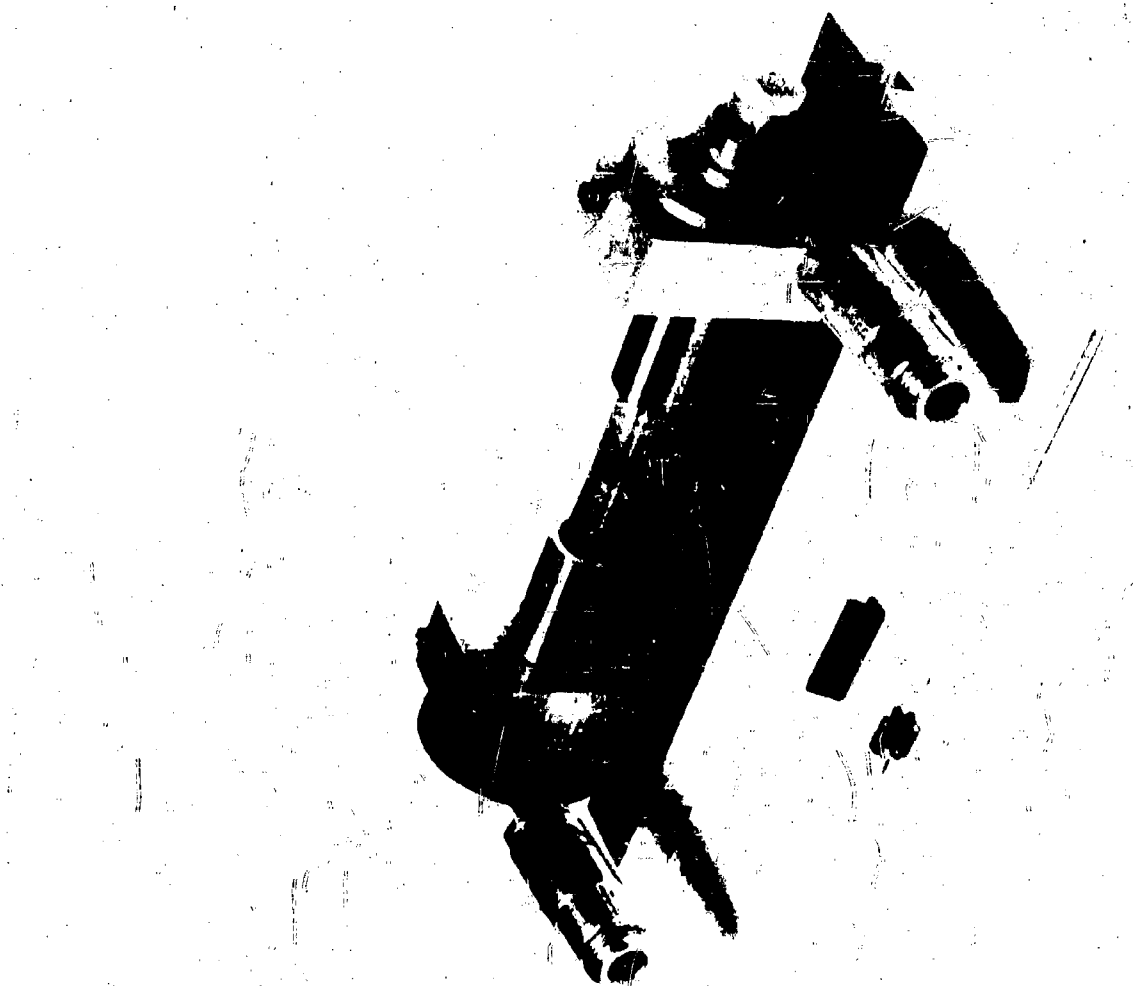


FIG. II-6. SCHEMATIC OF TEST SET - UP

4 2 1 3 0

FIG. II-7 L-BAND HELIX TYPE PARAMETRIC AMPLIFIER



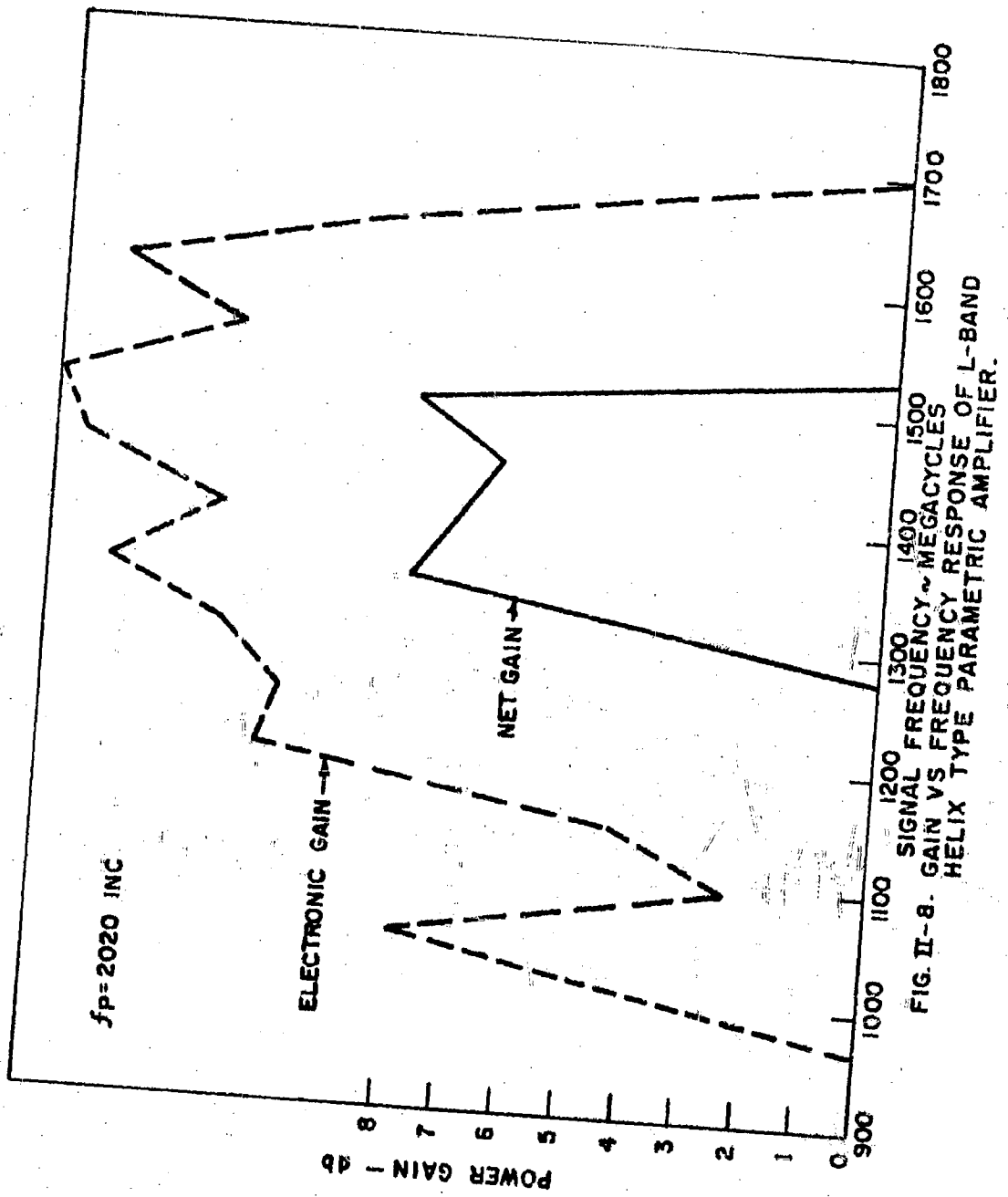


FIG. II-8. GAIN VS FREQUENCY - MEGACYCLES  
HELIX TYPE PARAMETRIC RESPONSE OF L-BAND  
AMPLIFIER.

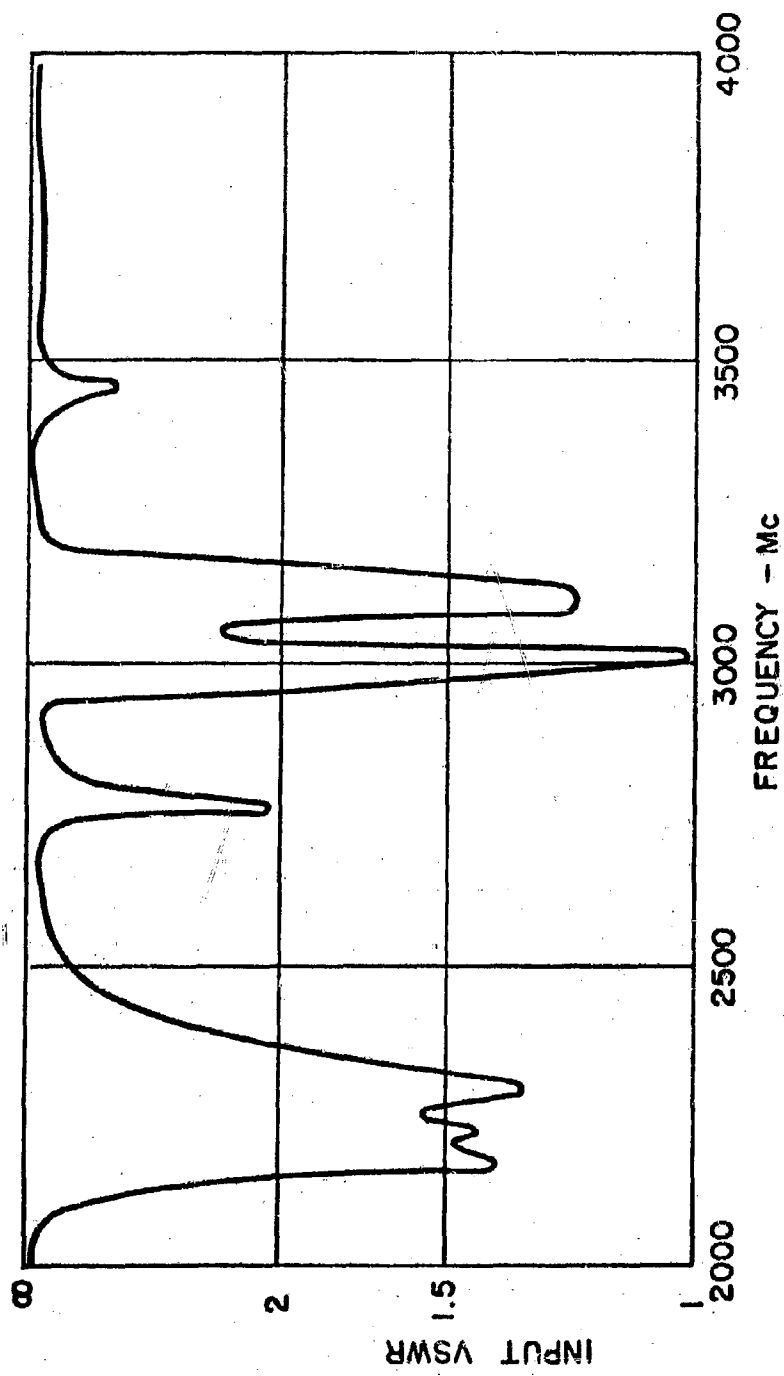


FIG.II-9. INPUT VSWR AS A FUNCTION OF FREQUENCY FOR THE HELIX STRUCTURE PERIODICALLY LOADED BY THREE DIODES AND  $Q = 0.5$

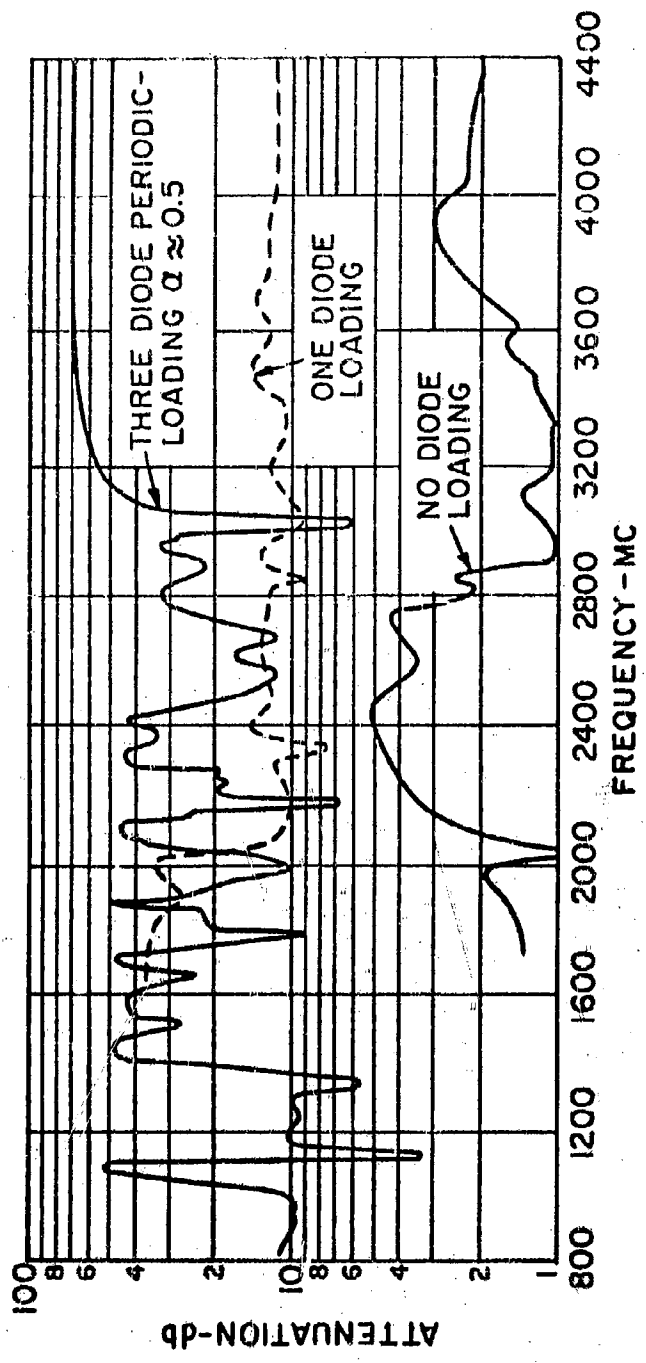


FIG. II-10. ATTENUATION AS A FUNCTION OF FREQUENCY FOR HELIX  
FOR DIFFERENT LOADING CONDITIONS.

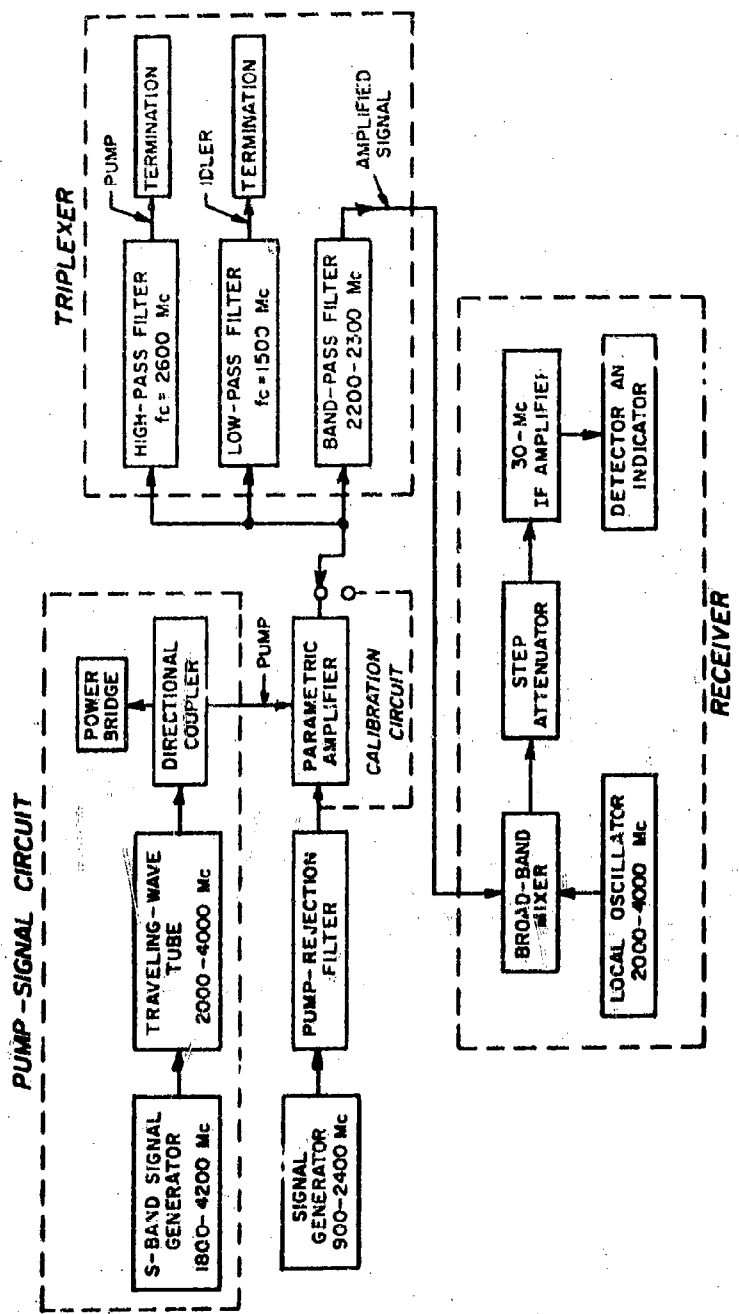


FIG. II-11. BLOCK DIAGRAM OF THE CIRCUIT USED FOR TESTING THE GAIN CHARACTERISTICS OF A HELIX PARAMETRIC AMPLIFIER FOR THE FREQUENCY BAND 2200 TO 2300 MEGACYCLES.

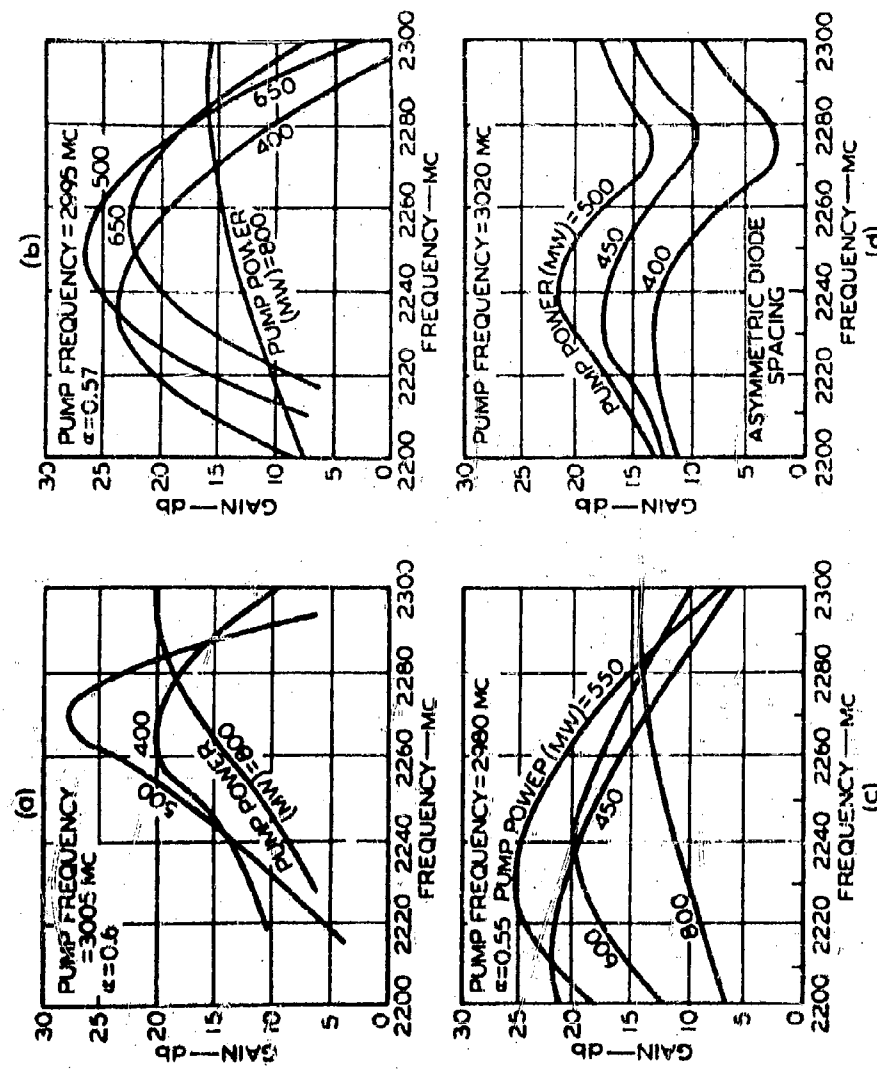


FIG. II-12. GAIN AS A FUNCTION OF FREQUENCY FOR SEVERAL FIXED VALUES OF PUMP POWER

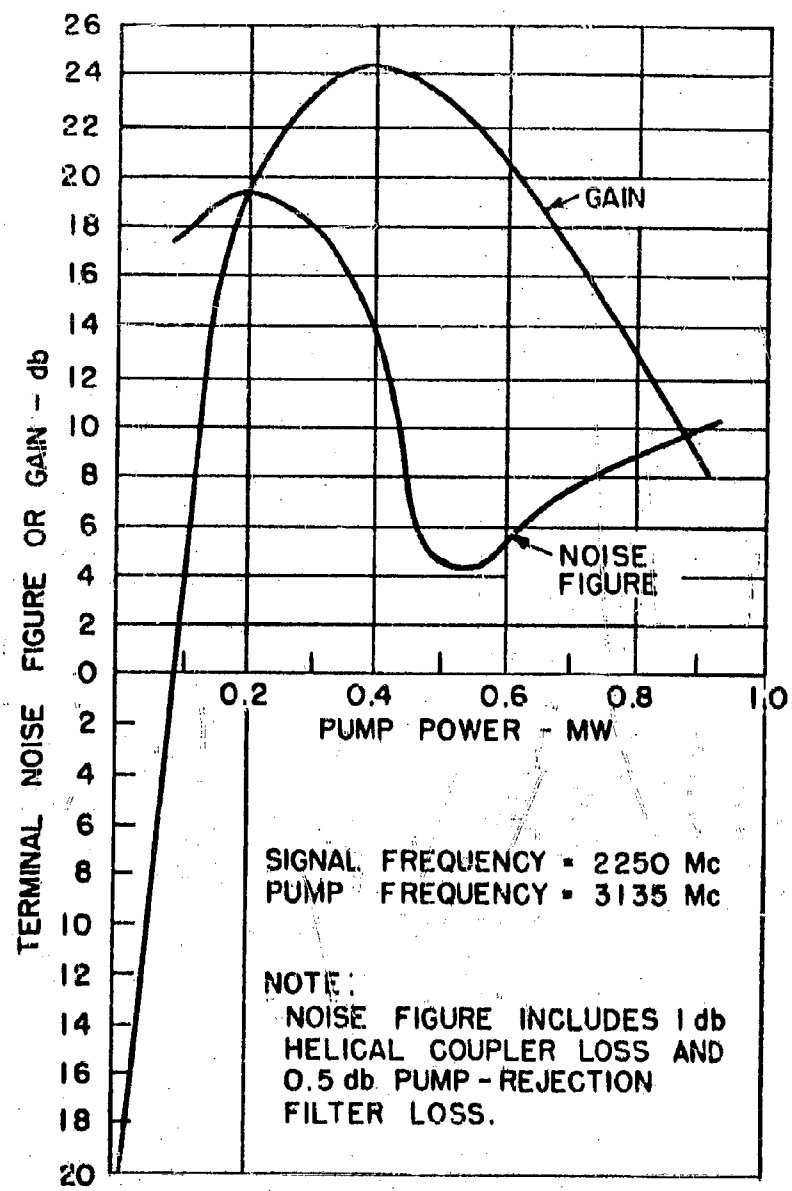


FIG.II - 13. NOISE FIGURE AND GAIN AS A FUNCTION OF PUMP POWER FOR A HELIX PARAMETRIC AMPLIFIER.

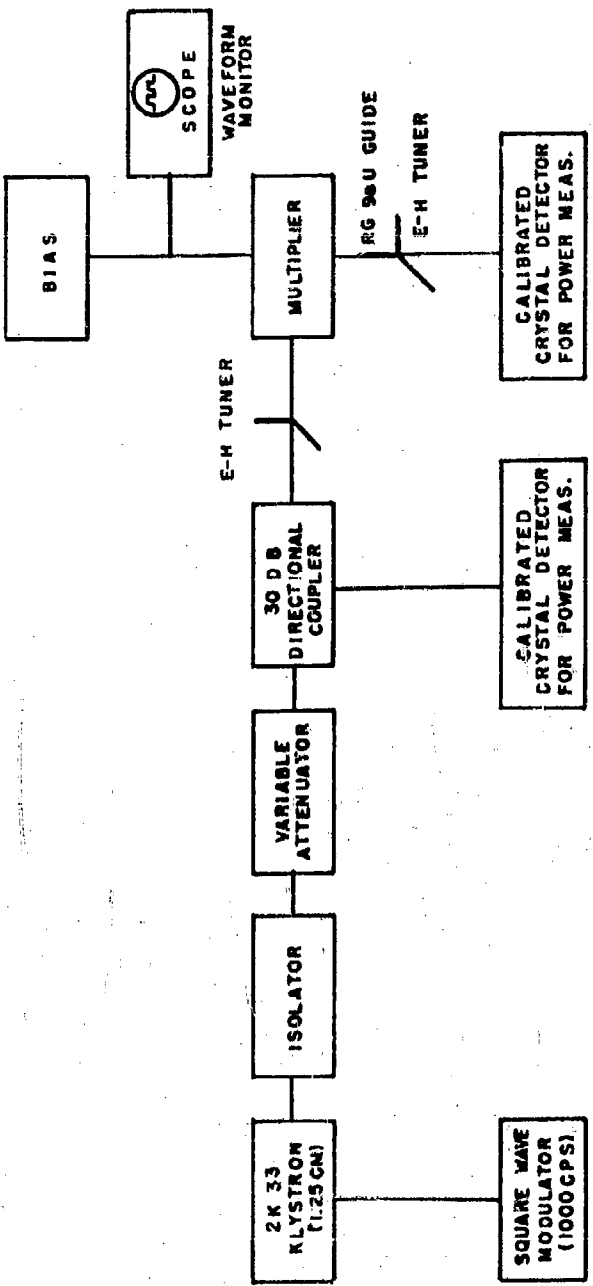
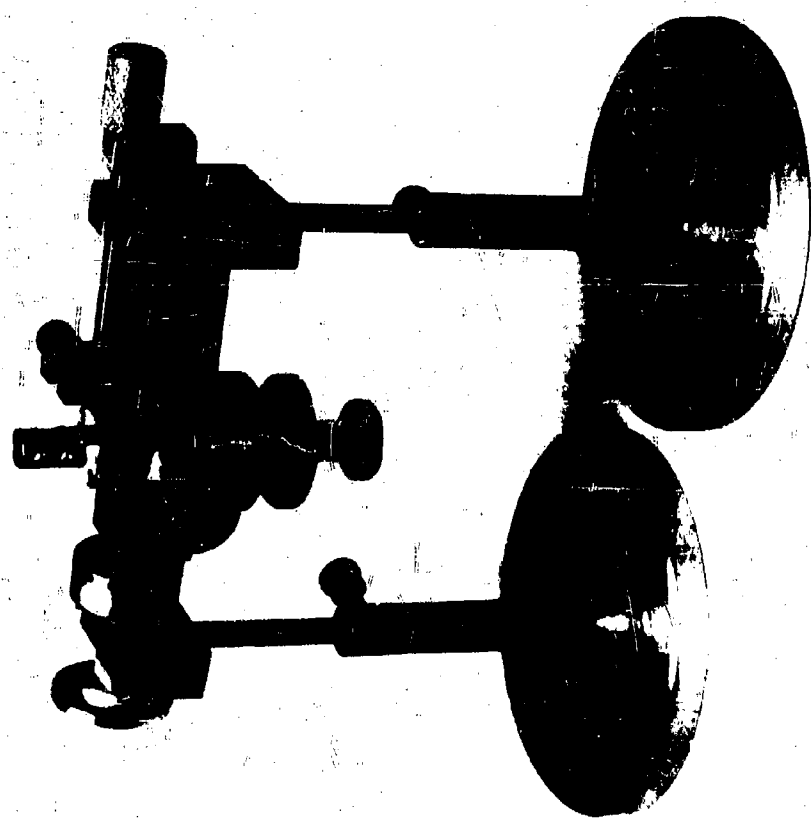


FIG. II-14. BLOCK DIAGRAM OF MEASURING APPARATUS

313302

FIG. II -15 HARMONIC GENERATOR



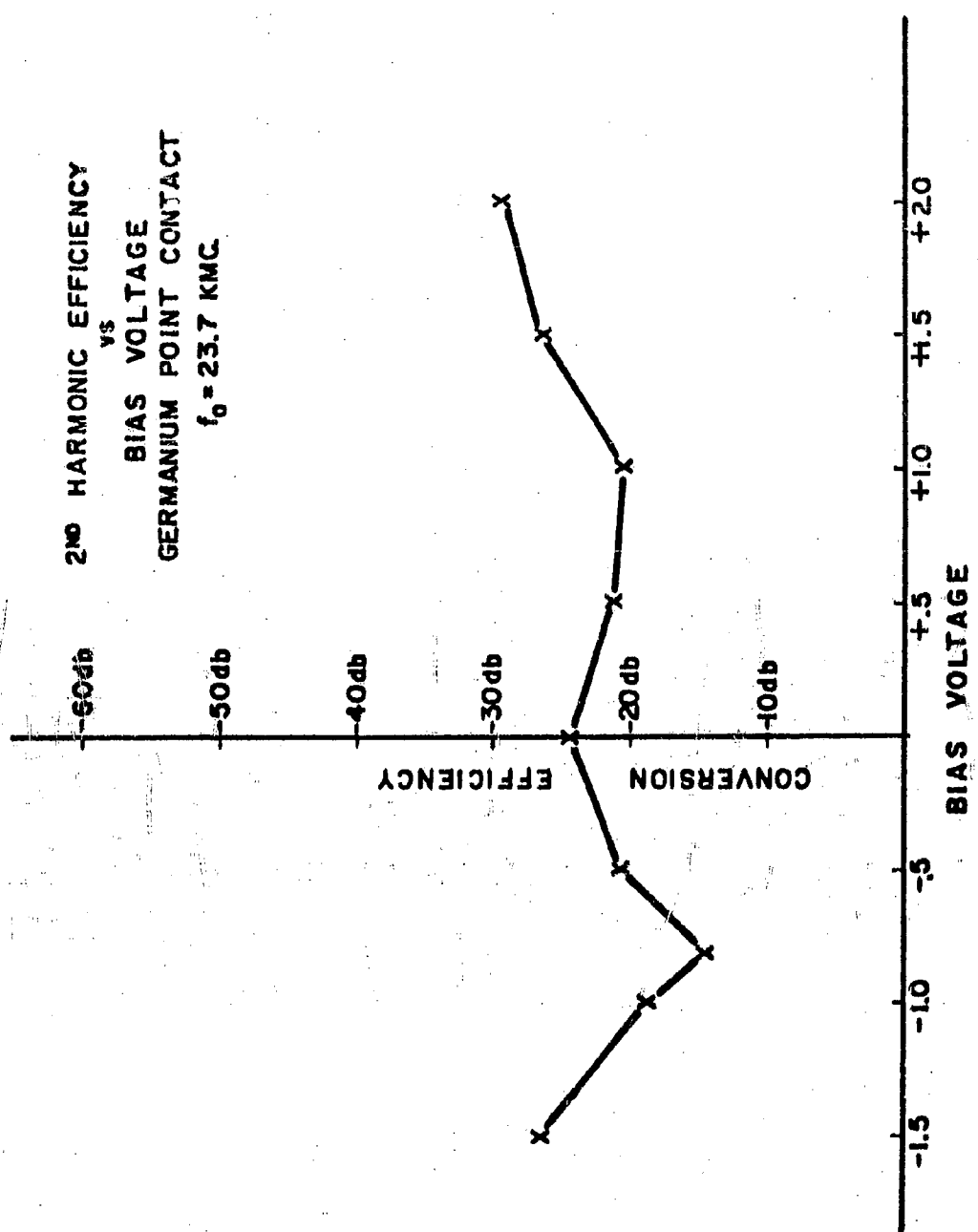


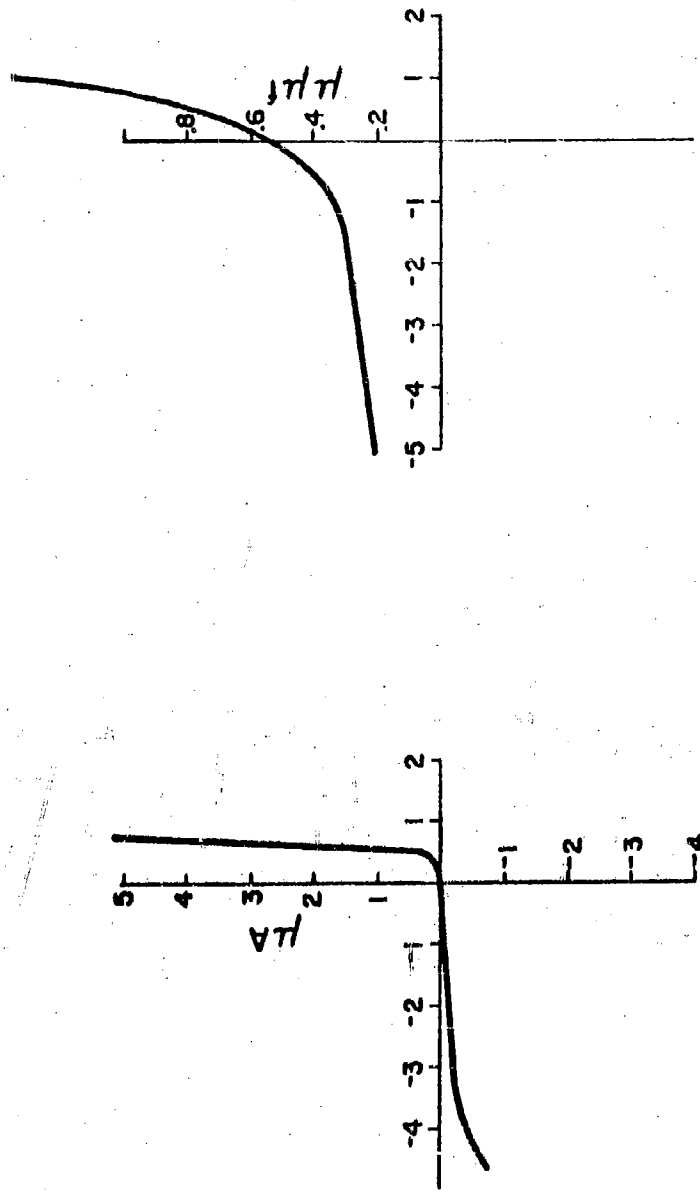
FIG.II-16

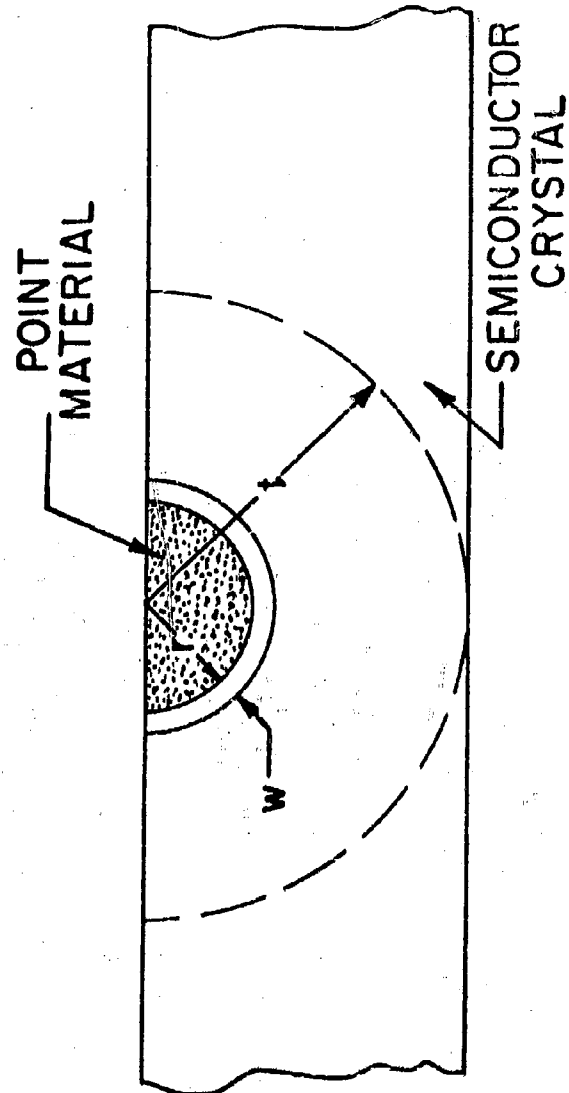
TYPICAL CHARACTERISTICS OF A GALLIUM ARSENIDE POINT CONTACT DIODE

CAPACITANCE ( $\mu\mu\text{f}$ ) vs. VOLTAGE

CURRENT vs. VOLTAGE

FIG. II-17





$$C = \frac{2\pi r^2}{w} K$$

$$R = \int_r^t \frac{\rho dr}{2\pi r^2} = \frac{\rho}{2\pi} \left( \frac{1}{r} - \frac{1}{t} \right)$$

**WHERE :  $t$  = CRYSTAL THICKNESS**

**w = BARRIER WIDTH**

**r = RADIUS**

FIG. II-18

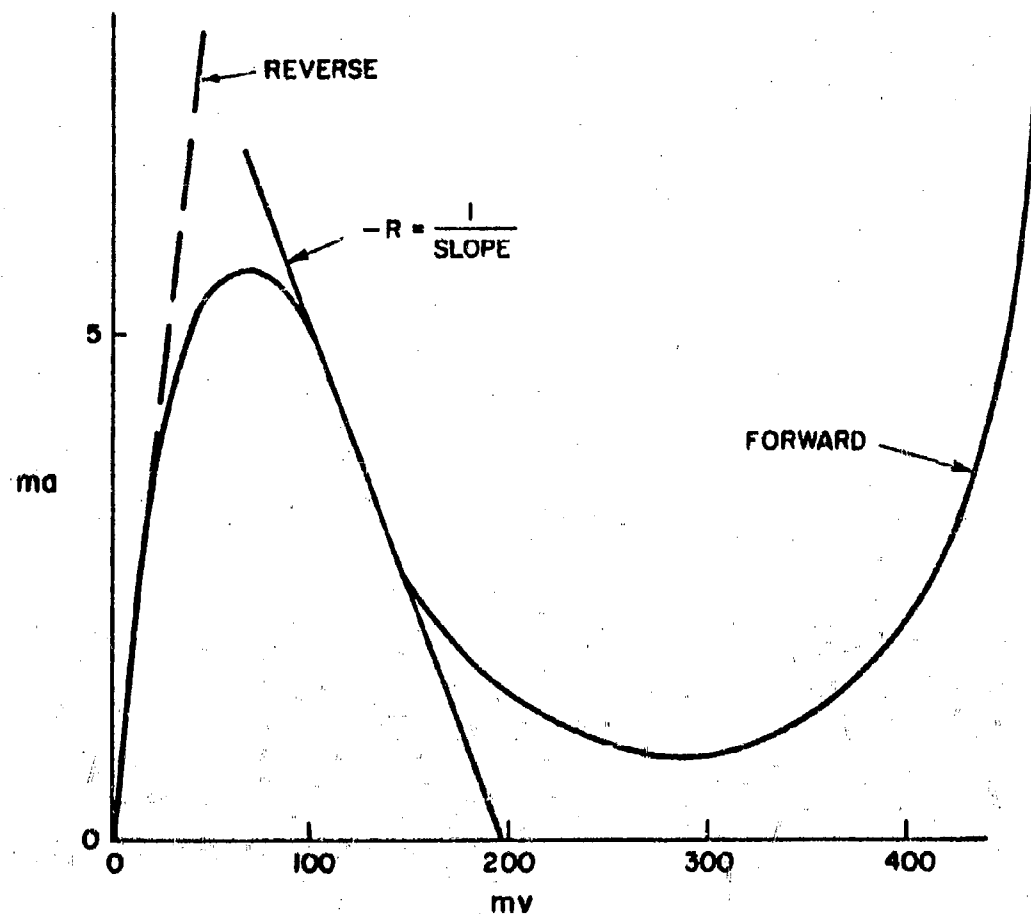


FIG. III-1. I-V CHARACTERISTIC OF TUNNEL DIODE

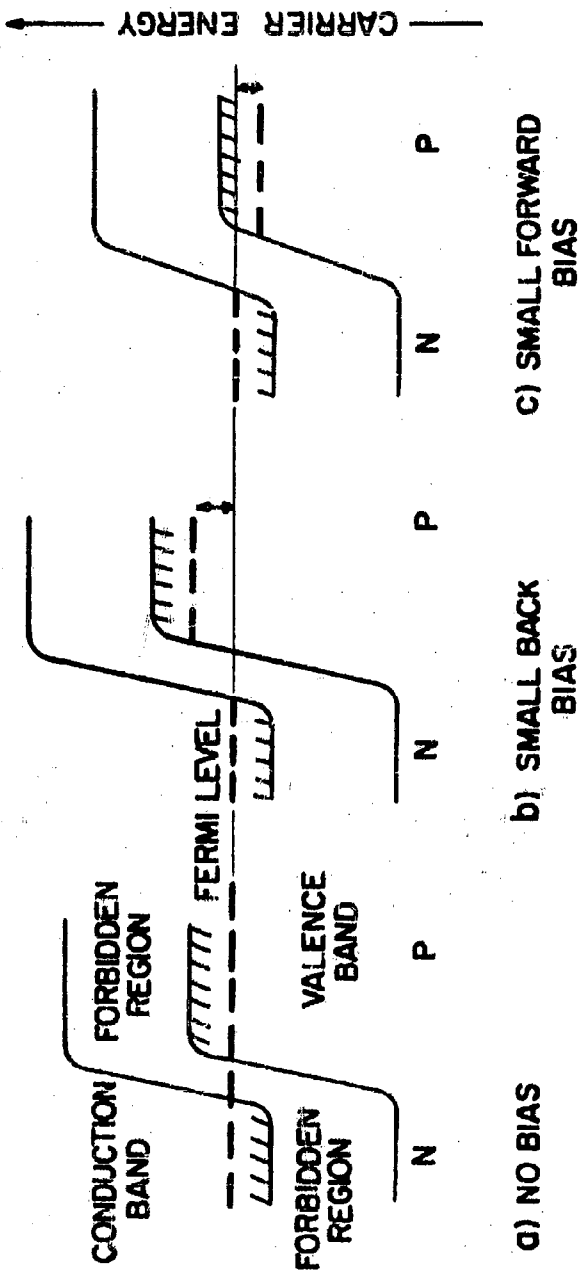


FIG. III-2. ENERGY BAND OF TUNNEL DIODE

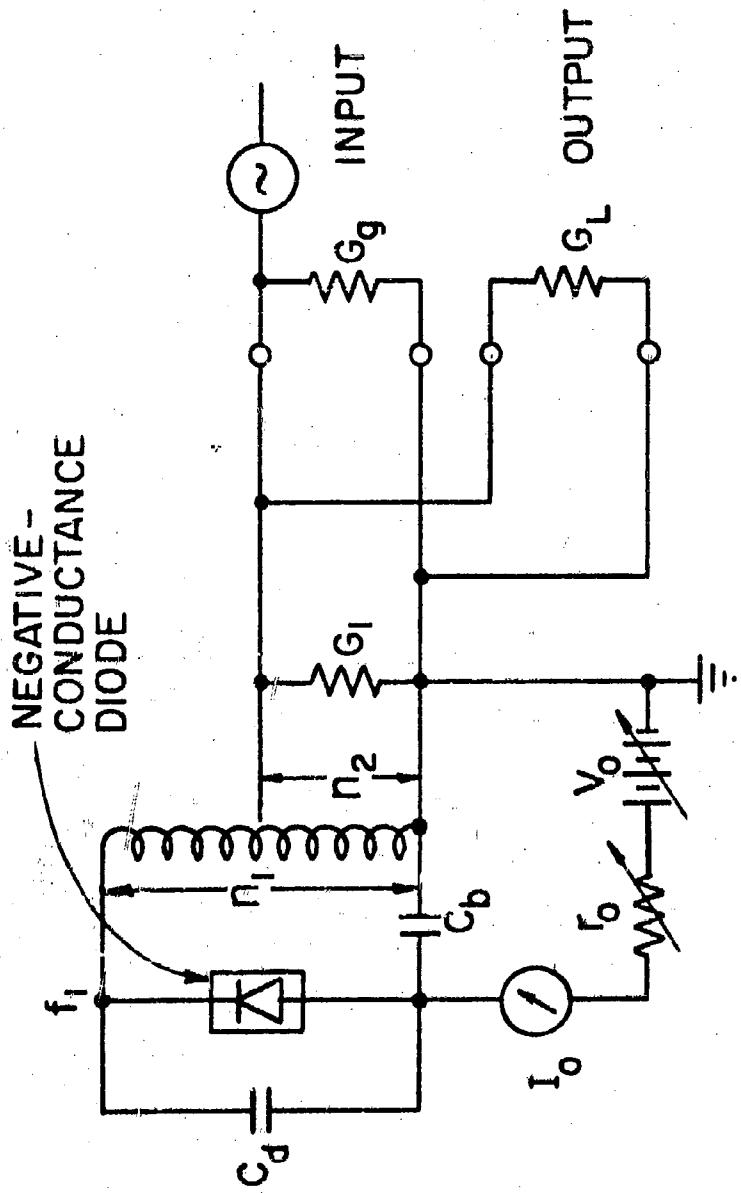


FIG. III-3. TUNNEL - DIODE AMPLIFIER CIRCUIT.

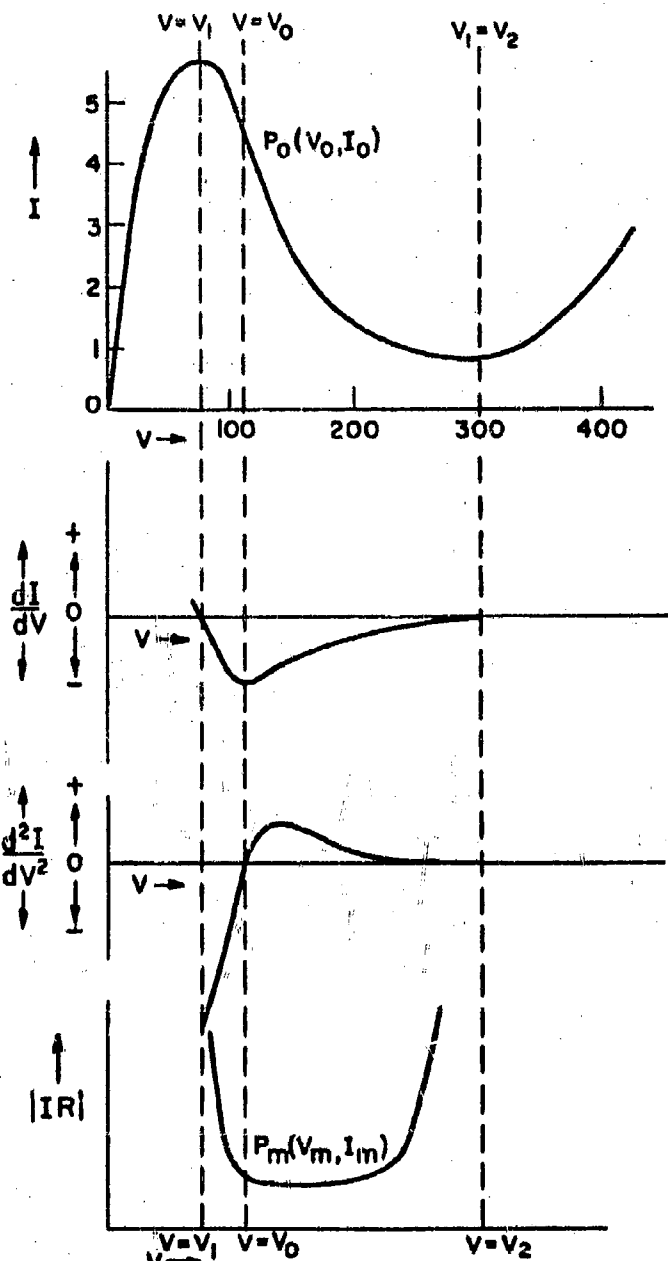
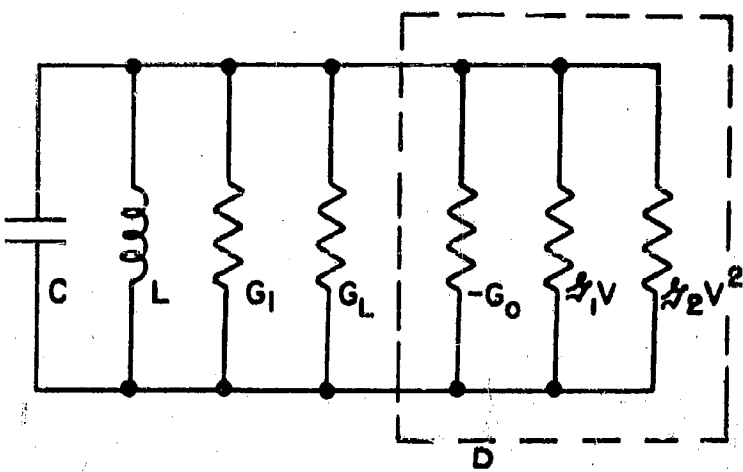


FIG.III-4. I-V CHARACTERISTIC OF TUNNEL DIODE



**FIG. III- 5 OSCILLATION CIRCUIT**

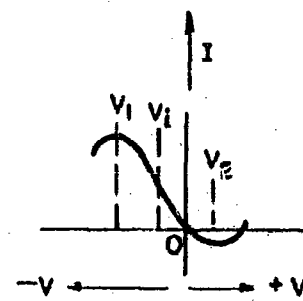


FIG. 6a I-V CURVE OF NEGATIVE CONDUCTANCE DEVICE

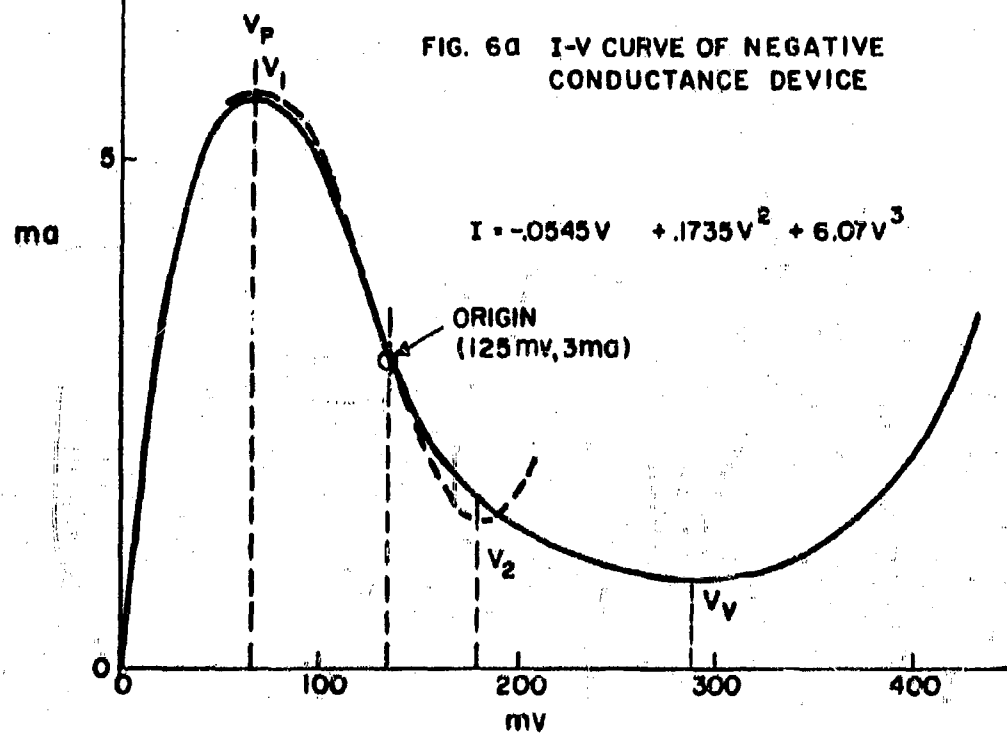


FIG. III-6. I-V CHARACTERISTIC OF TUNNEL DIODE

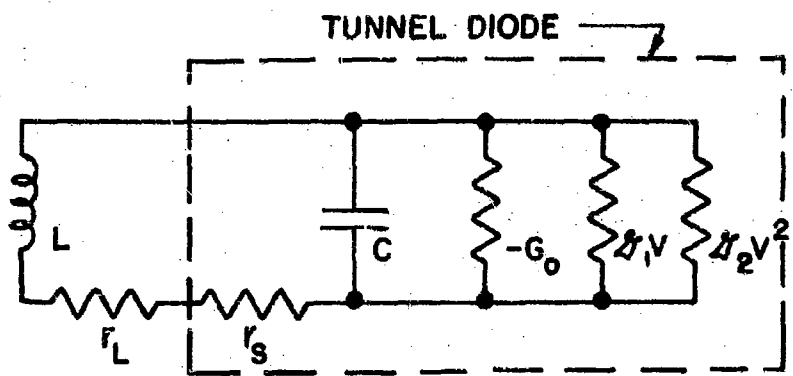
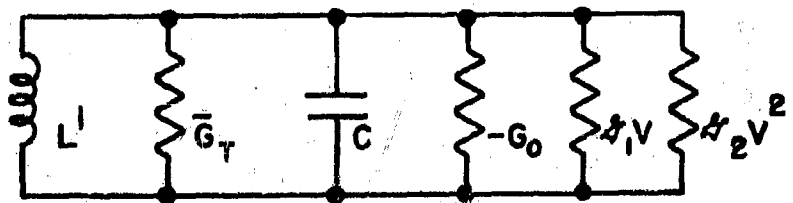


FIG. III - 7. TUNNEL - DIODE OSCILLATOR



$$L' = L \left( \frac{1 - r_Q^2}{Q_2} \right) \quad G_T = \frac{G_T}{1 + Q^2}$$

FIG. III - 8. EQUIVALENT CIRCUIT OF TUNNEL - DIODE OSCILLATOR

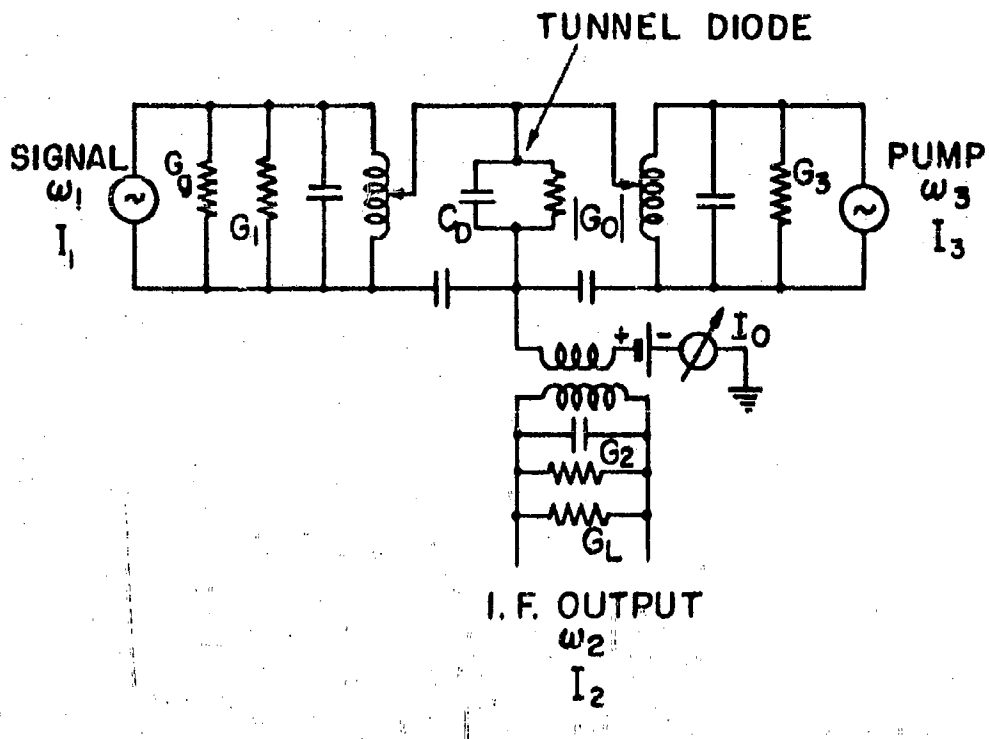
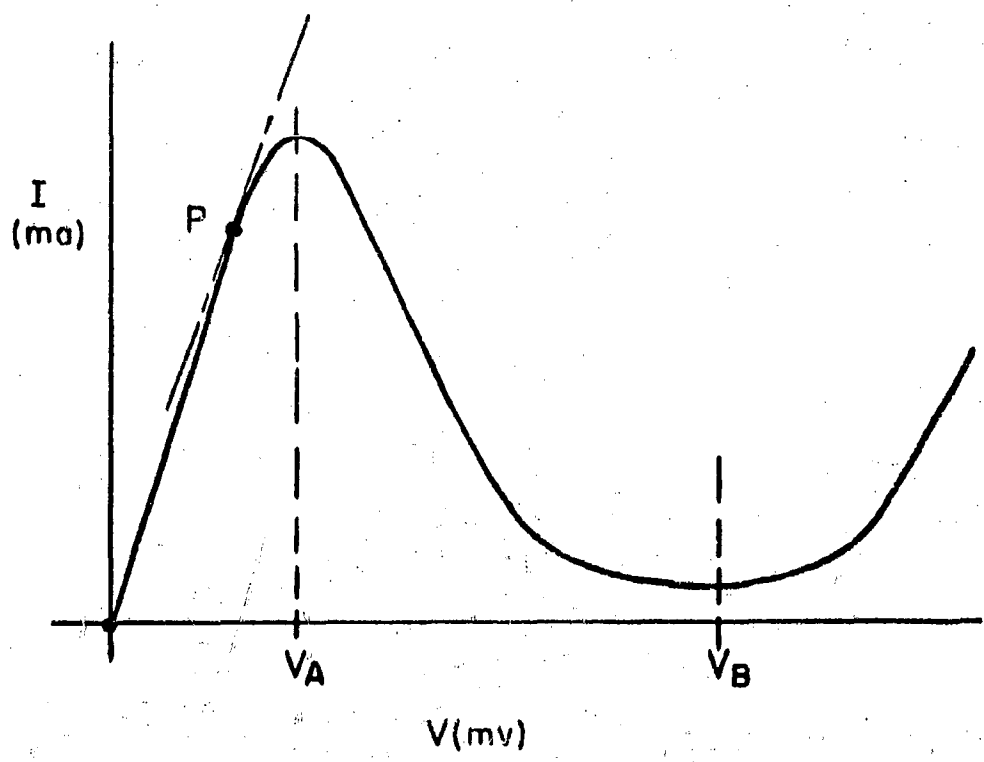


FIG. IV-I. SCHEMATIC DIAGRAM OF CONVERTER CIRCUIT



**FIG. IV-2. TUNNEL DIODE I-V CHARACTERISTIC**

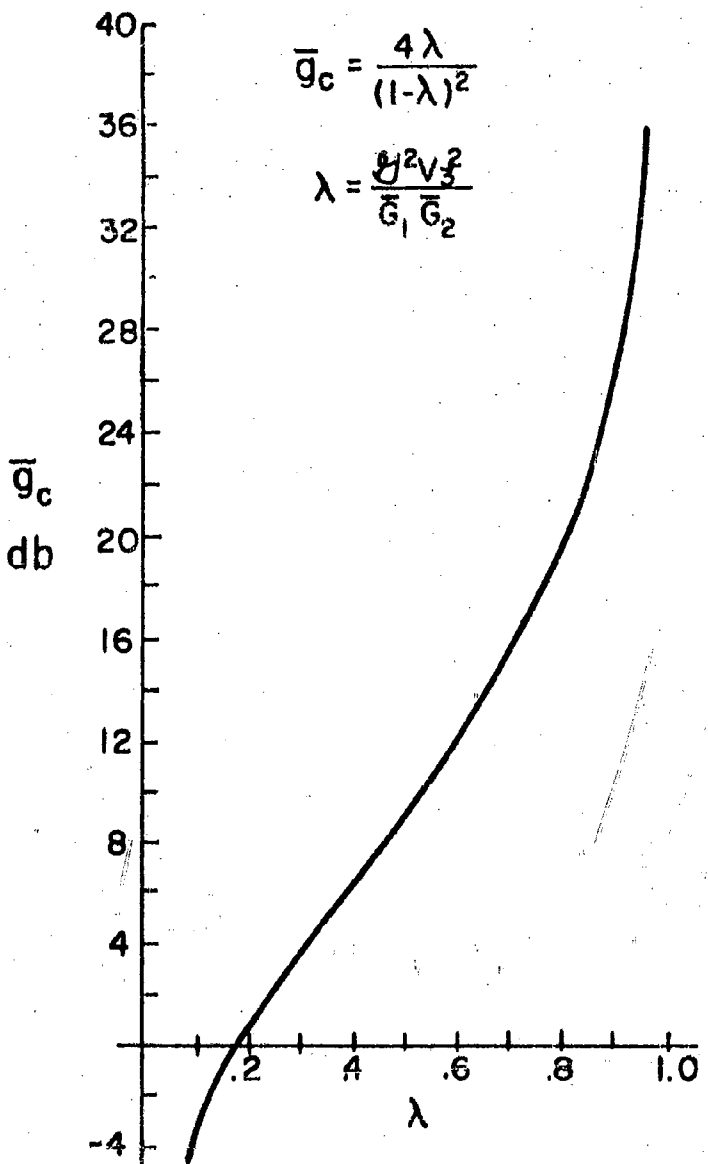


FIG. IV-3 "NORMALIZED" CONVERSION POWER RATIO

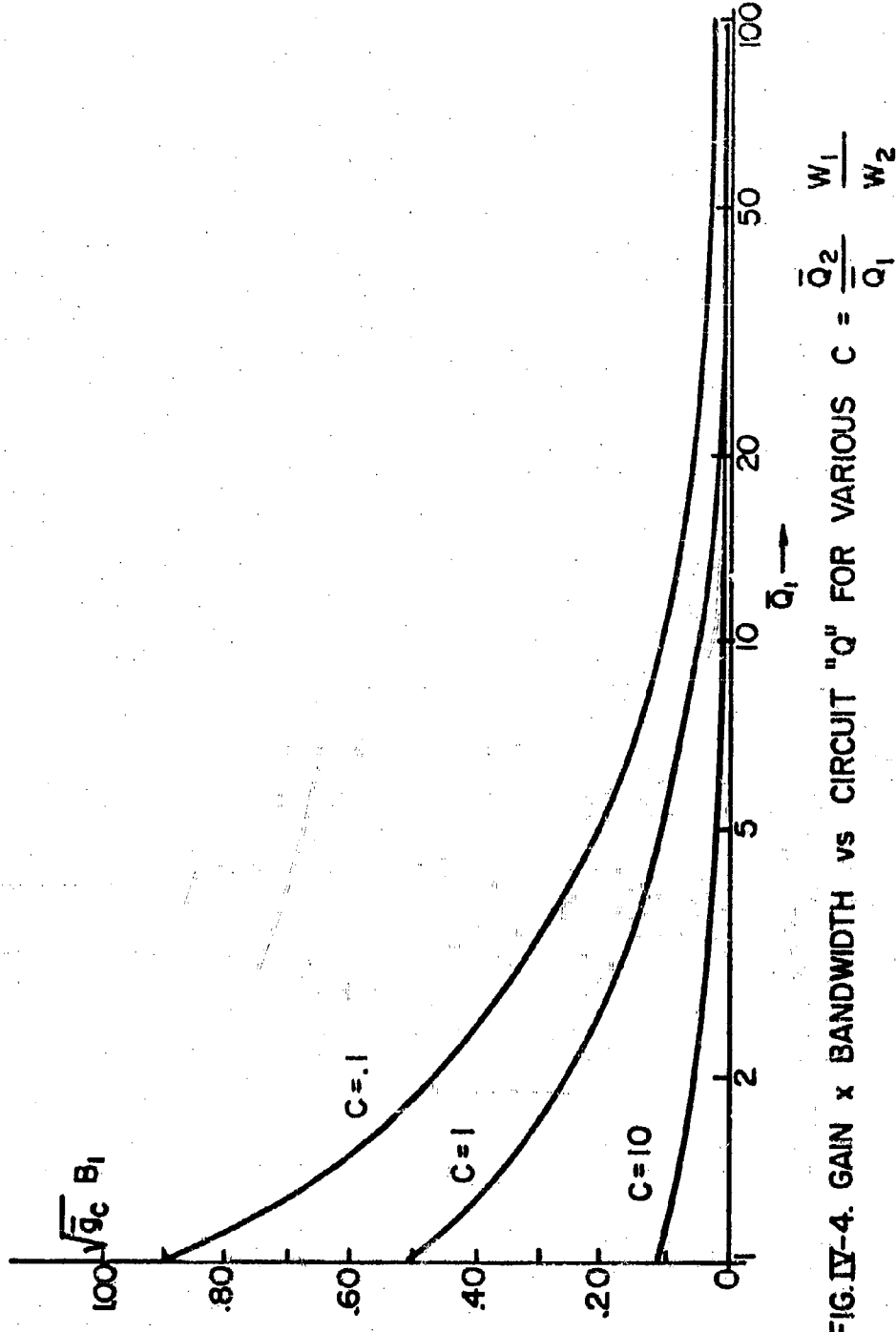


FIG. IV-4. GAIN  $\times$  BANDWIDTH vs CIRCUIT "Q" FOR VARIOUS  $C = \frac{\bar{Q}_2}{\bar{Q}_1} \frac{W_1}{W_2}$

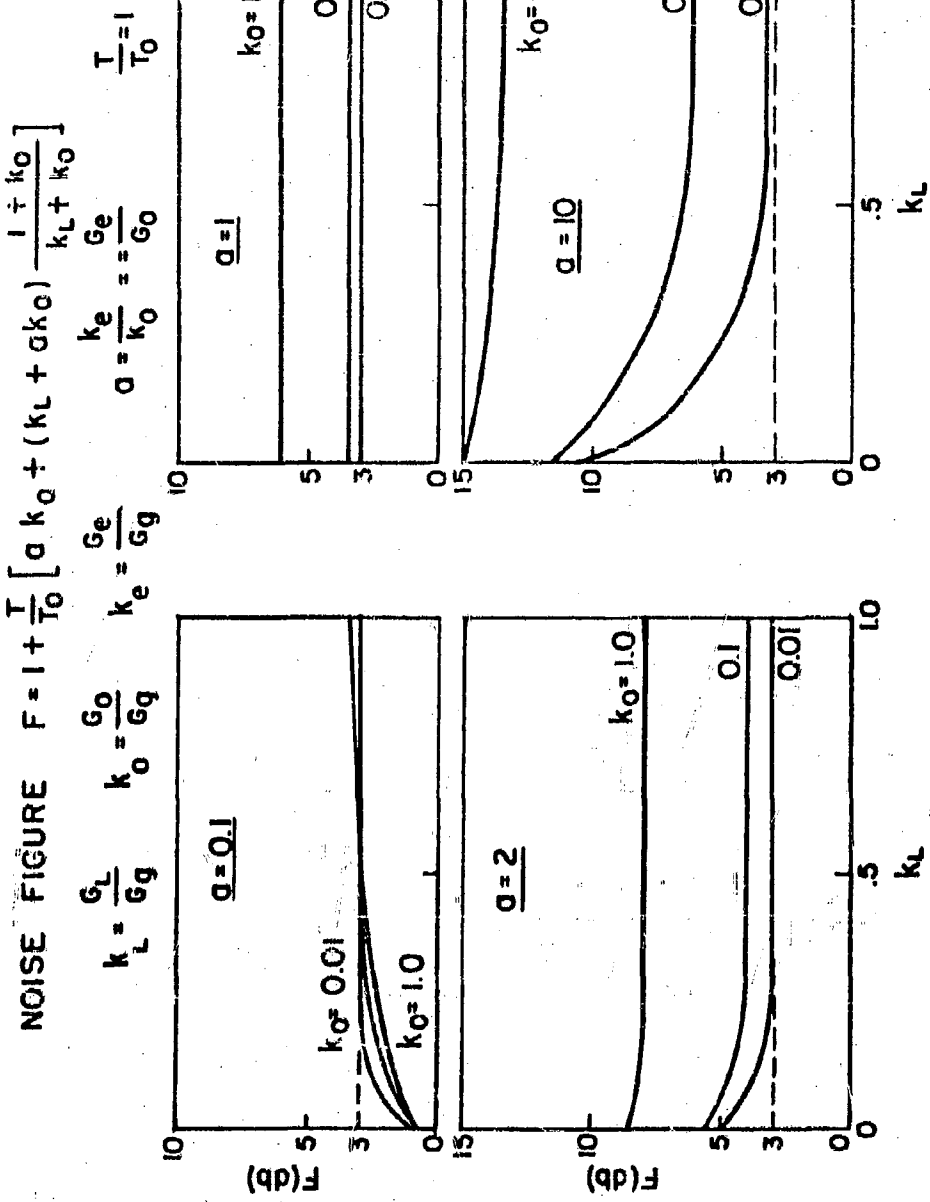
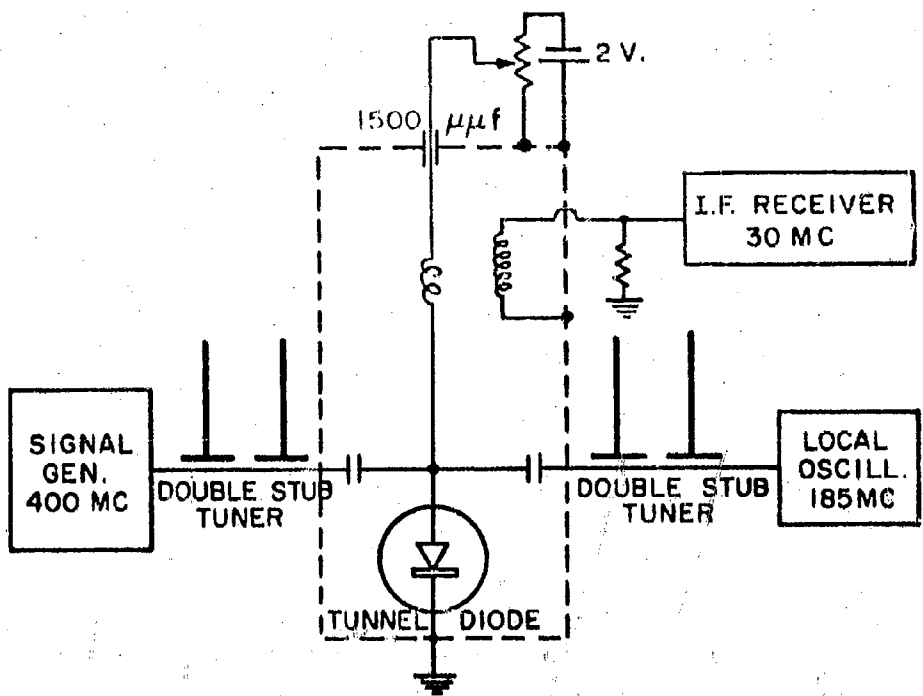


FIG. IV-5. NOISE FACTOR AS A FUNCTION OF DIODE AND CIRCUIT CONDUCTANCES



**FIG. IV-6. TUNNEL DIODE CONVERTER CIRCUITS.**

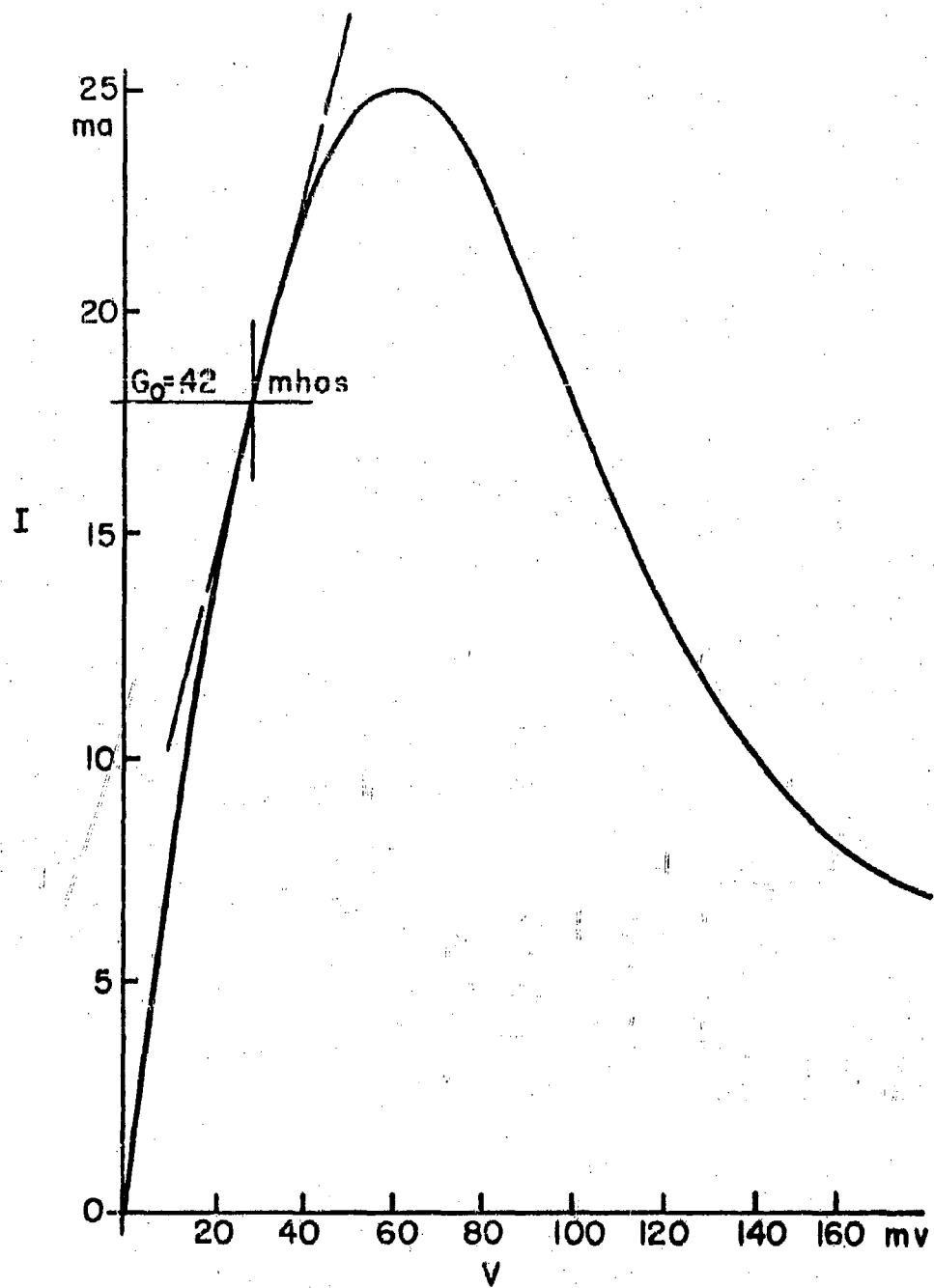


FIG. IV-7 TUNNEL DIODE GERMANIUM

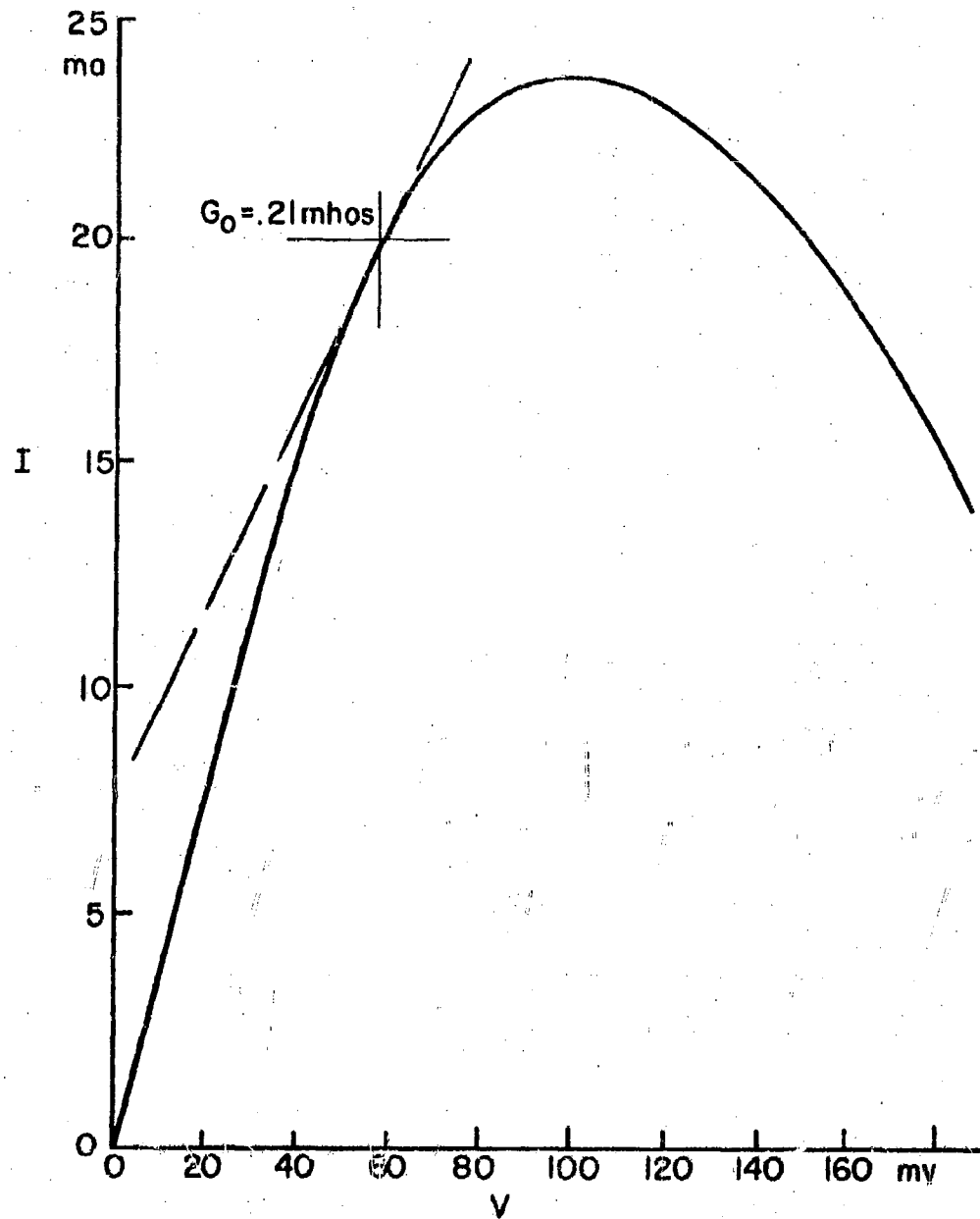
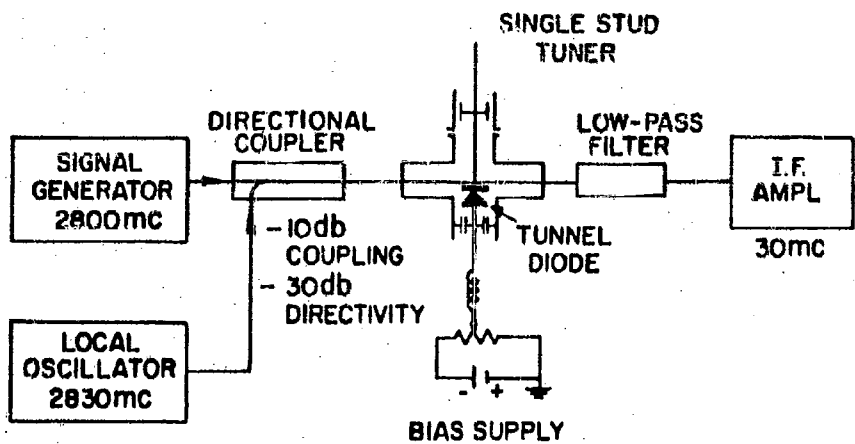


FIG. IV-8. TUNNEL DIODE GALLIUM ARSENIDE



BLOCK DIAGRAM OF "S"-BAND DOWN CONVERTER

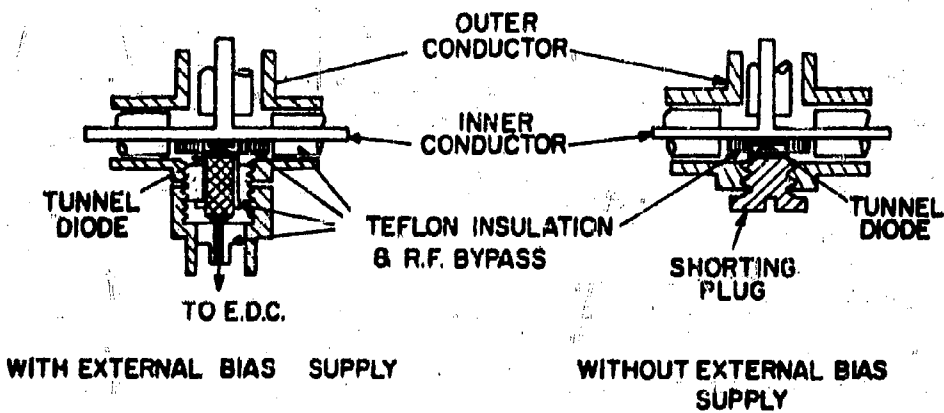


FIG. IV-9. DETAIL OF TUNNEL DIODE MOUNT IN "BNC" CONNECTOR

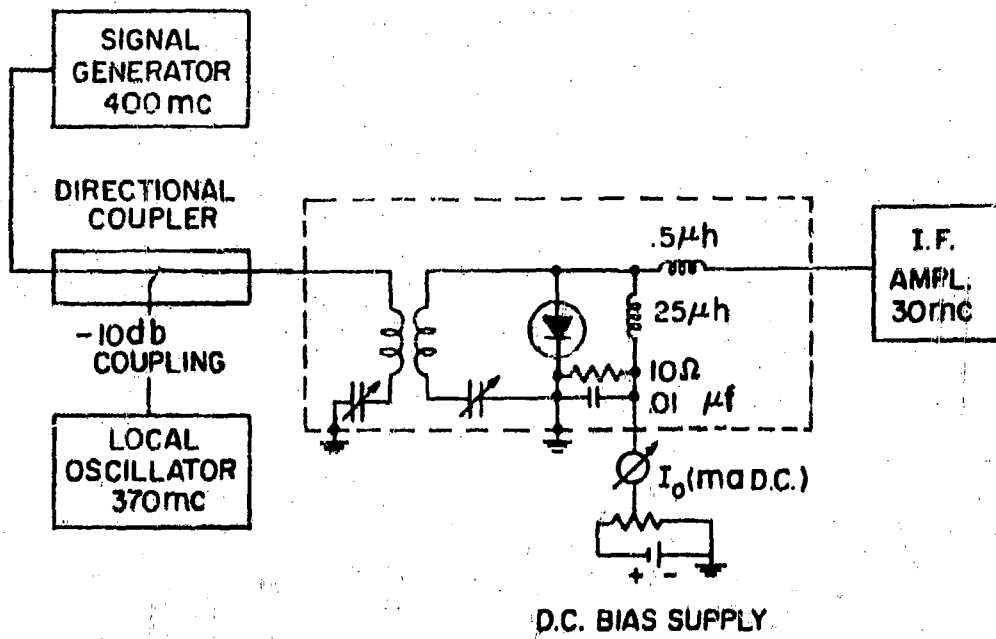


FIG. IV-10. BLOCK DIAGRAM OF "LUMPED CONSTANT" CIRCUIT

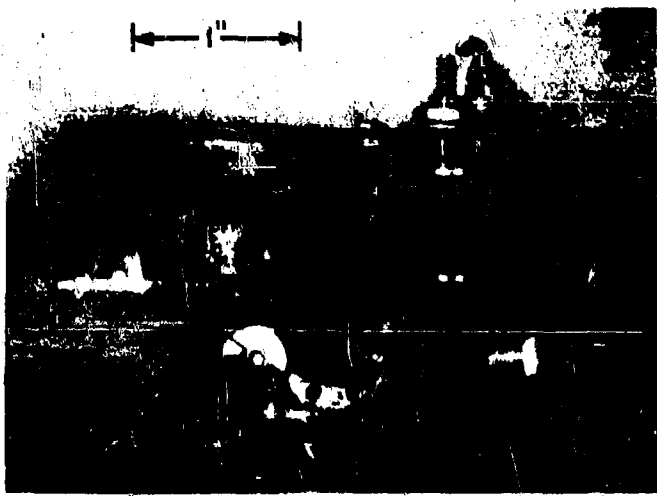


FIG. IV -II PHOTOGRAPH OF  
TUNNEL DIODE DOWN CONVERTER

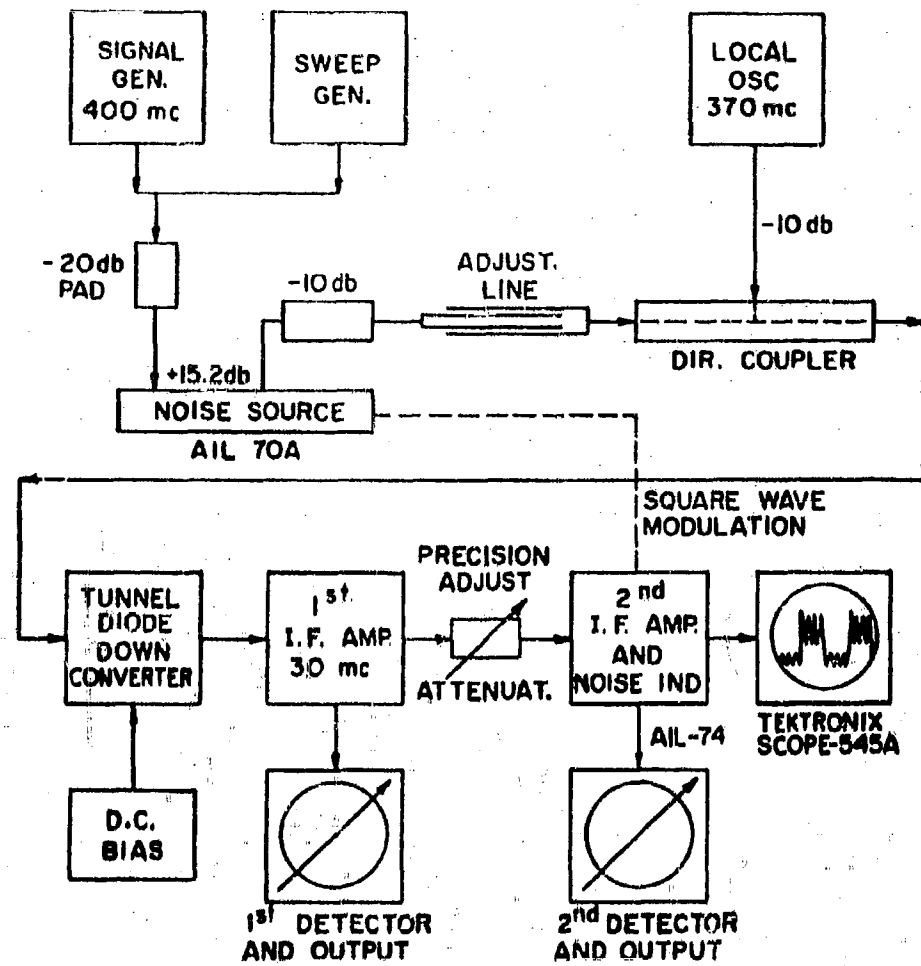
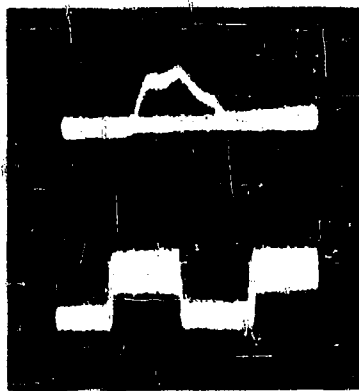


FIG. IV-12. COMPLETE TEST SET-UP FOR TUNNEL DIODE DOWN CONVERTER



BANDWIDTH  
1 cm = 3 mc

MODULATED NOISE

FIG. IV-13. SCOPE TRACING OF BANDWIDTH AND NOISE OUTPUT.

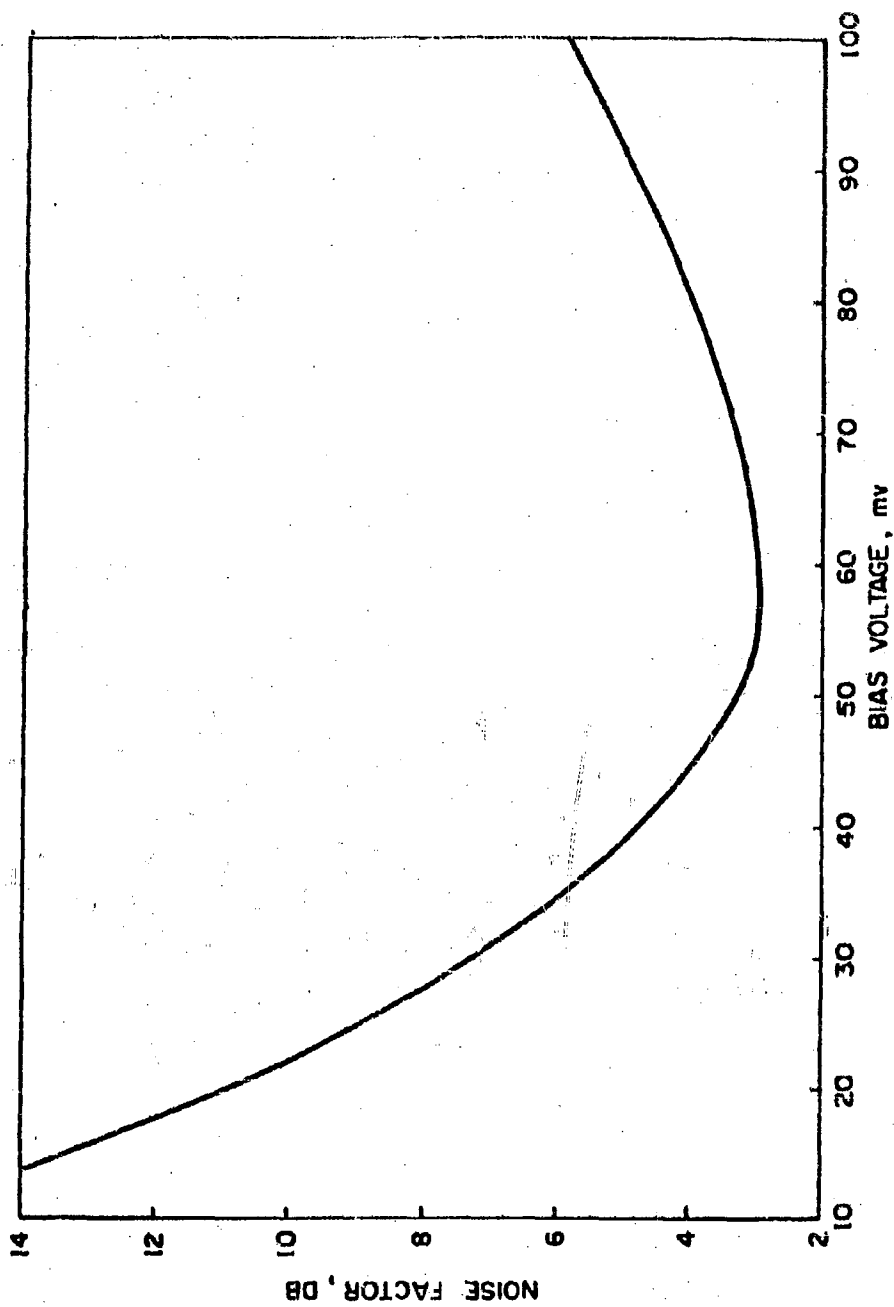


FIG. IV-14.4 NOISE FACTOR AS A FUNCTION OF BIAS VOLTAGE

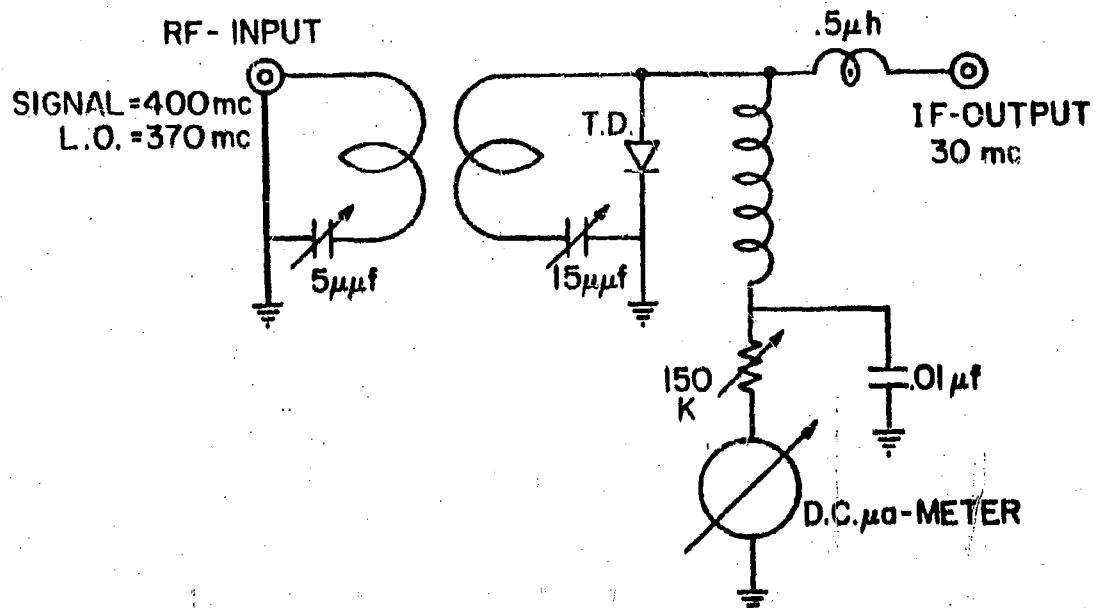


FIG. IV-15. LUMPED PARAMETER TUNNEL DIODE DOWN CONVERTER WITH SELF BIAS SCHEME

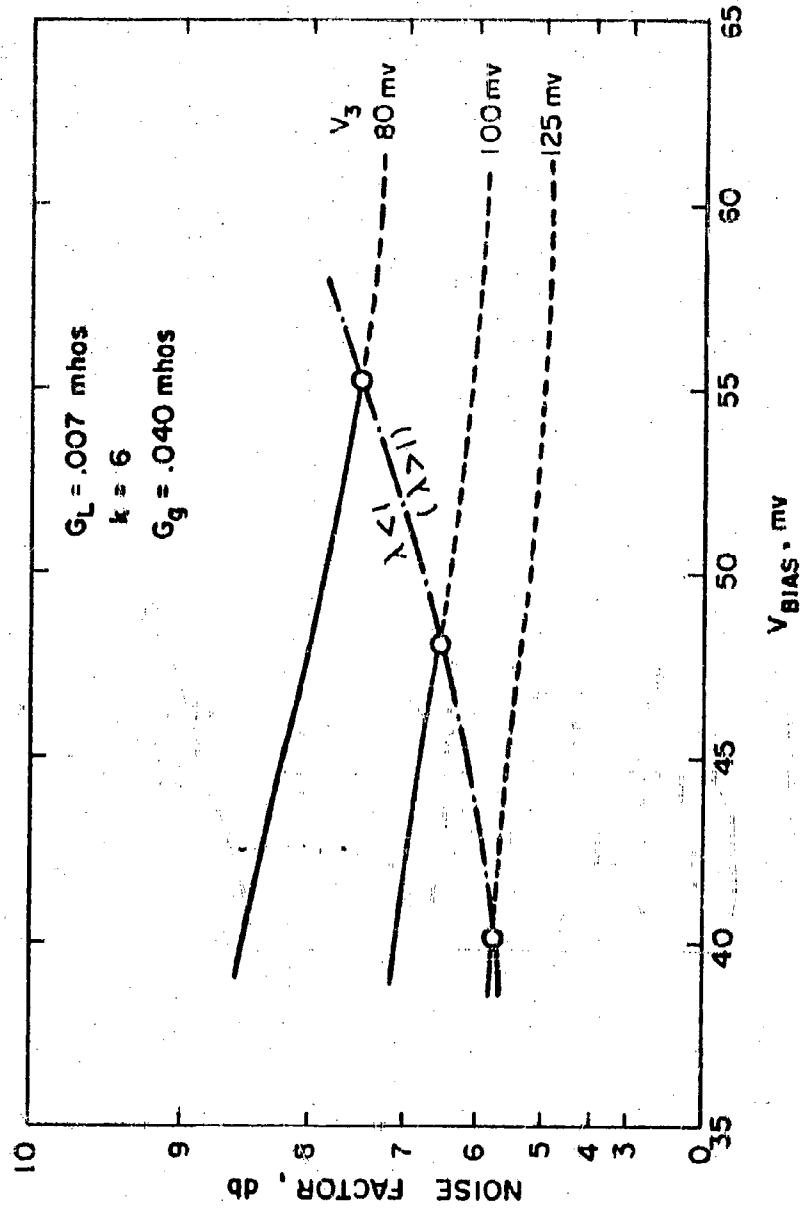


FIG. IV-16 NOISE FACTOR AS A FUNCTION OF BIAS VOLTAGE

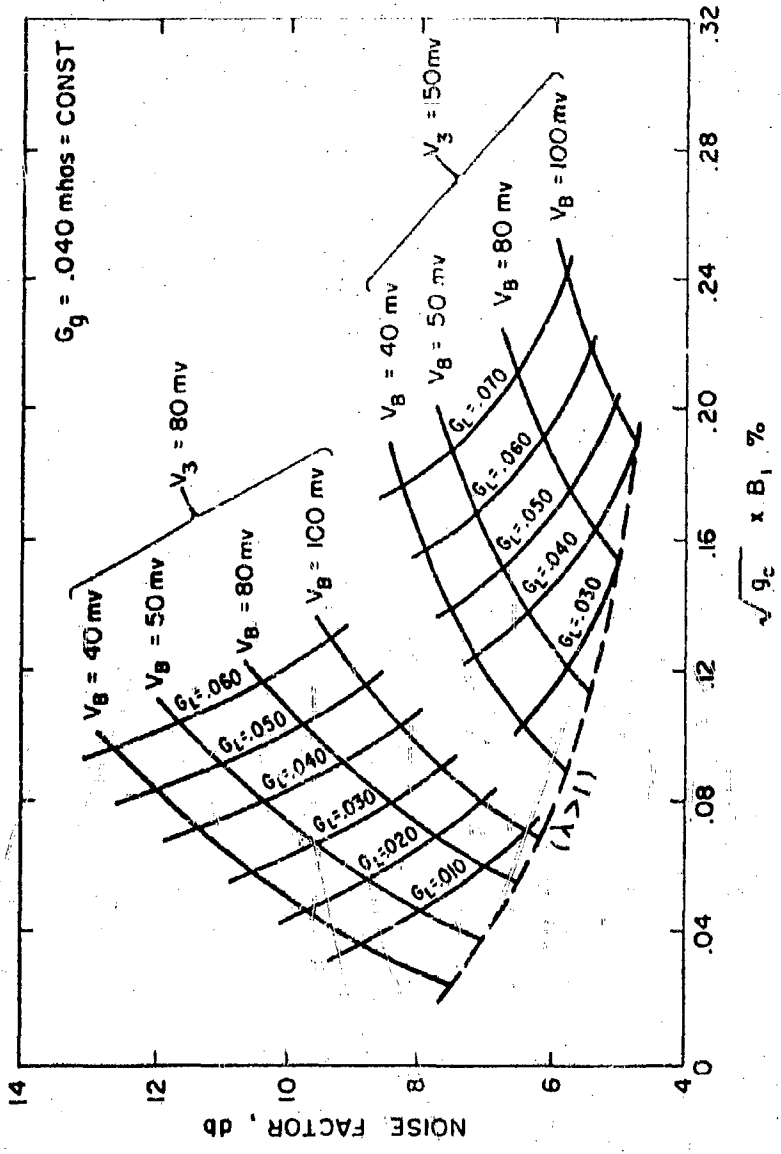
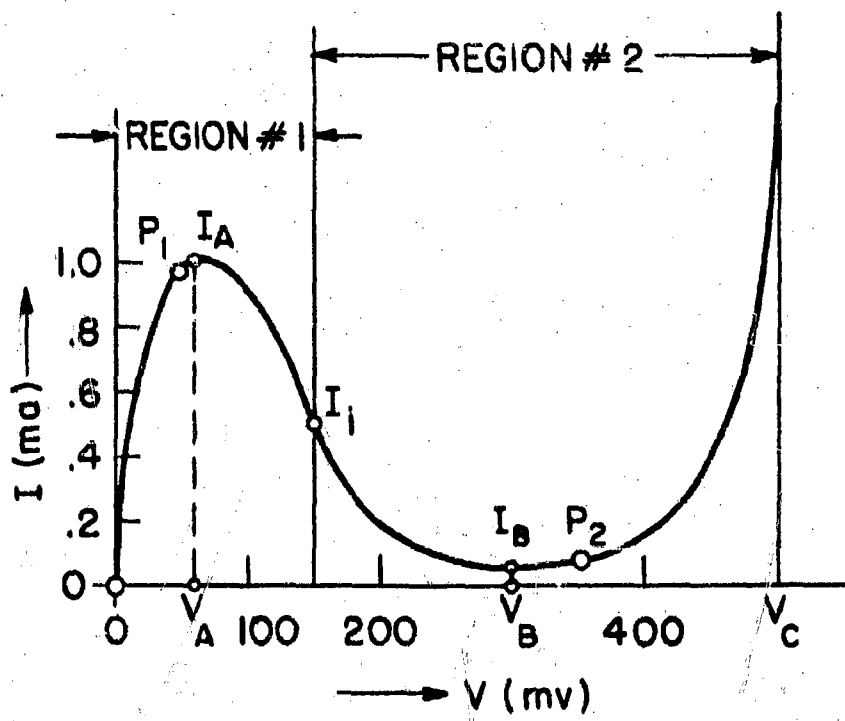


FIG. IV-17 NOISE FACTOR AS A FUNCTION OF GAIN BANDWIDTH PRODUCT



**FIG. IV-18. CHARACTERISTIC OF TUNNEL DIODE**

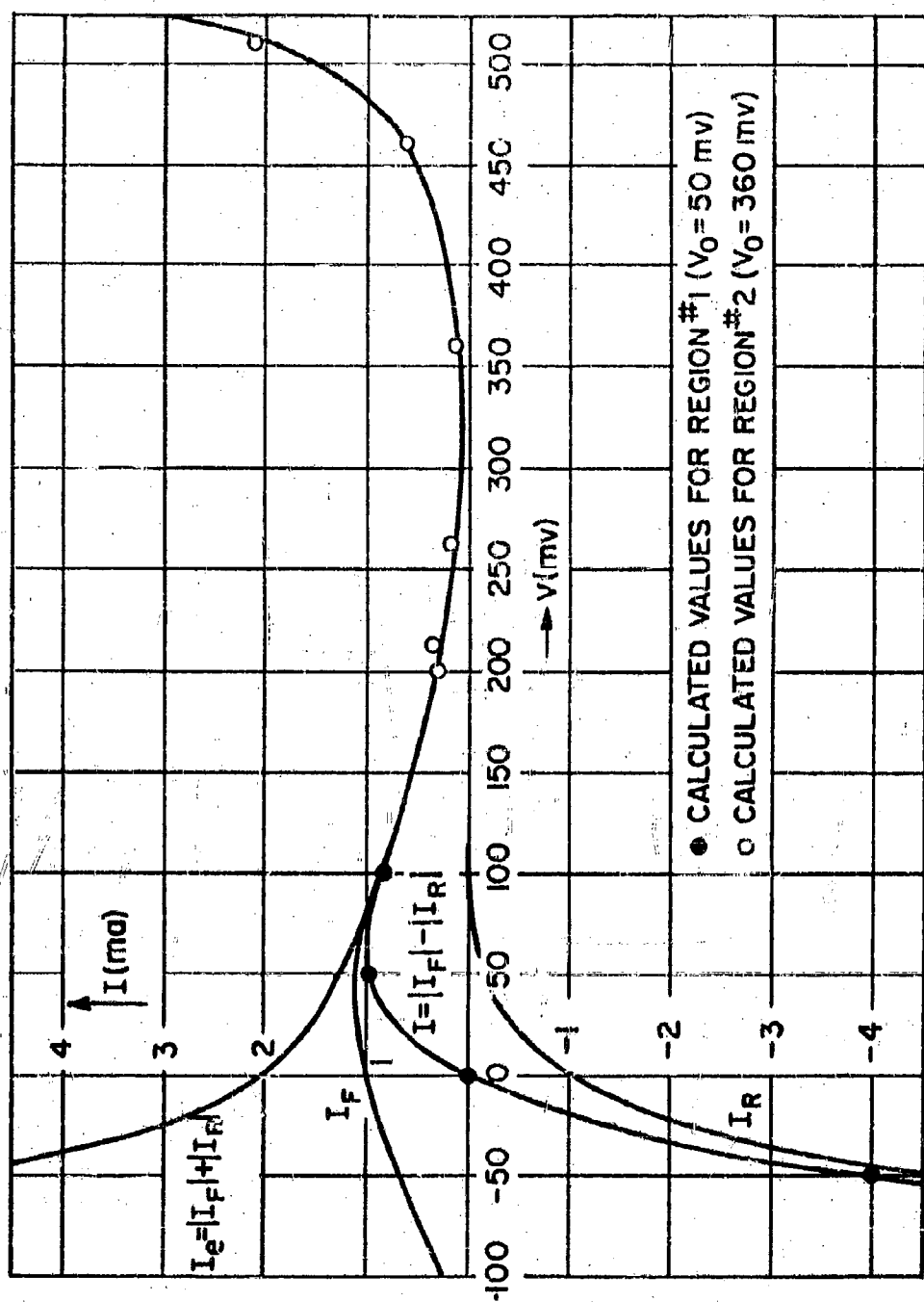


FIG IX-19. CHARACTERISTIC OF TEST DIODE

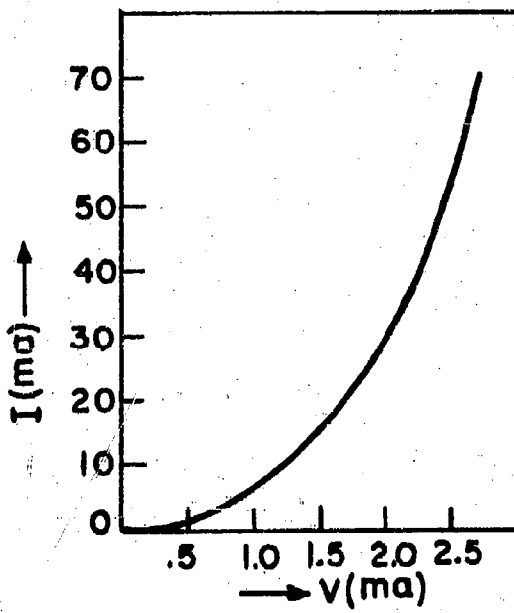


FIG. IV-20. I-V CHARACTERISTICS OF  
DIODE SIMILAR TO IN21

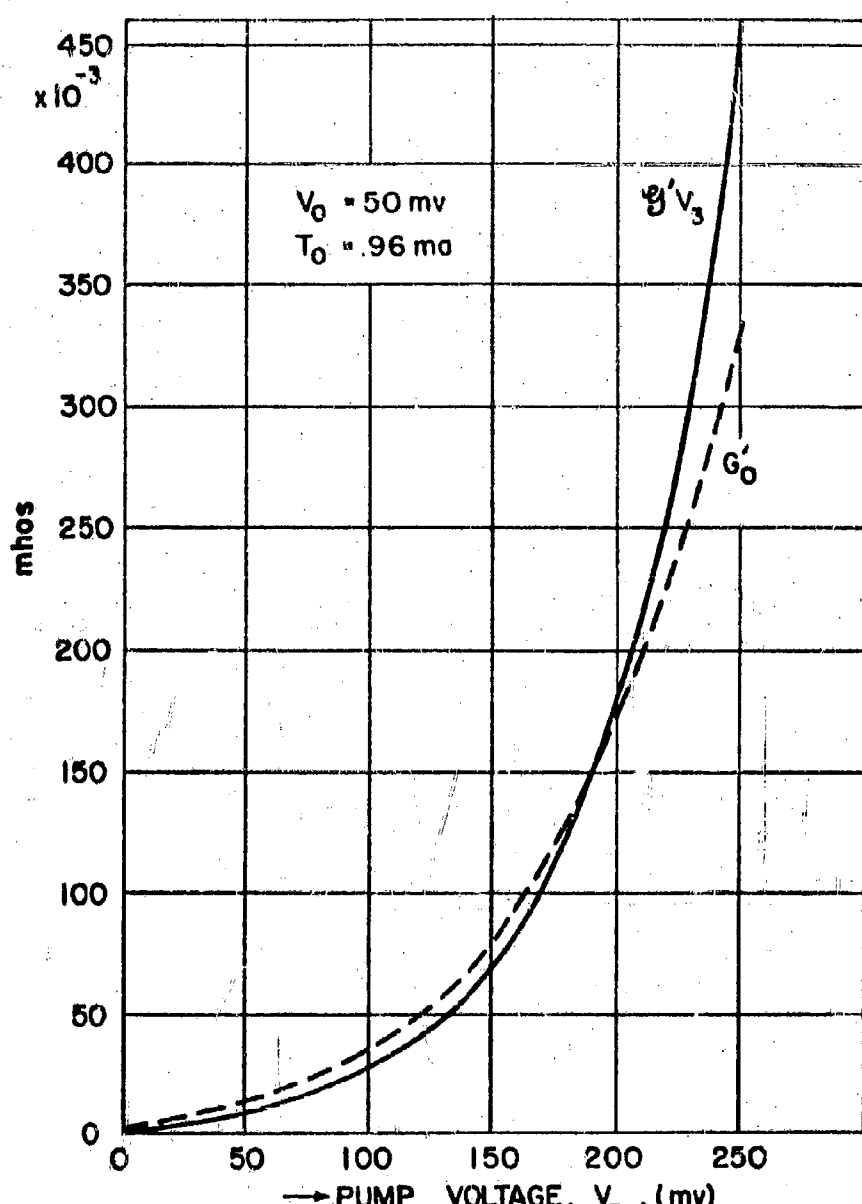


FIG.IV-21 LINEARITY ( $G'_0$ ) AND NON LINEARITY ( $g'V_3$ )  
TERMS vs PUMP VOLTAGE

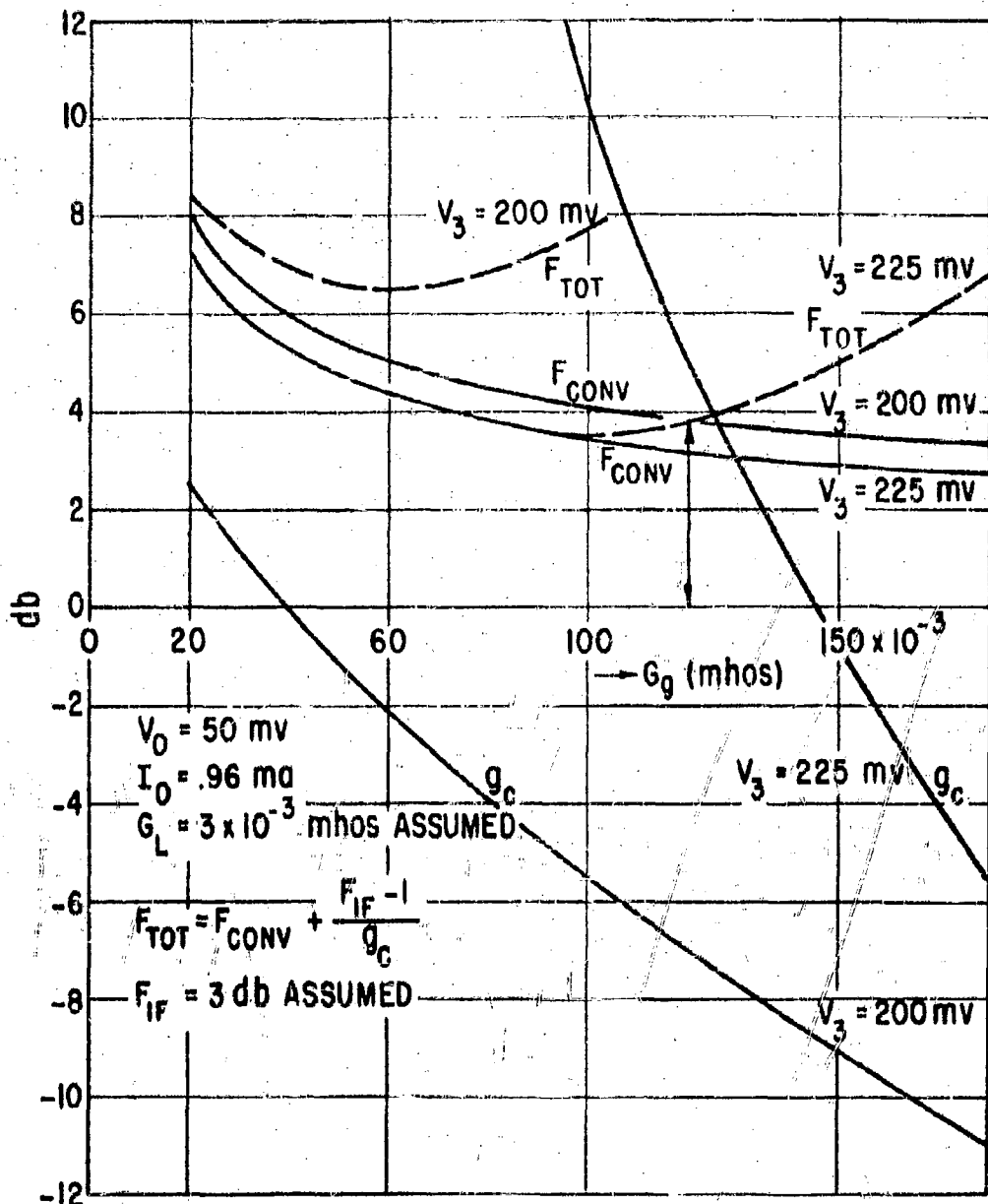
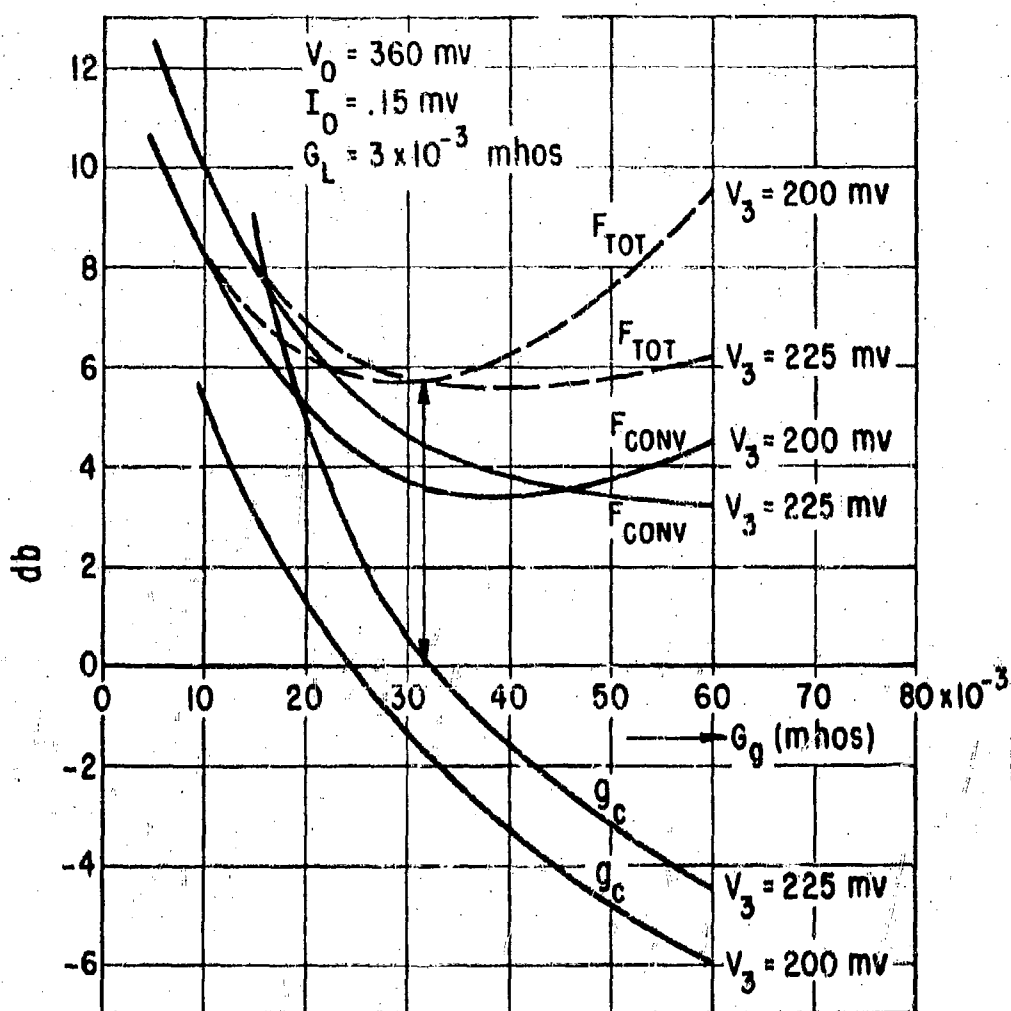


FIG. IV-22 CALCULATED VALUES OF NOISE FACTOR AND GAIN



**FIG. IV-23**  
**CALCULATED VALUES OF NOISE FACTOR AND GAIN**

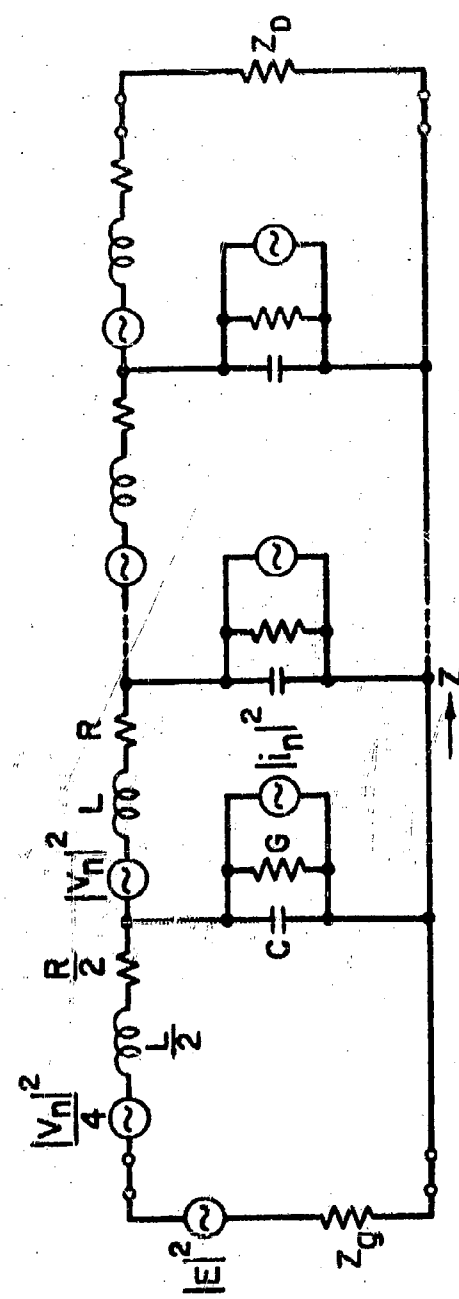


FIG. V-1. LOSSY TRANSMISSION LINE WITH DISTRIBUTED  
NEGATIVE RESISTANCES AND NOISE SOURCES

$$G'_P = \frac{G_P}{1-N}$$

$$N = \frac{R_O - R_D}{R_O + R_D}$$

$$M = \frac{R_O - R_g}{R_O + R_g} = 0$$

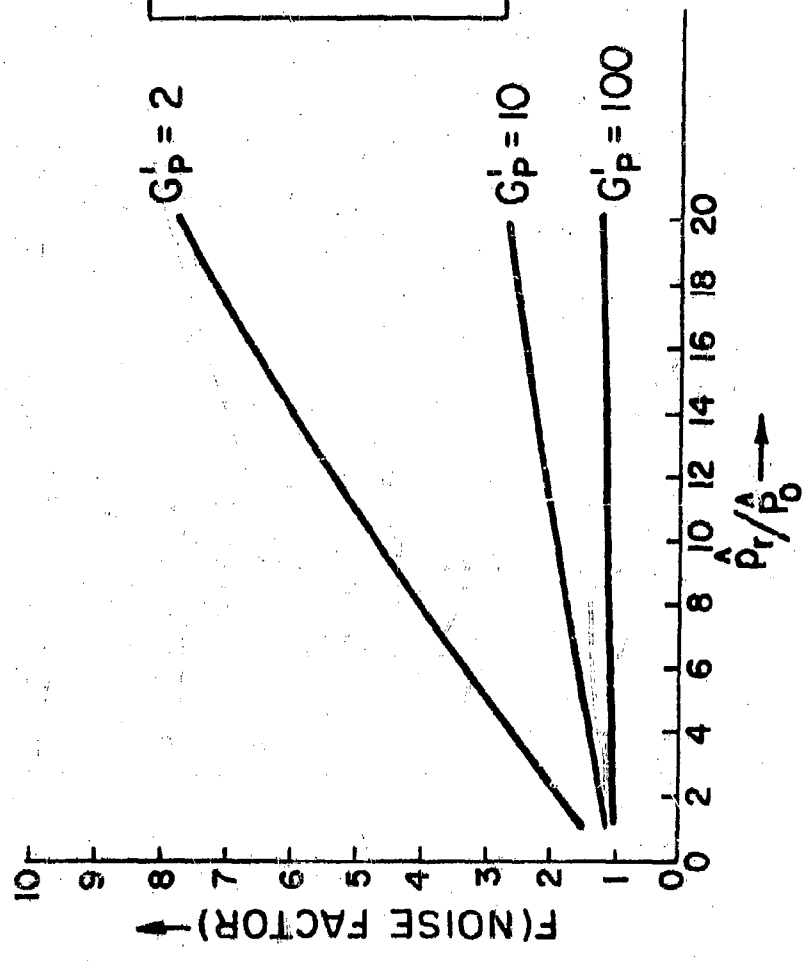


FIG. V-2. NOISE FACTOR OF A MATCHED-INPUT  
WITH DISTRIBUTED NOISE SOURCES

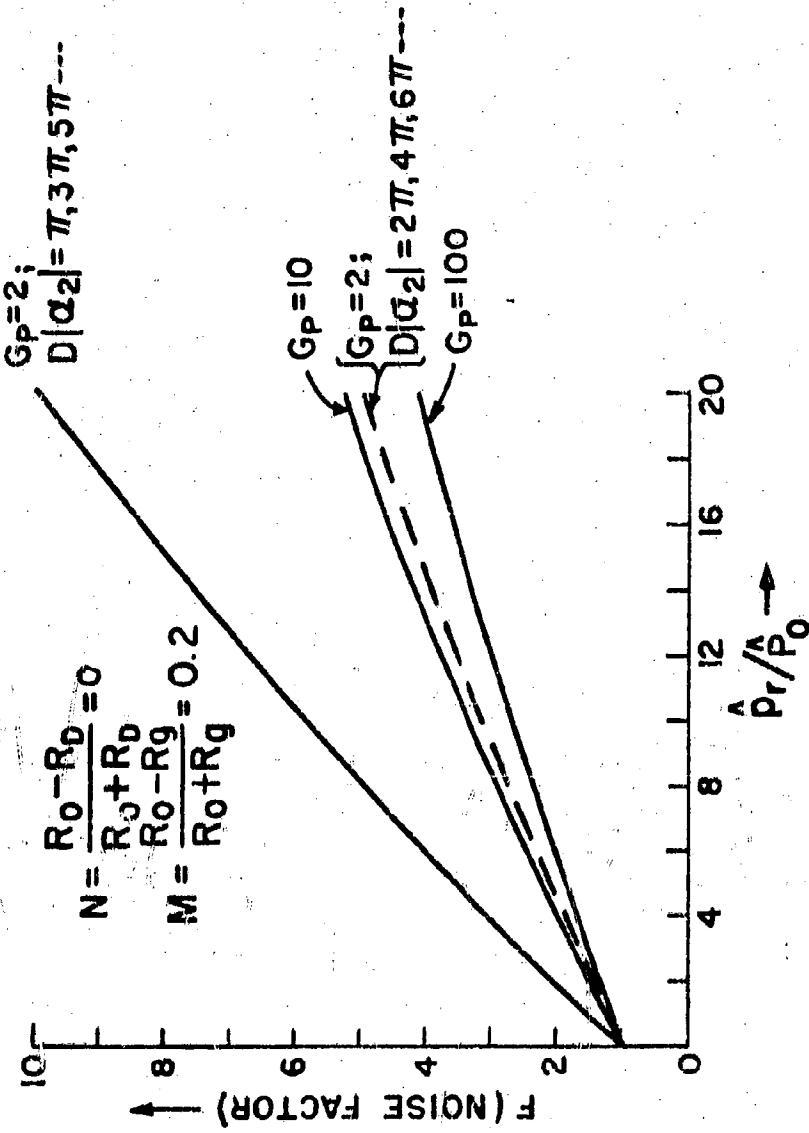


FIG. VII-3. NOISE FACTOR OF A MISMATCHED-INPUT LINE WITH DISTRIBUTED NOISE SOURCES ( $M = 0.2$ )

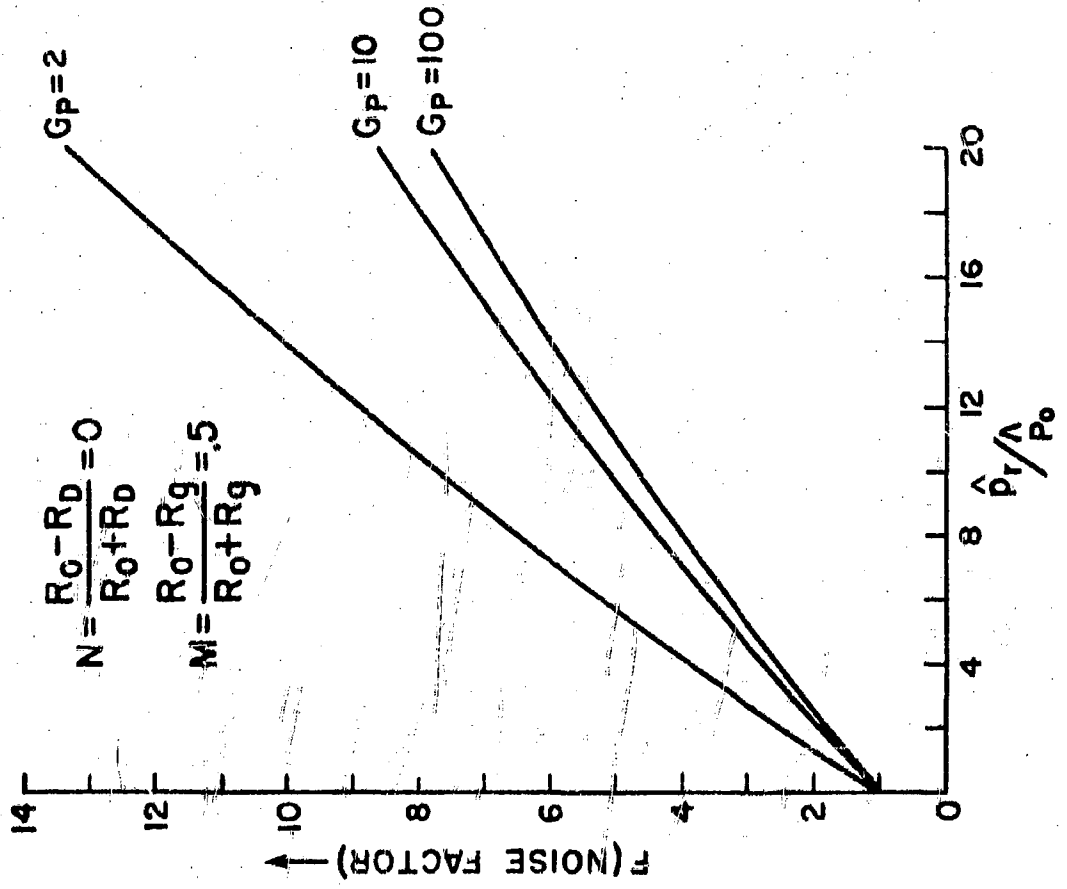


FIG. VII-4

11424

FIG. V-5 TRAVELLING WAVE TUNNEL DIODE AMPLIFIER

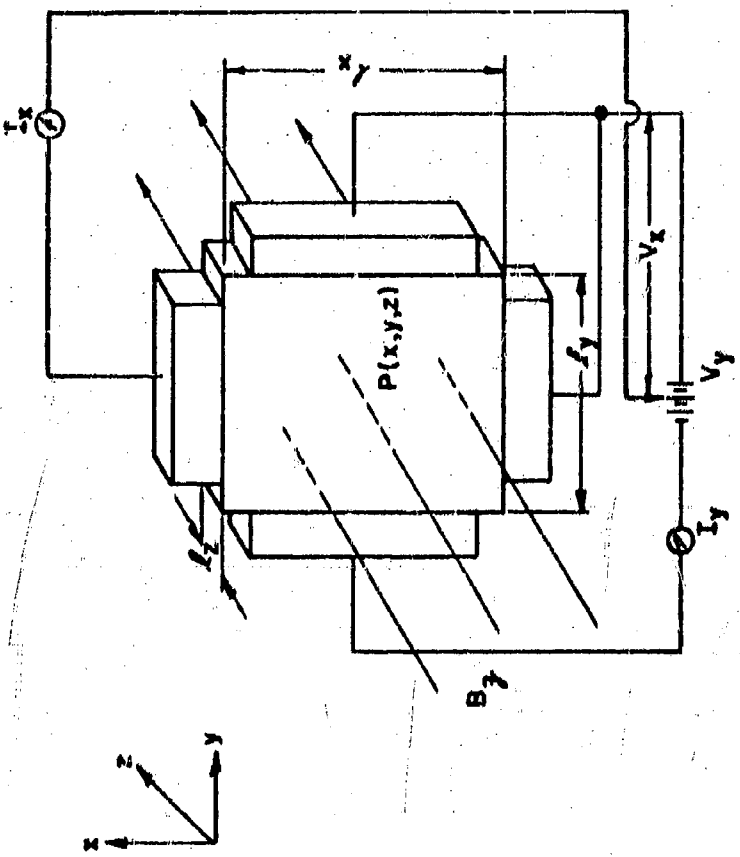


FIG. II-6 A HALL EFFECT MAGNETO RESISTANCE MEASUREMENT

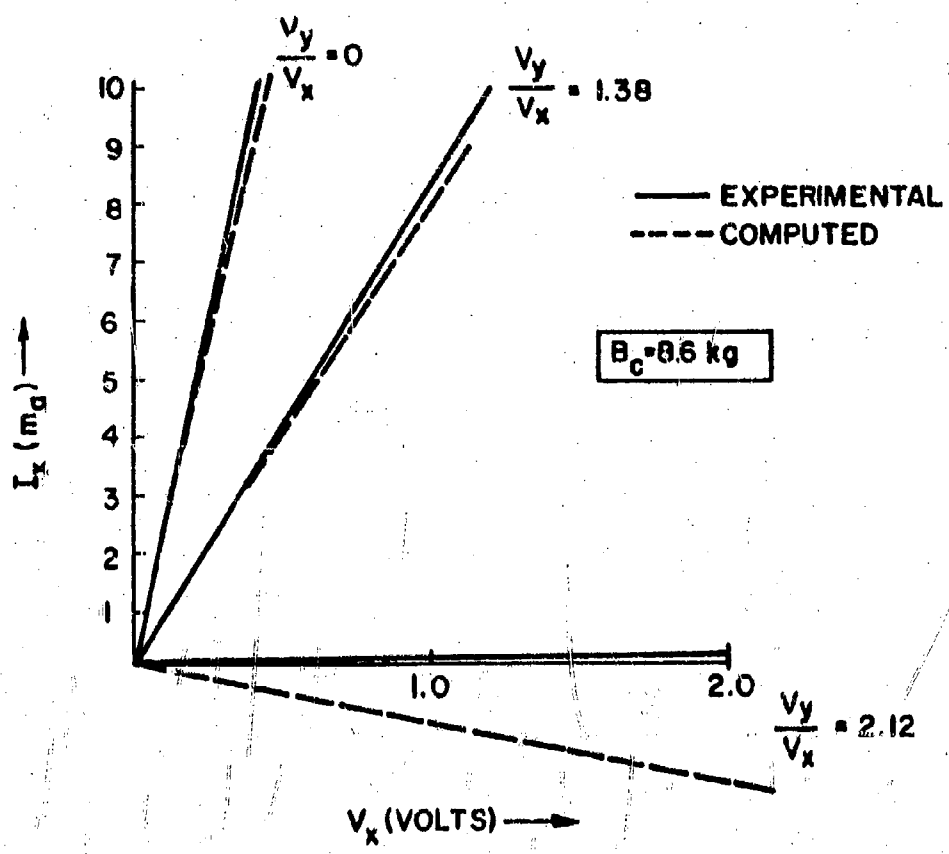


FIG. IV - 7 MAGNETO - RESISTANCE AS FUNCTION OF CROSS ELECTRICAL FIELDS

— EXPERIMENTAL  
- - - CALCULATED

$V_x = .2V$

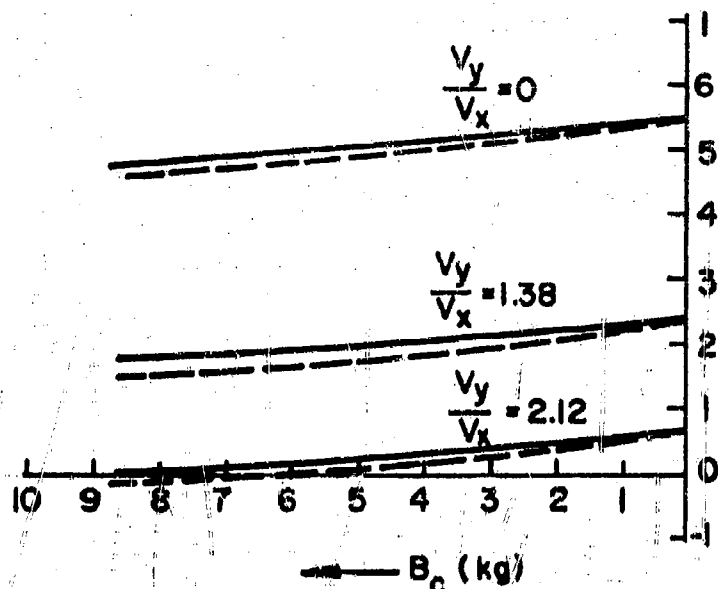


FIG. V-8 - MAGNETO - TRANSCONDUCTANCE AS FUNCTION OF CROSS ELECTRICAL FIELDS.

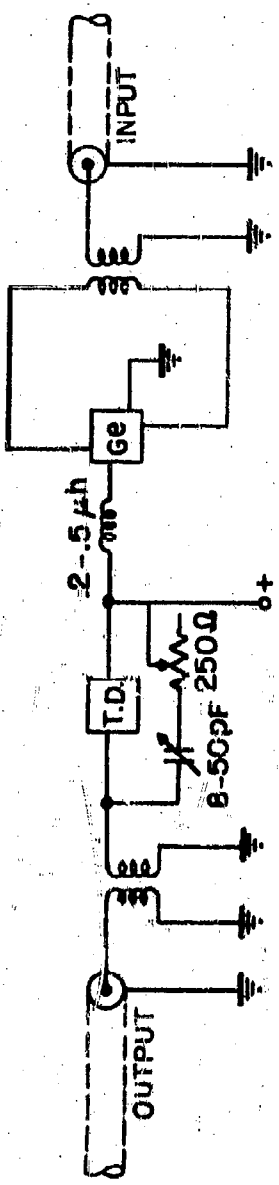


FIG V-9 INTEGRATED TUNNEL-DIODE-HALL-ISOLATOR AMPLIFIER

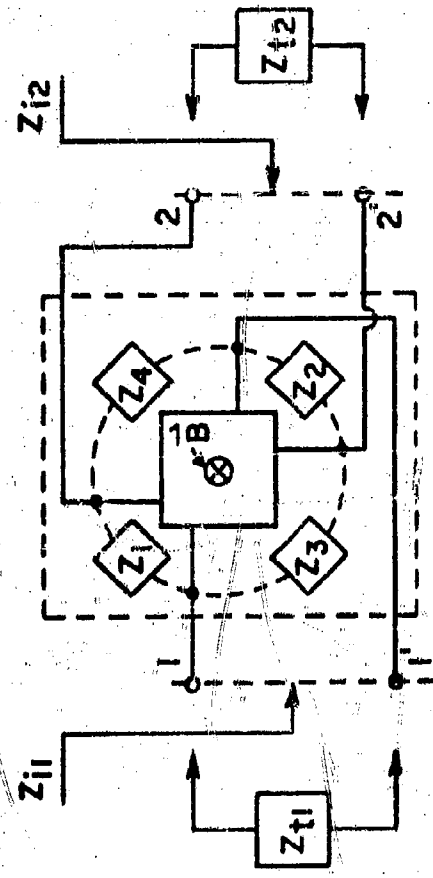
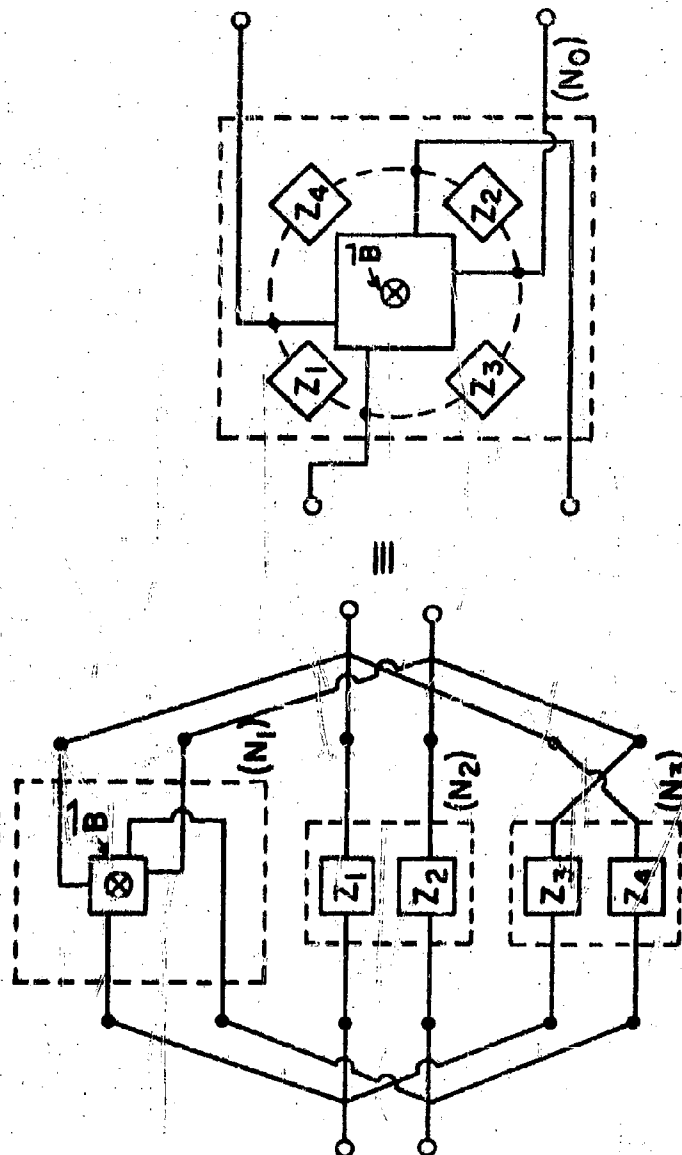


FIG. V-10 THE GENERALIZED FORM OF THE PRACTICAL HALL-EFFECT ISOLATOR

FIG. X-II SHOWING PRACTICAL HALL-EFFECT ISOLATOR AS COMPOSITION OF THREE DISTINCT 2-TERMINAL-PAIR NETWORKS.



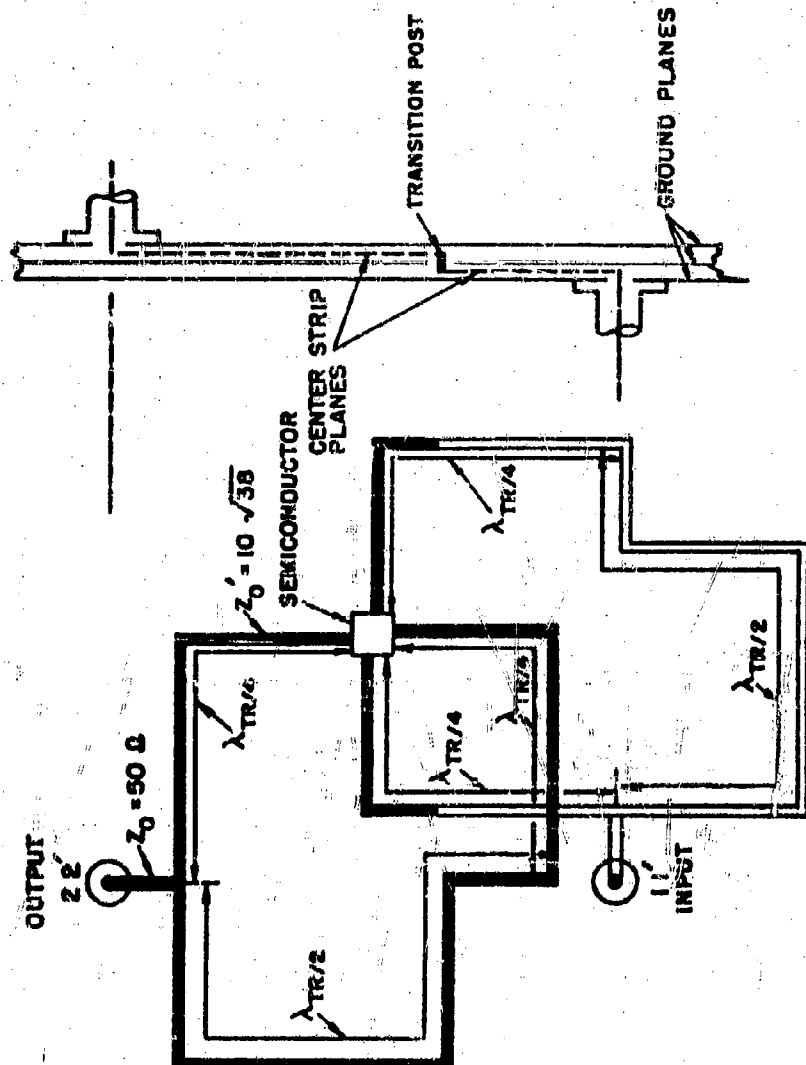
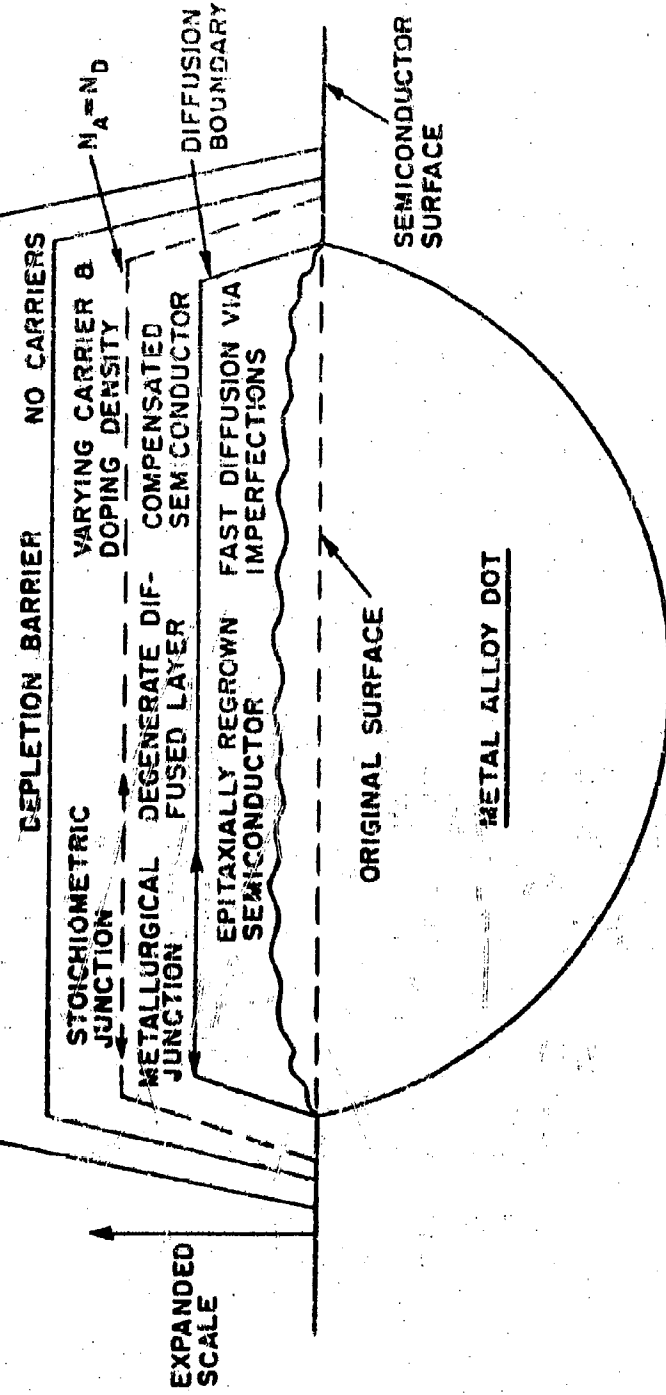


FIG T-12-4-CONTACT HALL ISOLATOR IN STRIP LINE

**SEMICONDUCTOR  
DEGENERATE BASE REGION**

**PERTINENT  
PROPERTIES**



**FIG. VI-1 EXPANDED DIAGRAM OF A DEGENERATE ALLOY JUNCTION.**

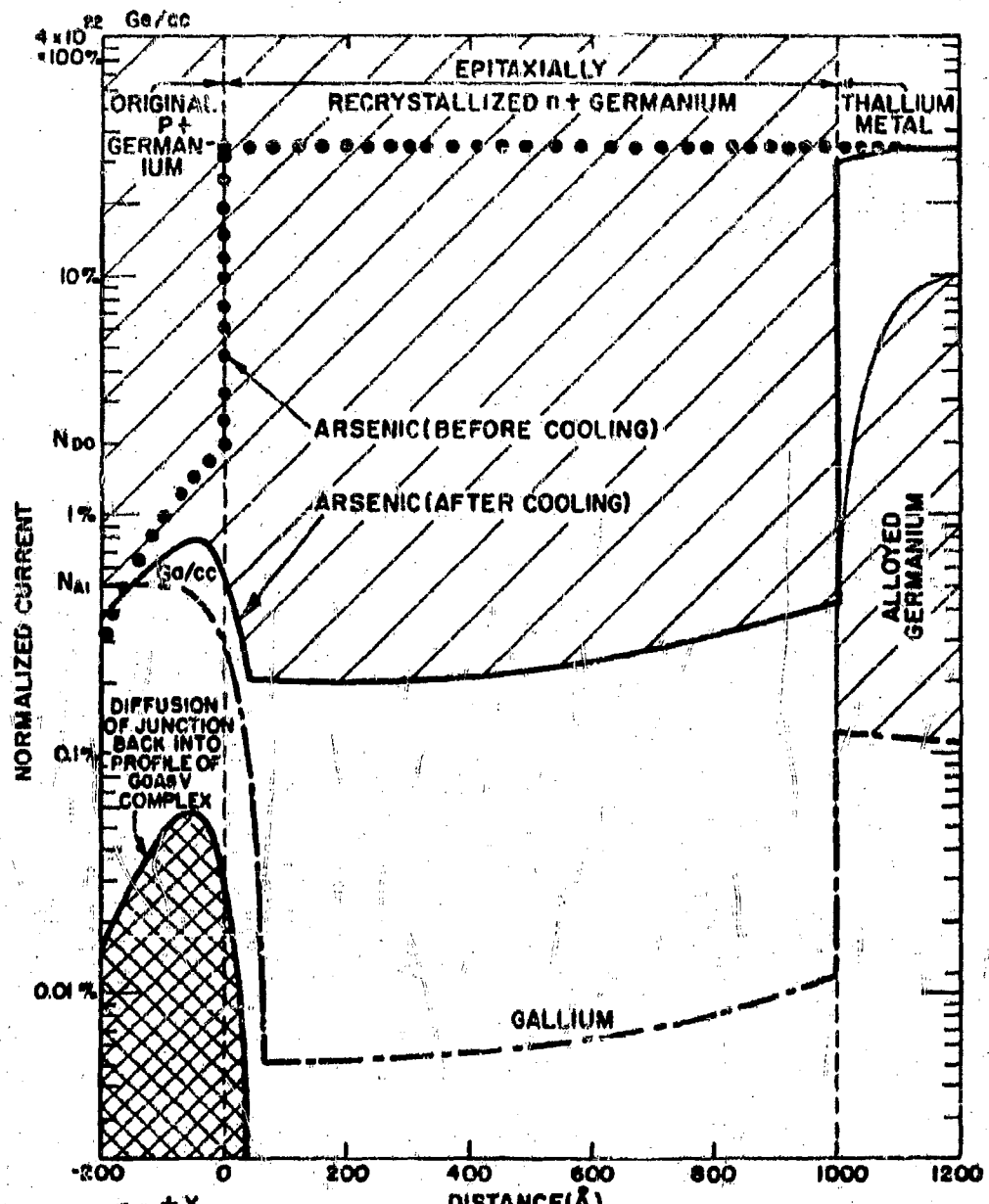


FIG. VI-2. QUENCH ALLOYING OF A Tl:As DOT  
TO Ge ( $2 \times 10^{20}$  Ga/cc)

DIODE	ATMOSPHERE	TIME AT TEMP.	HEAT AND COOL	ETCH
1	90% N <sub>2</sub>	~18 SEC.	INSTANTANEOUS	AFTERWARDS
2	10% H <sub>2</sub>	30 SEC.	SLOWER	
3	H <sub>2</sub>			FOR EACH POINT

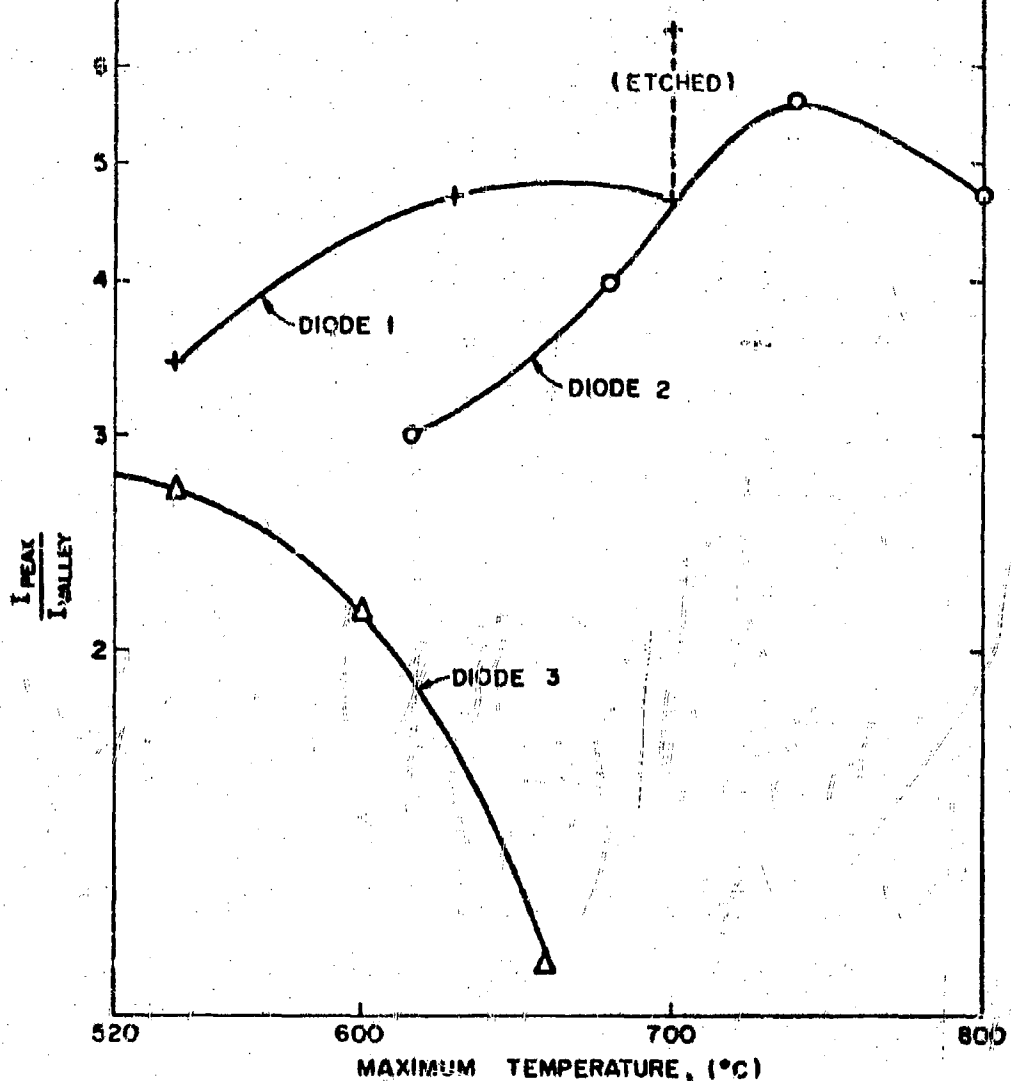


FIG.VI-3.TYPICAL PEAK TO VALLEY CURRENT RATIOS OF REHEATED DIODES WITH TI:As DOTS

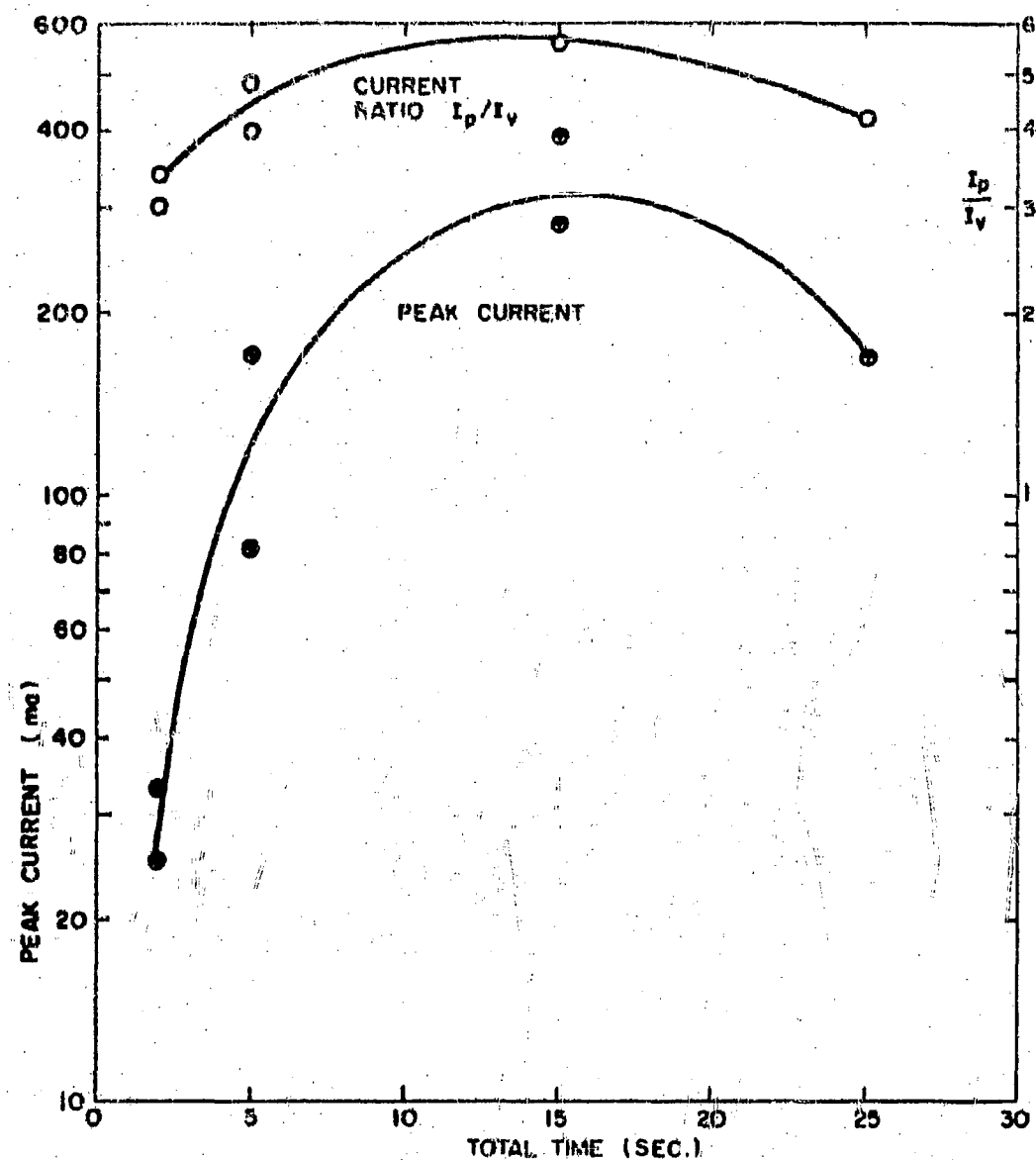
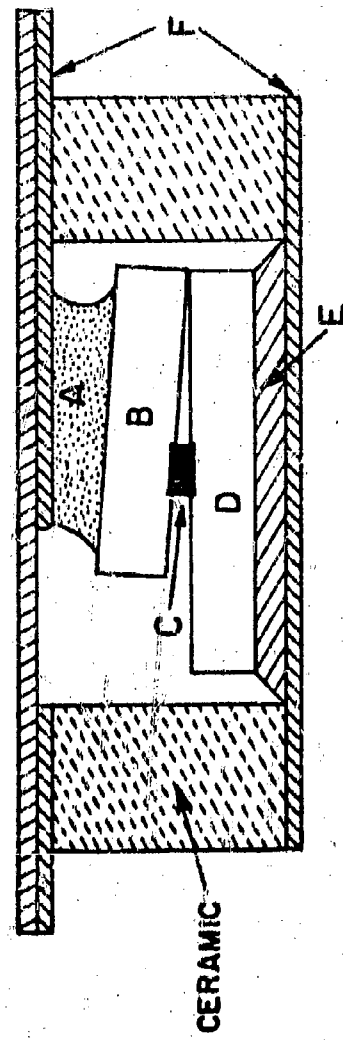


FIG. VI-4  
TWO REHEATED TI:As DOTS ON GERMANIUM AT 725°C.



- A. ALLOYED INDIUM DOT
- B. GALLIUM - SATURATED GERMANIUM
- C. ALLOYED TIN(3% ARSENIC) DOT
- D. ARSENIC - SATURATED GERMANIUM
- E. ARSENIC-DOPED SOLDER
- F. GOLD-PLATED KOVAR

FIG. VI-5. SANDWICH DIODE STRUCTURE

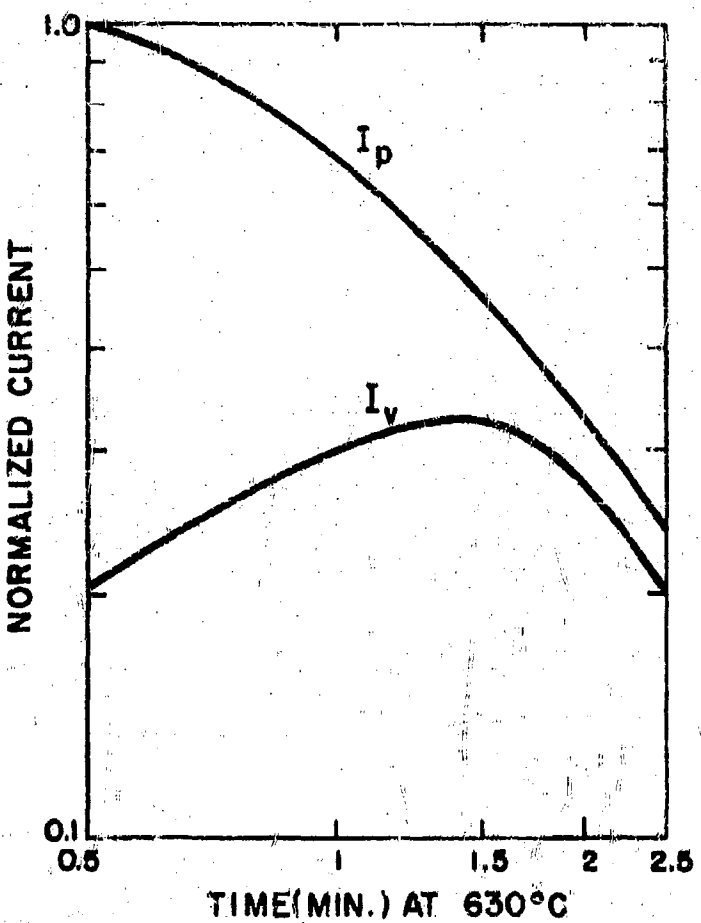
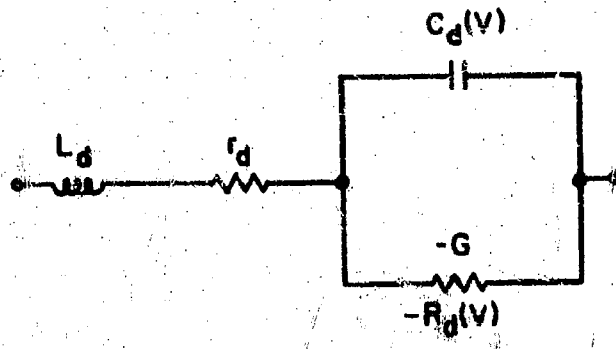


FIG. VI-6. TYPICAL DEGRADATION OF A  
3 PERCENT GALLIUM DOT ON  
GERMANIUM ( $2 \times 10^{19}$  As/cc)



**FIG. VI-7. EQUIVALENT CIRCUIT OF TUNNEL DIODE**

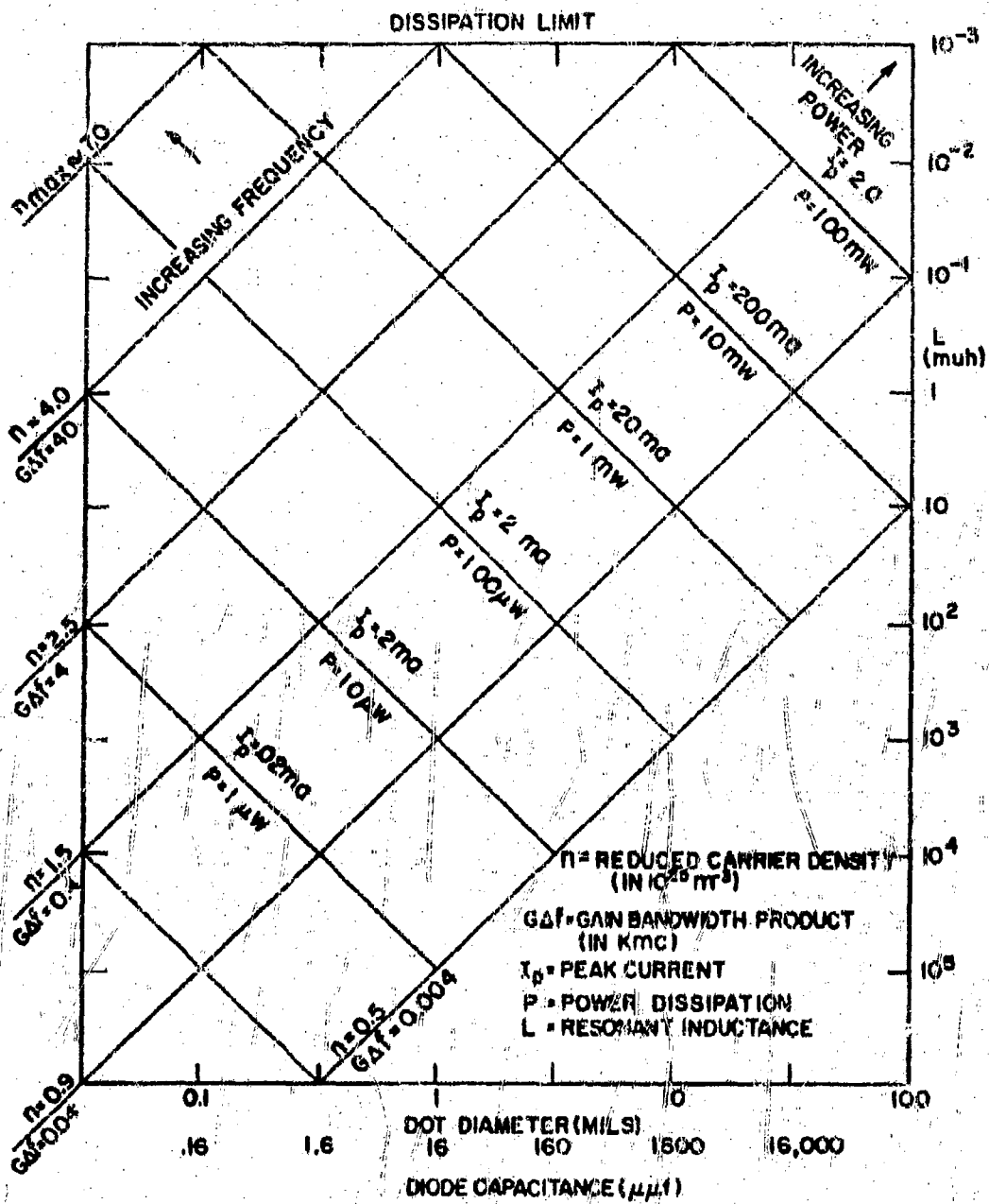


FIG. VI-8. GERMANIUM TUNNEL DIODE CHART

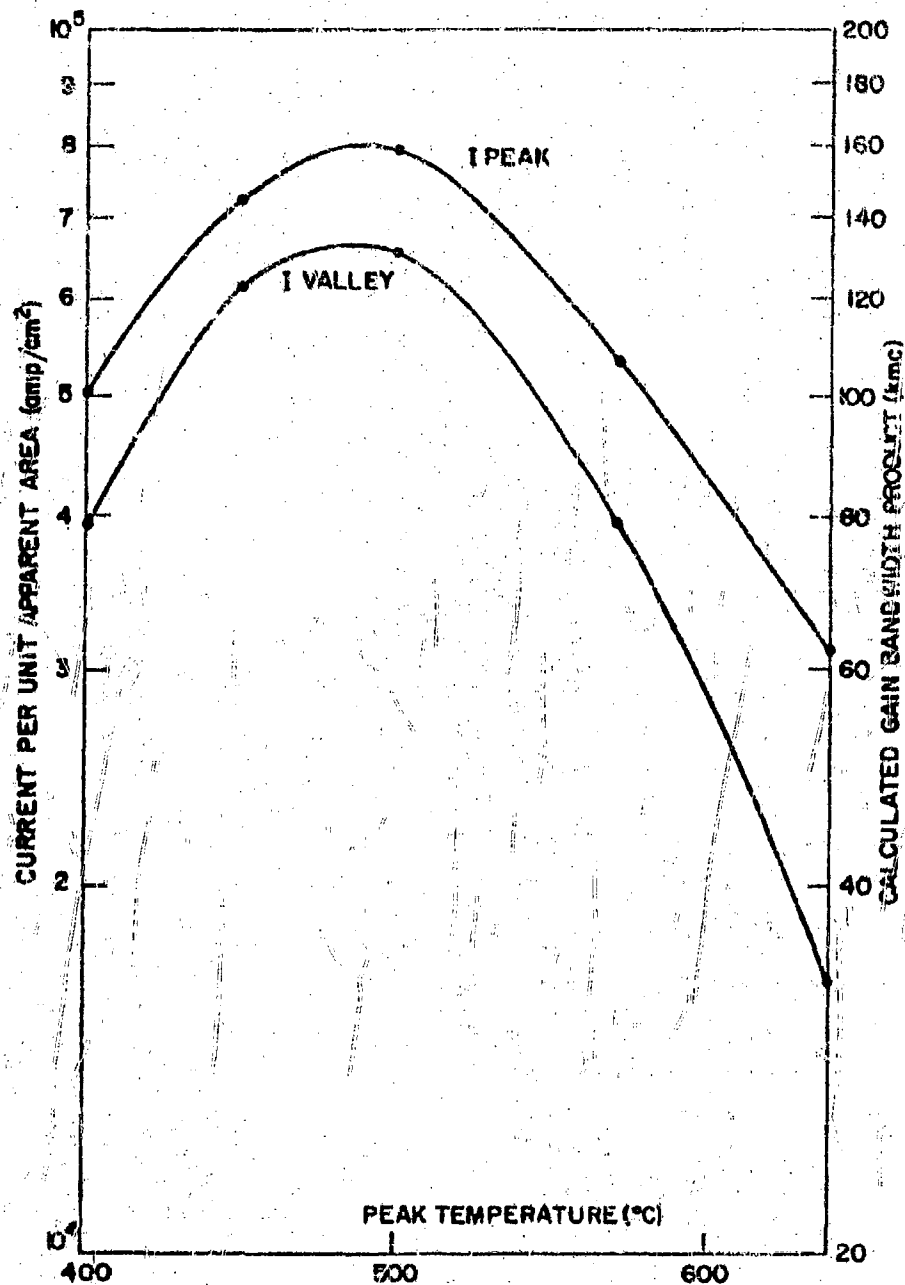


FIG. VI-9. TYPICAL Sn-Zn EUTECTIC DOTS ON GaSb ( $1.7 \times 10^{18}$  Te/cc)

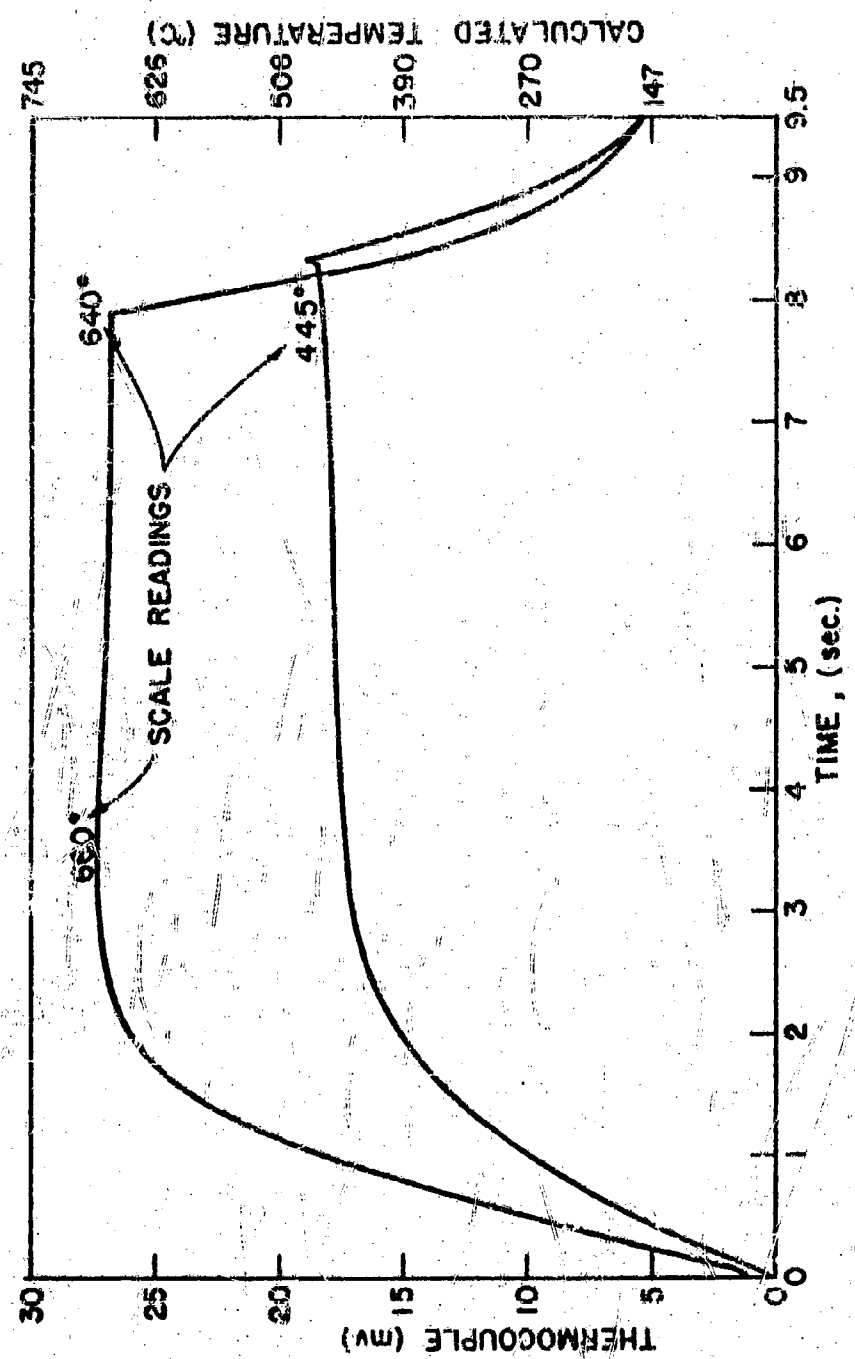


FIG. II-10. FURNACE RESPONSE TO THE SWITCHING OF FULL VOLTAGE  
(ALL TUNNEL DIODES WERE QUENCHED SIMILARLY)

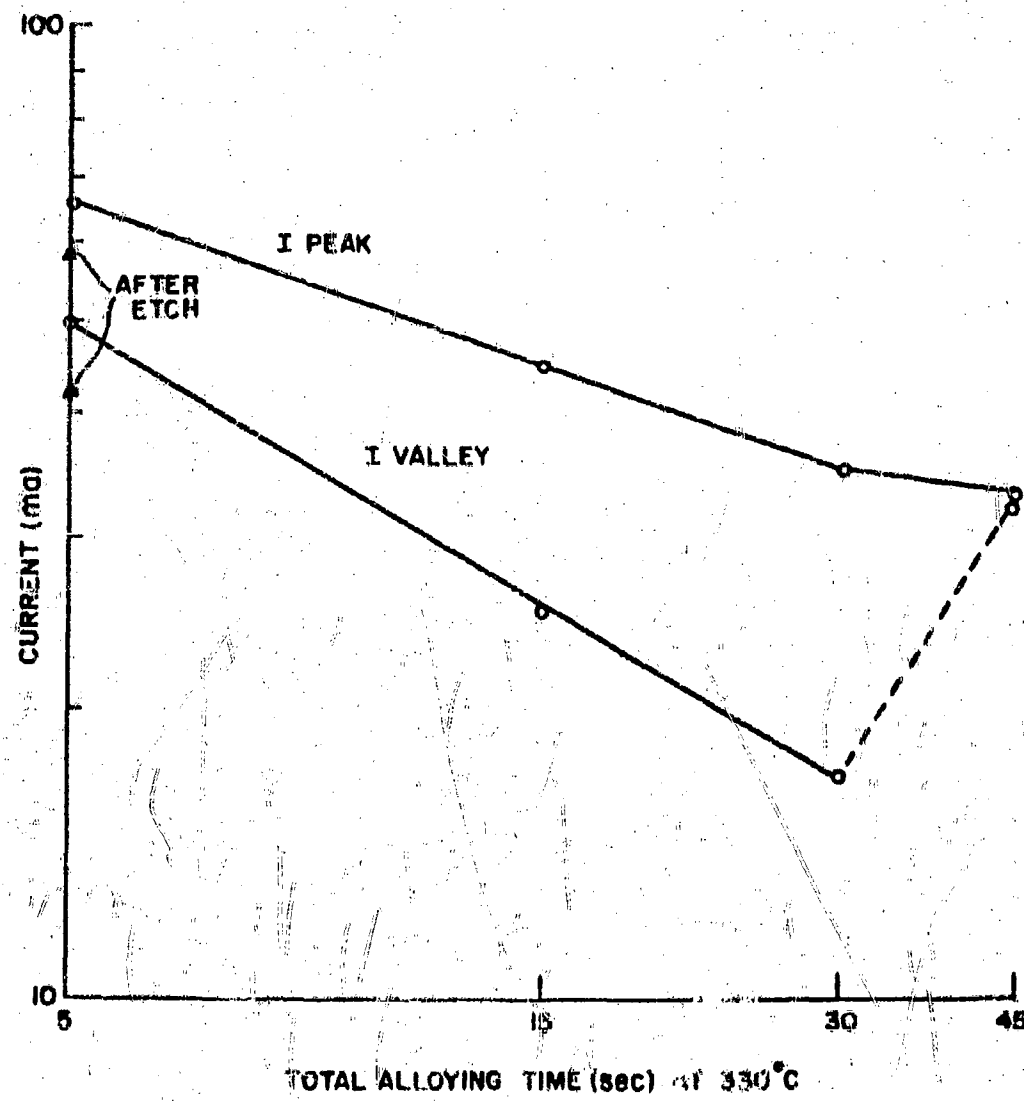
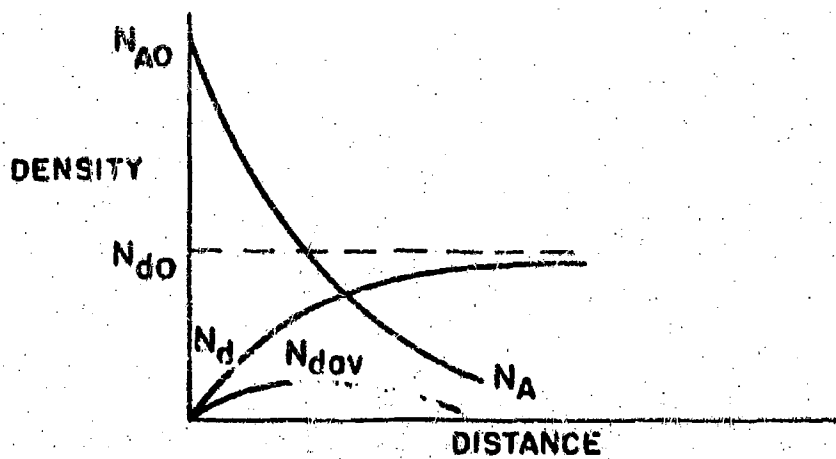
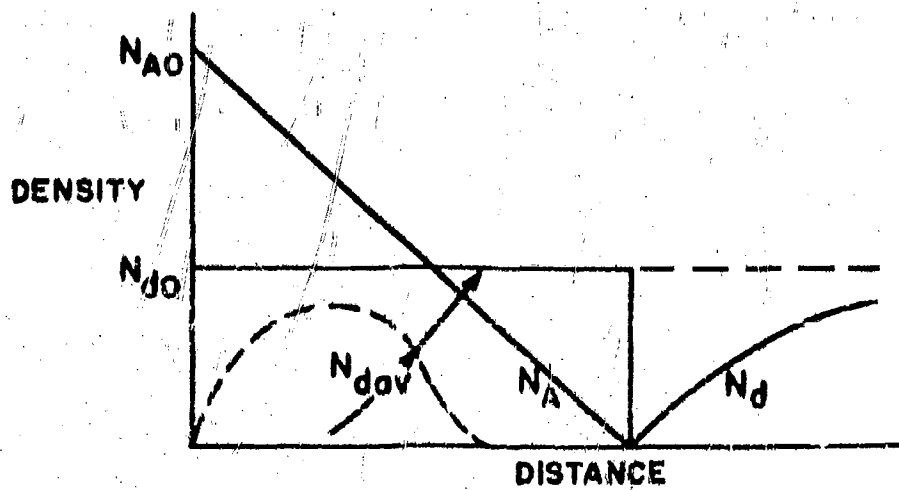


FIG. VII-II, TYPICAL DEGRADATION SN-Cd DOTS ON GLASS ( $1.5 \times 10^{18}$  Te/CC)



**FIG. VI-12. DENSITY PROFILES BEFORE REACTION RATE EXCEEDS DIFFUSION.**



**FIG. VI-13. DENSITY PROFILES AFTER REACTION RATE EXCEEDS DIFFUSION.**

**UNCLASSIFIED**

**UNCLASSIFIED**